NeXTEM

Next-Generation
Transmission
Electron Microscopy

October 8–10, 2018

PACIFIC NORTHWEST NATIONAL LABORATORY

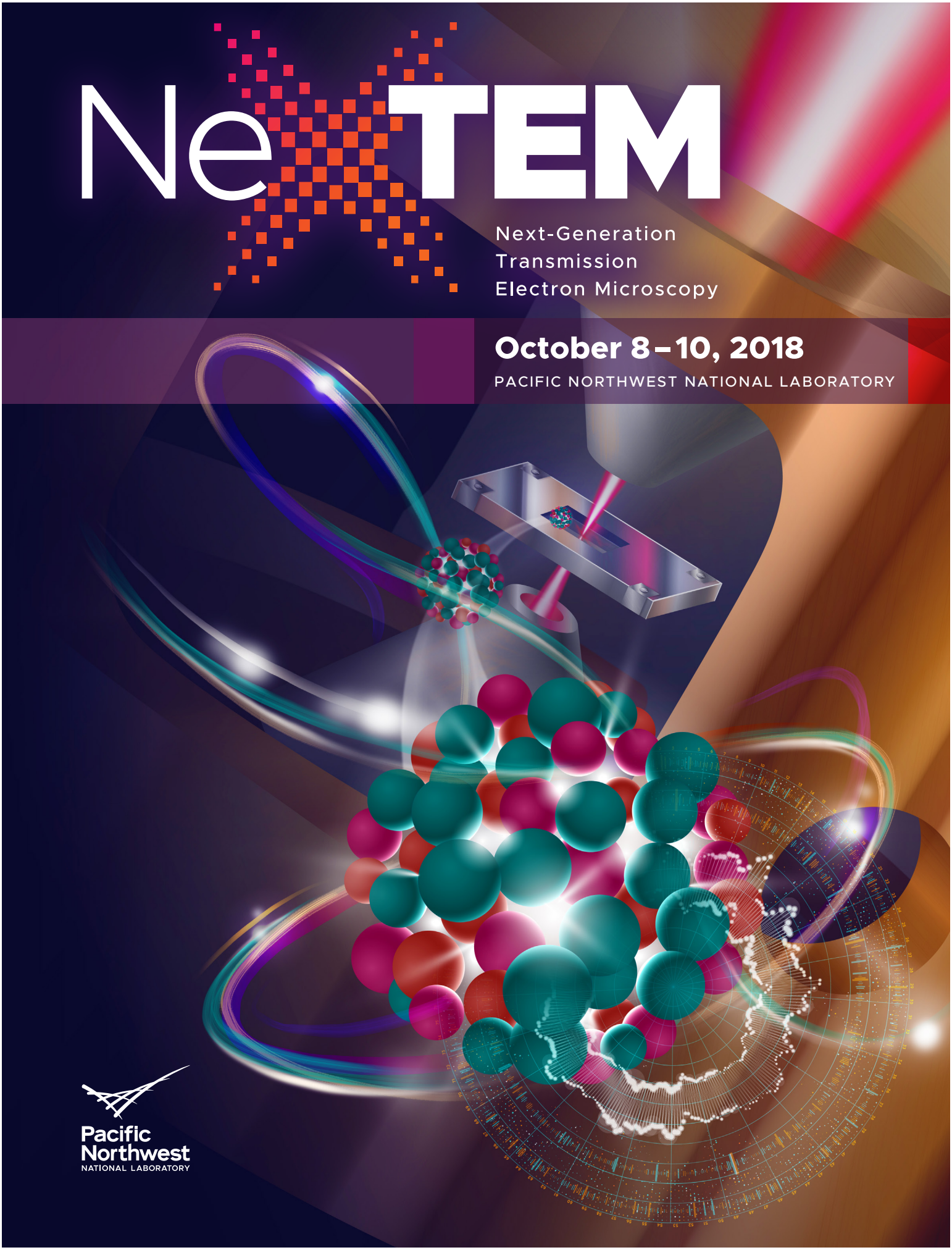

Pacific Northwest
NATIONAL LABORATORY

NexTEM
Next-Generation
Transmission
Electron Microscopy

WELCOME!

It is our pleasure to welcome you to the inaugural Next-Generation Transmission Electron Microscopy (NexTEM) meeting at Pacific Northwest National Laboratory! The landscape of electron microscopy is changing dramatically. Advanced instrumentation is allowing us to look deeper into materials than ever before. A variety of in situ platforms are granting us access to systems in near-native environments. And the machine learning revolution is starting to help us extract meaning from the vast amounts of data produced by today's microscopes. NexTEM is focused on the intersection and convergence of these rapidly evolving domains.

Over the next three days, we welcome experts from around the world who will discuss exciting developments on the frontier of microscopy. NexTEM will showcase cutting-edge science, ranging from Lorentz to 4D STEM and in situ irradiation to vibrational EELS. We have brought together scientists, instrument designers, and data analysis experts to celebrate successes and identify challenges still facing the community. The workshop is organized to allow ample time for both sharing research and finding new connections, with the aim to uncover unique solutions to longstanding problems.

Most importantly, we hope that NexTEM will frame a vision for the more meaningful, efficient, and dynamic microscopy of tomorrow. We're glad that you can join us!

Warm regards,

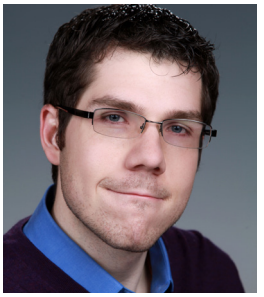

Steven R. Spurgeon
STAFF SCIENTIST
Energy and Environment Directorate
Pacific Northwest National Laboratory

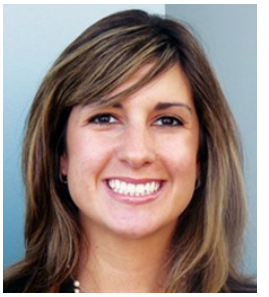

Mitra L. Taheri
HOEGANAES PROFESSOR
Department of Materials Science and Engineering
Drexel University

AGENDA AT A GLANCE: MONDAY, OCTOBER 8, 2018

8:30 a.m. – 10:00 a.m.

SESSION 1: High-Resolution Imaging and Spectroscopy

Chair: Matthew Olszta,
Pacific Northwest National Laboratory

10:30 a.m. – 12:00 p.m.

SESSION 2: In Situ and Extreme Environments

Chair: Daniel Schreiber,
Pacific Northwest National Laboratory

1:00 p.m. – 2:00 p.m.

SESSION 3: Data Analytics and Image Processing

Chair: Bradley Johnson,
Pacific Northwest National Laboratory

2:00 p.m. – 3:00 p.m.

SESSION 4: Instrumentation Development

Chair: Bradley Johnson,
Pacific Northwest National Laboratory

AGENDA AT A GLANCE: TUESDAY, OCTOBER 9, 2018

8:00 a.m. – 9:00 a.m.

SESSION 5: Data Analytics and Image Processing

Chair: Libor Kovarik,
Pacific Northwest National Laboratory

9:00 a.m. – 10:00 a.m.

SESSION 6: Instrumentation Development

Chair: Libor Kovarik,
Pacific Northwest National Laboratory

1:00 p.m. – 2:00 p.m.

SESSION 7: In Situ and Extreme Environments

Chair: Matthew Olszta,
Pacific Northwest National Laboratory

2:00 p.m. – 3:00 p.m.

SESSION 8: High-Resolution Imaging and Spectroscopy

Chair: Matthew Olszta,
Pacific Northwest National Laboratory

AGENDA AT A GLANCE: WEDNESDAY, OCTOBER 10, 2018

8:00 a.m. – 9:00 a.m.

SESSION 9: In Situ and Extreme Environments

Chair: Edgar Buck,
Pacific Northwest National Laboratory

9:00 a.m. – 10:00 a.m.

SESSION 10: Data Analytics and Image Processing

Chair: Edgar Buck,
Pacific Northwest National Laboratory

10:30 a.m. – 11:30 a.m.

SESSION 11: Instrumentation Development

Chair: Alice Dohnalkova,
Pacific Northwest National Laboratory

AGENDA

MONDAY, October 8, 2018

7:00 a.m. – 8:00 a.m.	**REGISTRATION**	
8:00 a.m. – 8:30 a.m.	**Welcome & Meeting Overview**	**Malin Young, Deputy Director, Science and Technology, PNNL** Pacific Northwest National Laboratory
8:30 a.m.–10:00 a.m.	**SESSION 1: High-Resolution Imaging and Spectroscopy** Chair: Matthew Olszta, Pacific Northwest National Laboratory	
8:30 a.m.	**Ultra-high Energy Resolution EELS**	**Ondrej Krivanek** Nion Co.
9:00 a.m.	**Prospects and Challenges for Quantitative High-Resolution TEM**	**Rafal Dunin-Borkowski** Research Centre Jülich
9:30 a.m.	**Imaging and Diffraction Based Strain Mapping in S(T)EM–From Single Atom Columns to Microns**	**Benedikt Haas** Humboldt-Universität zu Berlin
10:00 a.m.–10:30 a.m.	**Open Discussion**	All Attendees
10:30 a.m.–12:00 p.m.	**SESSION 2: In Situ and Extreme Environments** Chair: Daniel Schreiber, Pacific Northwest National Laboratory	
10:30 a.m.	**Exploring the Local Behavior of Magnetic Nanostructures via In Situ Lorentz TEM**	**Amanda Petford-Long** Argonne National Laboratory
11:00 a.m.	**In Situ STEM Characterization of 2-Dim Materials at High Energy and Spatial Resolution**	**Jacob Jokisaari** University of Illinois at Chicago
11:30 a.m.	**The Possibility of an Integrated Electron Microscopy Toolset for Studying Superimposed Extreme Environments**	**Khalid Hattar** Sandia National Laboratories
12:00 p.m.–1:00 p.m.	**Breakout Brainstorming (Working Lunch)**	All Attendees
1:00 p.m.– 2:00 p.m.	**SESSION 3: Data Analytics and Image Processing** Chair: Bradley Johnson, Pacific Northwest National Laboratory	
1:00 p.m.	**Accelerating the Pace of Discovery with In Situ 4D STEM**	**James LeBeau** North Carolina State University
1:30 p.m.	**EMsoft: Open Source Software for Electron Microscopy Simulations**	**Marc DeGraef** Carnegie Mellon University

2:00 p.m.–3:00 p.m.	**SESSION 4: Instrumentation Development** Chair: Bradley Johnson, Pacific Northwest National Laboratory	
2:00 p.m.	**Seeing is Believing–New Horizons for In Situ Microscopy**	**Jordan Moering** Protochips
2:30 p.m.	**Tools for In Situ and Operando TEM, and Other Imaging Platforms**	**Julio Rodriguez Manzo** Hummingbird Scientific
3:00 p.m.–3:30 p.m.	**Open Discussion**	All Attendees
3:30 p.m.–5:00 p.m.	**Breakout 1**	All Attendees
5:00 p.m.–6:15 p.m.	**Reception** **Poster Session (Discovery Hall)**	All Attendees

TUESDAY, October 9, 2018

7:00 a.m.–8:00 a.m.	**REGISTRATION**	
8:00 a.m.–9:00 a.m.	**SESSION 5: Data Analytics and Image Processing** Chair: Libor Kovarik, Pacific Northwest National Laboratory	
8:00 a.m.	**The Lab on a Beam: Big Data and Artificial Intelligence in Scanning Transmission Electron Microscopy**	**Sergei Kalinin** Oak Ridge National Laboratory
8:30 a.m.	**4D-STEM Experimental and Simulation Methods**	**Colin Ophus** Lawrence Berkeley National Laboratory
9:00 a.m.–10:00 a.m.	**SESSION 6: Instrumentation Development** Chair: Libor Kovarik, Pacific Northwest National Laboratory	
9:00 a.m.	**Recent Developments and Current State of the STEM; A JEOL Perspective**	**Tom Isabell** JEOL USA, Inc.
9:30 a.m.	**Recent Advances in Electron Microscopy Developments**	**Jan Ringnalda** ThermoFisher Scientific
10:00 a.m.–12:00 p.m.	**Microscopy Facility Tours (EMSL Quiet Wing, 3410 Suite and RPL Radiological Microscopy Suite)**	
12:00 p.m.–1:00 p.m.	**Breakout Brainstorming (Working Lunch)**	All Attendees

1:00 p.m.– 2:00 p.m.	**SESSION 7: In Situ and Extreme Environments** Chair: Matthew Olszta, Pacific Northwest National Laboratory	
1:00 p.m.	**Multimodal Methods for In Situ Transmission Electron Microscopy**	**Renu Sharma** National Institute of Standards and Technology
1:30 p.m.	**Liquid Phase Electron Microscopy Study of Dynamic Phenomena at Solid-Liquid Interfaces**	**Haimei Zheng** Lawrence Berkeley National Laboratory
2:00 p.m.–3:00 p.m.	**SESSION 8: High-Resolution Imaging and Spectroscopy** Chair: Matthew Olszta, Pacific Northwest National Laboratory	
2:00 p.m.	**Electron Microscopy for the Quantum Information Era**	**Juan Carlos Idrobo** Oak Ridge National Laboratory
2:30 p.m.	**Advantages of Direct Detection and Electron Counting for Electron Energy Loss Spectroscopy Data Acquisition**	**Paolo Longo** Gatan
3:00 p.m.–3:30 p.m.	**Open Discussion**	All Attendees
3:30 p.m.–5:00 p.m.	**Breakout 2**	All Attendees
5:00 p.m.–5:30 pm	**Return to Hotels**	All Attendees
5:30 p.m.–6:00 pm	**Bus Pickup from Local Hotels**	All Attendees
6:00 p.m.–9:00 pm	**Dinner** **Terra Blanca Winery** Sponsored by JEOL USA	

WEDNESDAY, October 10, 2018

7:00 a.m. – 8:00 a.m.	**REGISTRATION**	
8:00 a.m.–9:00 a.m.	**SESSION 9: In Situ and Extreme Environments** Chair: Edgar Buck, Pacific Northwest National Laboratory	
8:00 a.m.	**Environmental TEM Study of Catalytic Nanoparticles In A Reactive Gas Environment**	**Libor Kovarik** Pacific Northwest National Laboratory
8:30 a.m.	**Characterizing Formation, Growth, Dissolution, and Transformation of Nanoscale Objects in Aqueous and Non-Aqueous Suspensions**	**R. Lee Penn** University of Minnesota

9:00 a.m.–10:00 a.m.	**SESSION 10: Data Analytics and Image Processing** Chair: Edgar Buck, Pacific Northwest National Laboratory	
9:00 a.m.	**Frame-Series Imaging and Spectroscopy as a Flexible Experiment-Design Dimension**	**Lewys Jones** Trinity College Dublin
9:30 a.m.	**Knowledge from Atomically Resolved Images: Deep Learning Meets Statistical Physics**	**Maxim Ziatdinov** Oak Ridge National Laboratory
10:00 a.m.–10:30 a.m.	**Open Discussion**	All Attendees
10:30 a.m.–11:30 a.m.	**SESSION 11: Instrumentation Development** Chair: Alice Dohnalkova, Pacific Northwest National Laboratory	
10:30 a.m.	**Analyzing Infrared Quasiparticles with Nanoscale Spatial Resolution using Monochromated Electron Energy Loss Spectroscopy**	**Jordan Hachtel** Oak Ridge National Laboratory
11:00 a.m.	**An Attempt to Integrate Electron Tomography and In Situ Deformation for 3D Dislocation Dynamics**	**Mitsu Murayama** Virginia Tech
11:30 a.m.–12:00 p.m.	**Group Photo**	All Attendees
12:00 p.m.–1:00 p.m.	**Breakout Brainstorming (Working Lunch)**	All Attendees
1:00 p.m.–3:00 p.m.	**Breakout Writing**	All Attendees
3:00 p.m.–3:30 p.m.	**Closing Remarks**	**Steven Spurgeon** Pacific Northwest National Laboratory **Mitra Taheri** Drexel University
3:30 p.m.–5:00 p.m.	**LIGO Tour**	
5:00 p.m.–6:30 p.m.	**Reception at LIGO**	
6:30 p.m.	**Bus Returns Attendees to Discovery Hall**	

THURSDAY, October 11, 2018

7:00 a.m. – 11:30 a.m.	**Optional B-Reactor Tour** (available only to those who registered for the B-Reactor tour)
7:00 a.m.	**Motorcoach Departs Discovery Hall**
11:30 a.m.	**Motorcoach Returns to Discovery Hall**

NexTEM

Next-Generation
Transmission
Electron Microscopy

We appreciate the support of our sponsors.

Thank you!

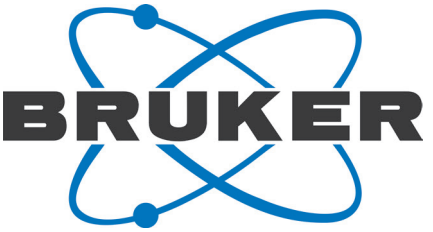

EMsoft: Open Source Software for Electron Microscopy Simulations

Marc De Graef[1]
[1.] Department of Materials Science and Engineering, Carnegie Mellon University, Pittsburgh PA, USA

The open source EMsoft package, available from GitHub [1], consists of a series of modules for crystallography, symmetry, scattering, rotations, etc… as well as multiple application programs that use the modules. The bulk of the package is written in fortran 2008, with some components in C, as well as OpenCL for specific computations on a Graphical Processing Unit (GPU). Package configuration is done with the CMake environment, and the majority of the generated output is formatted in the Hierarchical Data Format (HDF5, [2]). The use of the CMake build environment facilitates maintenance of the code for all three major operating systems, Mac OS X, Windows 10, and Linux (currently tested on CentOS 7 and Ubuntu 16). The package is intended to cover Electron Microscopy (EM) imaging and diffraction modalities for both Scanning and Transmission EM; the package does not cover high-resolution EM modalities, since there are many other options available for HREM.

The basic equations underlying dynamical electron scattering can be used interchangeably for image and diffraction simulations for both SEM and TEM. EMsoft provides tools for the following diffraction modalities: Electron Back-Scatter Diffraction (EBSD), Electron Channeling Patterns (ECP), Transmission Kikuchi Diffraction (TKD), Convergent Beam Electron Diffraction (CBED), and Precession Electron Diffraction (PED). For imaging, the following modalities are currently available: Bright Field/Dark Field (BF/DF) diffraction contrast imaging, STEM Diffraction Contrast Imaging (STEM-DCI), and Electron Channeling Contrast Imaging (ECCI). In a future release, photon-based modalities will be added, including High Energy Diffraction Microscopy (HEDM), and Computational Polarized Light Microscopy (CPLM).

The main goal of the EMsoft package is to provide a series of physics-based modular forward models that can be used to accurately simulate images and diffraction patterns for arbitrary crystal symmetry and for a range of crystal defects, including dislocations, stacking faults, anti-phase boundaries, ellipsoidal (Eshelby) inclusions, voids, and second phase particles; the current release includes aperiodic structures as well (octagonal, decagonal, dodecagonal, and icosahedral). The package uses the atomic scattering factors and absorptive form factors parameterized in [3]; the main simulation approaches are based on the Bloch wave formalism and the scattering matrix formalism and have been implemented in a single form for both SEM and TEM modalities. For defect image simulations, the code can handle molecular dynamics data sets as well as phase field and discrete dislocation dynamics data.

In this contribution, we will begin with a description of the general philosophy used to design and maintain the EMsoft package, and we will provide a brief overview of the structure of the package as well as the available user help (wiki pages [4], EMsoft Google Users Group [5]). Then we will provide detailed examples of the use of the package, in particular the new dictionary indexing algorithm used for EBSD, TKD, ECP, and PED patterns described in the

next paragraphs. We will conclude with a brief future outlook, detailing ongoing code development efforts.

The Dictionary Indexing (DI) algorithm [6,7] provides a general approach to the automated unsupervised indexing of electron diffraction patterns and research directions. The DI approach relies on the availability of a physics-based forward model for the particular diffraction modality; this model, along with a uniform sampling of orientation space, *SO(3)*, and accurate knowledge of the detector geometry, allows for the generation of a dictionary of simulated diffraction patterns. These patterns are typically interpolated from a so-called "master pattern". For the EBSD modality, this involves first a Monte Carlo simulation to determine the energy, depth, and directional distributions of the back-scattered electrons (BSEs); this simulation is carried out on a GPU and takes only a few minutes. Then the Monte Carlo data is combined with a dynamical scattering simulation (Bloch waves) of the BSE yield on the Kikuchi sphere; this data is then stored on a square grid using an equal-area Lambert-type projection. When combined with the orientation sampling and the detector geometry, the master pattern allows for the fast generation of individual diffraction patterns by means of simple bilinear interpolation. A typical dictionary for a cubic crystal contains on the order of 330,000 individual patterns, corresponding to a sampling of orientation space with an average 1.4° angular step size; for lower symmetry structures, the dictionary size increases correspondingly.

The dictionary patterns are then compared with all the experimental patterns using a pattern matching algorithm; among many possible similarity metrics we have selected the normalized dot product between two patterns because it can be compute rapidly using a GPU, but other metrics, such as cross-correlation and mutual information, work equally well. At no point during the comparison are any features extracted from the diffraction pattern, which is very different from the commercially available approaches, which rely on the Hough Transform (HT) to find the most intense Kikuchi bands. We will show that the DI approach is significantly more robust against pattern noise than the HT approach. Once the orientation of an individual experimental pattern has been determined, a refinement step can be used to eliminate any artifacts arising from the discrete sampling of orientation space.

We will provide several example applications of the DI approach for EBSD and TKD patterns, including: polycrystalline Nickel; shot-peened Al 7075-T651; a three-phase mixture of garnet, clinopyroxene, and a glassy phase; and a large scale serial sectioning super alloy data set consisting of more than 117 million EBSD patterns. We will conclude with a brief review of current and future development of the EMsoft package [8].

References:

[1] http://github.com/marcdegraef/EMsoft.
[2] http://hdfgroup.org.
[3] A Weickenmeier and H Kohl, Acta Crystal. A, **47** (1991), p. 590.
[4] http://github.com/marcdegraef/EMsoft/wiki.
[5] https://groups.google.com/forum/?hl=en#!forum/emsoft-users.
[6] YH Chen *et al*, Microsc. MicroAnal. **21** (2015), p. 739.
[7] K. Marquardt *et al*, American Mineralogist, **102** (2017), p. 1843.
[8] The author acknowledges funding from a DoD Vannevar Bush Faculty Fellowship (N00014-16-1-2821), and the computational facilities of the Materials Characterization Facility at Carnegie Mellon University under grant # MCF-677785.

Imaging and Analyses of Iron Deposits within Chronic Myocardial infarction

Alice Dohnalkova[1] and Libor Kovarik[1]
[1.] Pacific Northwest National Laboratory, Environmental Molecular Sciences Laboratory, Richland, WA, USA

A collaboration project with Dr. Rohan Dharmakumar and Ivan Cokic, The Cedars-Sinai Medical Center, Los Angeles, CA and University of California, Los Angeles, CA, USA

Myocardial infarction (MI) is a type of acute coronary syndrome that often results in impaired blood flow to the heart, necrotic damage to the heart cells in the territory of the blocked coronary artery, and eventually a formation of a collagen scar in its place. Emerging evidence indicates that persistent microvascular obstruction (PMO) is more predictive of major adverse cardiovascular events than MI size. But it remains unclear how PMO drives adverse remodeling in chronic MI setting. We hypothesized that PMO resolves into chronic iron nanocrystals deposition within MI territories, which in turn are proinflammatory and favor adverse remodeling post-MI [1].

Canines (n=40) were studied with non-invasive characterization of PMO with gadolinium-enhanced cardiac magnetic resonance (CMR) imaging to characterize the spatiotemporal relationships among PMO, iron deposition, infarct resorption, and left ventricular remodeling between day 7 (acute) and week 8 (chronic) post-MI. Histology was used to assess iron deposition and to examine relationships between iron content with macrophage infiltration. High resolution transmission electron microscopy was used to determine the ultrastructure of the iron released from hemoglobin during the hemorrhage reperfusion which can lead to chronic iron deposition, associated with recruitment of macrophages, and its incorporation into the cell within the cardiac tissue. Iron crystallinity was determined by selected area diffraction (SAD), and the chemical composition of the iron composite was identified by the energy- dispersive X-ray spectroscopy (EDS).

Briefly, samples positive for iron from *ex-vivo* sections were dissected into 1 mm^3 cubes and fixed in 2.5% glutaraldehyde (Electron Microscopy Sciences, Hatfield, PA) and processed by washing them with dH_2O and a gradual dehydration by using ethanol series (25%, 33, 50, 75, and 3×100% ethanol). The traditional stains for contrast enhancement such as OsO_4 were purposely omitted to preserve the redox state of the newly formed biominerals. Samples were then infilgtrated in LR white acrylic resin (EMS), and polymerized at 60°C for 24 hours. The hardened resin blocks were sectioned on a Leica EM UC6 ultramicrotome using a 45° diamond knife (DiATOME, Biehl, Switzerland). 70-nanometer-thick sections were collected on copper grids coated with ultrathin carbon on holey carbon support (Ted Pella, Redding, CA) and imaged on a Tecnai T-12 TEM (FEI, Hillsboro, OR) with a LaB6 filament, operating at 120 kV. Images were collected digitally with a 2×2K Ultrascan 1000 CCD (Gatan, Pleasanton, CA). For the atomic resolution imaging, the previously identified areas of interest were correlatively imaged using Titan scanning transmission electron microscope (S/TEM, FEI), operating at 300 kV. To identify the cryatallinity of the newly formed Fe minerals, the diffraction patterns were collected

and analyzed. The chemical elemental analysis was performed with energy-dispersive spectroscopy, using a Si(Li) detector (EDAX, Mahwah, NJ), coupled to the S/TEM.

PMO with or without reperfusion hemorrhage led to chronic iron deposition, and the extent of this deposition was strongly related to PMO volume. TEM of chronic MI sections, positive for iron in ex vivo T2* CMR, revealed the presence of electron-dense materials within macrophages that were organized into nodules (≈200 nm in diameter; Figure 1A). These iron deposits were aggregates of 2.5 nm highly crystalline nanocrystals in the ferric state (Fig 1B). S/TEM imaging and analysis of the particulate material showed a highly ordered atomic pattern, and the EDS spectrum revealed a strong presence of iron. The SAD confirmed the diffraction pattern to be an exact fit to the 6-line hydroxy ferrihydrite (HFO), $Fe_2O_3 \bullet 0.5H_2O$.

In conclusion, S/TEM, EDS, and SAD studies revealed for the first time that the iron deposits within chronic MI are found as nodules composed from nanocrystals of iron in ferric form. Moreover, the TEM images also showed that iron aggregates are located within membrane-enclosed structures, suggestive of lysosomes that seem to be loaded to their physical limits (diameter>1 μm). These findings may help to explain the proinflammatory burden and adverse structural remodeling in chronic MI with iron deposits.

References:

[1] A Kali et al., Circ Cardiovasc Imaging. 2016;9:e004996. DOI: 10.1161/CIRCIMAGING.115.004996
[2] A part of this research was performed at the Environmental Molecular Sciences Laboratory (EMSL), a national scientific user facility, located at PNNL.
[3] This work was supported in part by NIH Research project grant 131-437-9427-A3 to AD.

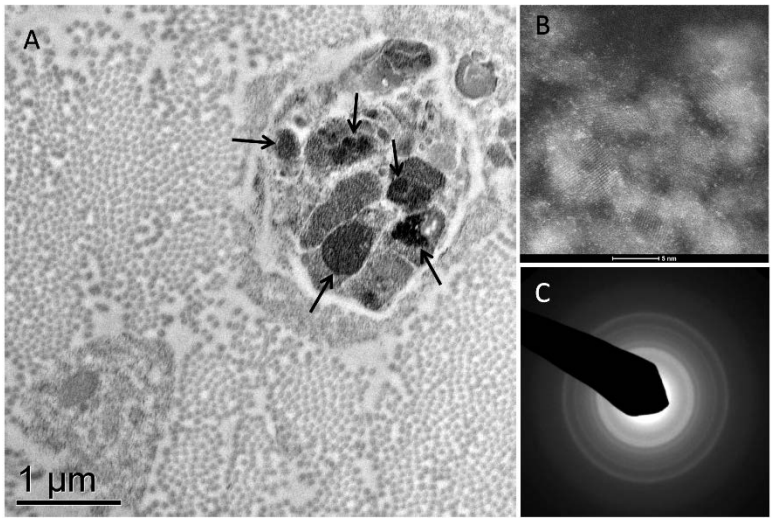

Figure 1. (A) TEM image of a macrophage cell in a cardiac tissue. Arrows point to the Fe deposits. (B) HAADF-STEM image of nanocrystalline Fe material within the nodules. (C) SAD pattern of the HFO.

Visualizing Oxygen Vacancy Ordering and Structural Evolution in Perovskite-Related Oxides by *In Situ* and Environmental TEM

Zhenzhong Yang[1], Le Wang[1], Steven R. Spurgeon[2], Mark Engelhard[3], Mark Bowden[3], Chongmin Wang[3], Zihua Zhu[3], and Yingge Du[1*]
[1.] Physical & Computational Sciences Directorate, Pacific Northwest National Laboratory (PNNL), Richland, WA 99352 USA
[2.] Energy & Environment Directorate, PNNL
[3.] Environmental Molecular Sciences Laboratory, PNNL

Transition metal oxides exhibit a broad range of structural, compositional, and functional properties, which can be further tuned or even drastically transformed by means of judicious elemental doping, strain and defect engineering. This talk will highlight our most recent effort aiming to modify complex oxides through heteroepitaxy for tunable O^{2-} transport, which have profound implications in energy conversion and storage devices.

The creation, clustering, and ordering of oxygen vacancies (VOs) in perovskite-structured oxides (ABO_3, B being a transition metal) give rise to a special class of materials, such as Brownmillerite (BM) structured $SrCoO_{2.5}$, $SrFeO_{2.5}$ (BM-SFO), and rhombohedral structured $SrCrO_{2.8}$ (R-SCrO). We show that by varying synthesis and processing conditions, the orientation of OVCs can be selectively controlled on the same lattice matched substrate. Optical ellipsometry, in-plane transport, ^{18}O isotope exchange, and scanning transmission electron microscopy studies reveal that these configurations offer distinct different physical and oxygen transport properties. A topotactic phase transition from BM-SFO (R-SCrO) to perovskite $SrFeO_3$ ($SrCrO_3$) can be promoted, delayed, or prohibited based on the interfacial strain conditions, highlighting the importance of interface engineering in designing robust and efficient ion conducting materials.

Prospects and Challenges for Quantitative High-Resolution TEM

R E Dunin-Borkowski[1], L Jin[1], A Kovács[1], J Caron[1], P Diehle[1], P Lu[1], A H Tavabi[1], F Zheng[1], V Migunov[1,2], F Winkler[1], J Barthel[1,2], C L Jia[1] and A Thust[1]
[1.] Ernst Ruska-Centre and Peter Grünberg Institute, Forschungszentrum Jülich, 52425 Jülich, Germany
[2.] Gemeinschaftslabor für Elektronenmikroskopie, RWTH Aachen University, 52074 Aachen, Germany

The introduction of aberration correction, monochromated and high brightness electron guns, improved specimen stages and holders, direct electron detectors and advanced software for instrument control have resulted in improvements in the spatial resolution and ability to interpret atomic-resolution images recorded using transmission electron microscopy (TEM). However, further advances are still possible in spatial and temporal resolution, spectroscopic sensitivity, three-dimensional characterization, sample stability and cleanliness and the use of advanced software to interpret measurements.

Here, we describe recent experimental measurements and discuss the need for future developments in methodology and instrumentation. Figure 1 shows an example of the retrieval of the three-dimensional atomic structure and shape of an MgO crystal from a single spherical aberration corrected high-resolution TEM image recorded at 300 kV [1]. The best fitting atomic structure model was refined in such a way that simulated images were matched to the experimental image *on an absolute scale*. The structure refinement was carried out column-by-column, allowing for the possibility of an atomically corrugated sample surface. It relied on the measurement or refinement of experimental parameters that described both the specimen and the microscope imaging parameters. A statistical confidence test was used to provide detailed quantitative statements about the uniqueness and reliability of the fitted crystal shape. Figure 2 shows a similar quantitative comparison between experimental images and simulations carried out on a high-resolution electron optical phase image of five monolayers of two-dimensional WSe_2 recorded at 80 kV using off-axis electron holography in a spherical and chromatic aberration corrected TEM [2]. The images show the result of iterative fitting of specimen tilt, absorption, image spread and aberrations by comparing the experimental phase image with simulations. Simulations based on scattering potentials derived from density functional theory were found to be necessary to achieve quantitative agreement between experimental and simulated phase images [3]. In contrast to the analysis of conventional high-resolution TEM images, access to the electron wavefunction allows residual aberrations to be removed, facilitating a quantitative description of the atomic structure of the material, including the detection of changes in electrostatic potential associated with local structural defects. With the recent introduction of combined spherical and chromatic aberration correction for high-resolution TEM, a spatial resolution of 50 pm can be achieved at 200 kV [4], while a value of better than 90 pm can be achieved at 50 kV, providing opportunities for imaging electron-beam-sensitive materials with high spatial resolution. In addition, the combination of spherical and chromatic aberration corrected high-resolution TEM with either off-axis electron holography or electron magnetic circular dichroism offers prospects for imaging magnetic fields on the atomic scale. Further improvements in spatial resolution are likely to require changes to the design of electron microscope columns to overcome problems such as “Johnson noise” [5], while more

precise measurements may require the automation of longer experiments, a better knowledge of microscope and specimen parameters and their stability [6], the use of ultra-high-vacuum technologies and improved specimen stages to provide clean and stable sample environments, quantitative comparisons of experimental measurements with both complementary techniques and advanced simulations, and new approaches for data handling and storage [7].

References:
[1] C L Jia et al., Nature Materials **13** (2014), 1044-1049.
[2] F Winkler et al., Phys. Rev. Lett. **120** (2018), 156101.
[3] S Borghardt et al., Phys. Rev. Lett. **118** (2017) 086101.
[4] L Jin et al., Ultramicroscopy **176** (2017), 99-104.
[5] S Uhlemann et al., Phys. Rev. Lett. **111** (2013), 046101.
[6] J Barthel and A Thust, Ultramicroscopy **134** (2013), 6-17.
[7] The authors are grateful to S B Mi, J Ungermann, Z-A Li, H Du, K Shibata, Y Tokura, M Riese, M Farle, N Kiselev, S Blügel, B E Kardynal, S Borghardt, P Hartel, M Haider, H Müller, P Tiemeijer and M Bischoff for contributions to this work.

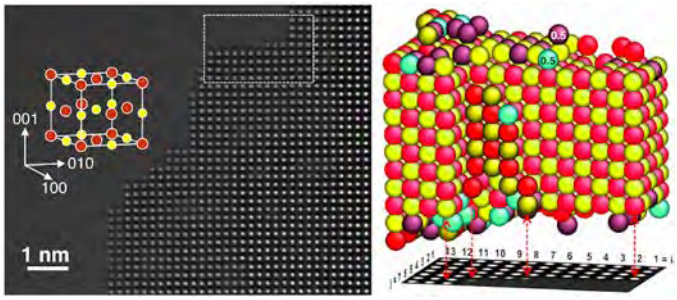

Figure 1. (Left) High-resolution TEM image of MgO viewed along [001] recorded using a spherical aberration corrected electron microscope operated at 300 kV. (Right) Three-dimensional structure model retrieved from the area indicated by the box based on quantitative comparisons with image simulations *on an absolute scale*. Red and yellow spheres indicate Mg and O atoms, respectively. Purple and green spheres indicate formally half-occupied Mg and O positions, respectively.

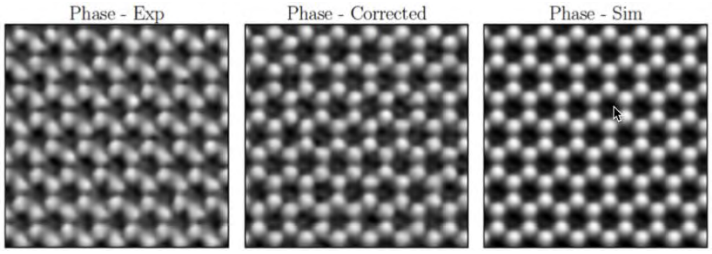

Figure 2. (Left) Spherical and chromatic aberration corrected high-resolution phase image recorded at 80 kV using off-axis electron holography from 5 monolayers of WSe_2. The specimen thickness was known from a comparison of the mean phase and amplitude with simulations. (Right) Simulated phase image generated for the known specimen thickness using density-functional-theory-derived potentials. (Center) Experimental image corrected for coherent aberrations, which were fitted iteratively through comparisons with the simulated image. The experimental image spread and specimen tilt were also fitted.

Imaging and Diffraction Based Strain Mapping in S(T)EM – From Single Atom Columns to Microns

Benedikt Haas[1], Johannes Müller[1], David Cooper[2], Jean-Luc Rouvière[2] and Christoph T. Koch[1]
[1] Institut für Physik & IRIS Adlershof, Humboldt-Universität zu Berlin, Berlin, Germany
[2] MINATEC Campus, CEA Grenoble & Université Grenoble Alpes, Grenoble, France

Mapping strain is essential for a variety of technologically relevant material systems. To enhance the performance of Si based transistors, the channel region is strained to enhance the charge carrier mobility and subsequently the achievable clock frequency of the device. The strain state is also crucial for the topological insulator system HgTe/CdTe where the deformation of the HgTe lattice gives rise to topologically protected states. Moreover, the local lattice spacing can also be used in certain systems to determine the chemistry with atomic resolution and with lower dose than it is necessary for spectroscopy. Three different methods are presented with decreasing spatial and increasing strain resolution and are applied to appropriate relevant materials science problems.

The first method is the determination of atom positions from registered HAADF image series. With this technique the position of columns can be measure with pm accuracy [1]. Fig. 1 (a) shows an HAADF image of a ZnTe/CdSe multilayer sample for photovoltaic applications. Here, the interface chemistry is critical for the device performance. In (b) the two interfaces A and B are shown in a registered HAADF image and (c) is the obtained local lattice spacing. The roughly 10% smaller values at the interfaces demonstrate that they consist of ZnSe, which is detrimental to the performance.

A second technique of strain measurement is to create a moiré pattern between the scanning probe and a crystal potential to augment deformations [2]. Here it is combined with adaptive sampling in the form of rectangular scan grids: Fig. 2 (a) shows a typical HAADF image of Si[110] and (b) the corresponding Fourier transform (FT). Utilizing an appropriate rectangular scan grid produces square symmetry in image (c) and FT (d). Subsequently, 2D scanning moirés can be obtained from e.g. SiGe/Si transistors in [110] ZA as seen in (e). From the patterns precise strain maps are calculated, shown in (f) and (g).

The third technique is strain mapping from scanning nano-beam diffraction. A 4D-STEM data set consisting of diffraction patterns obtained at every position of a scan grid are used to calculate the local lattice constants. This method is also realized in our SEM that we have equipped with a transmission diffraction detector to enable low-voltage 4D-STEM: Fig. 3 (a) depicts a GaN/AlN/sapphire sample and (b) a corresponding SEM 30kV transmission diffraction pattern from the GaN region. From the 10x50 diffraction patterns a virtual dark field given in (c) and maps of the local lattice distances in (d) and (e) can be obtained which show that GaN & AlN are fully relaxed.

References:
[1] AB Yankovichet al., Nature Comm. **5** (2014), p. 1.
[2] S Kim et al., Appl. Phys. Lett. **103** (2013), p. 033523.
[3] BH acknowledges funding from Deutsche Forschungsgemeinschaft (KO 2911/12-1).

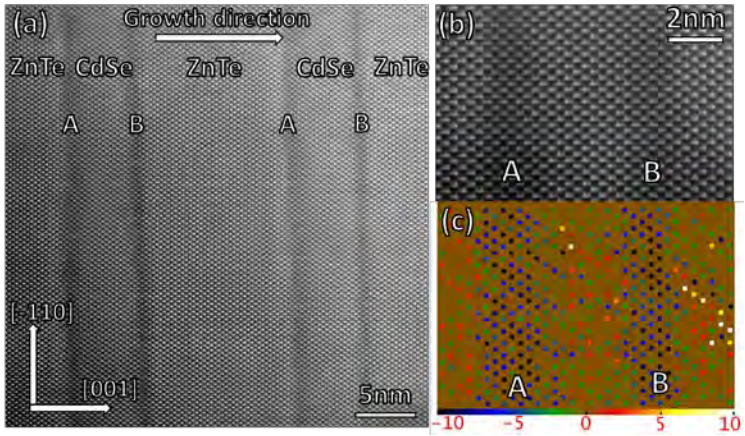

Figure 1. (a) HAADF image of ZnTe/CdSe superlattice. (b) Image of interfaces from registered series. (c) Map of relative lattice spacings for each column (in percent). The large negative values at the interfaces demonstrate ZnSe building up there.

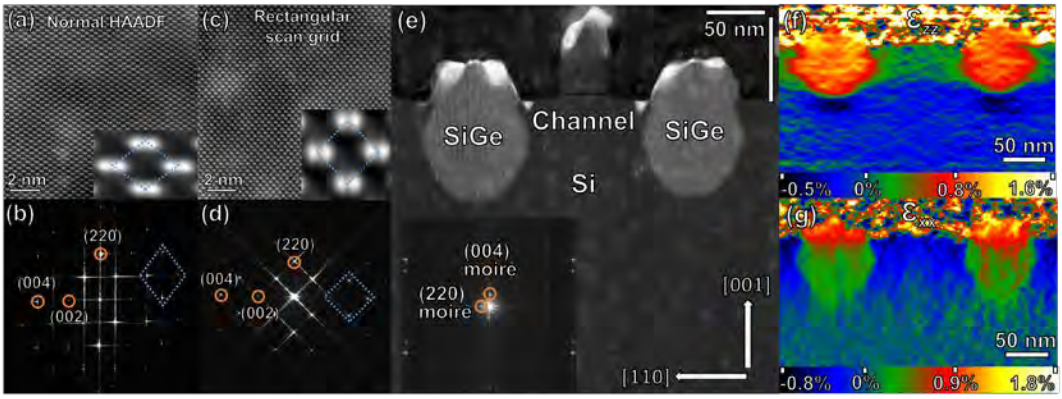

Figure 2. (a) HAADF image of Si[110] and (b) corresponding Fourier transform. (c) Modifying the scan grid can produce a square symmetry, as seen in the FT in (d). (e) This can be used to obtain 2D scanning moirés patterns of a SiGe/Si transistor in [110] ZA to obtain precise strain maps (f) & (g).

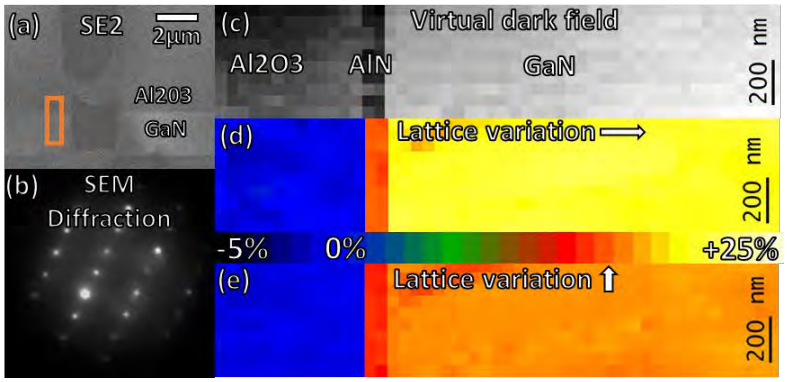

Figure 3. (a) Secondary electron image of GaN/AlN/sapphire sample with marked region of interest. (b) Diffraction pattern from SEM with homemade transmission setup. (c) Virtual dark field obtained from 4D-S(T)EM data set. (d) & (e) Local lattice distances in growth direction and perpendicular showing completely relaxed AlN and GaN layers.

Analyzing Infrared Quasiparticles with Nanoscale Spatial Resolution using Monochromated Electron Energy Loss Spectroscopy

Jordan A. Hachtel[1], Jacob R. Jokisaari[2], Ankit Agrawal[3], Shin Hum Cho[3], Delia J. Miliron[3], Robert F. Klie[2], Juan Carlos Idrobo[1]
[1.] Center for Nanophase Materials Sciences, Oak Ridge National Laboratory, Oak Ridge, TN USA.
[2.] Department of Physics, University of Illinois at Chicago, Chicago, IL USA.
[3.] McKetta Department of Chemical Engineering, University of Texas at Austin, Austin, Texas USA.

Electron energy loss spectroscopy (EELS) has been of the predominant methods to study the chemical, electronic, and optical properties of materials in the scanning transmission electron microscope. While, the natural spread of energies emerging from standard electron guns (300-700 meV) have long made the infrared regime difficult to access if not inaccessible to EELS. Recent developments in monochromation have both improved the energy resolution and dramatically reduced the background in the infrared, allowing for the detection of the small line-width excitations that populate this regime [1].

These newly accessible infrared excitations are largely quasi-particles such as surface plasmons and phonons. In the case of plasmons, the excitations normally occur in noble metals in the visible regime but the resonances can be pushed into the infrared by elongating the dimensions of the plasmonic nanostructures. Additionally, plasmon resonances can occur in semiconductors if the free-carrier concentration is driven to high levels via doping, for doped-semiconductor plasmons the resonances are often deep into the mid-infrared [2].

For vibrational phonon modes, the naturally low energies have prevented them from being studied in EELS effectively up until recently [3]. However, monochromation provides access to many of the phonon resonances in light materials with the spatial resolution of the electron microscope [4]. Furthermore, the microscope can couple to these phonon modes in 'aloof' mode, allowing for the vibrations to be probed without incurring beam damage on the sample, and opening up the possibility to examine highly beam-sensitive organic and liquid samples.

For both infrared plasmon resonances and phonon modes the small frequencies have mostly limited characterization attempts to macroscopic methodologies, meaning samples are studied via diffraction-limited techniques that cannot detect nanoscale variations in the infrared spectra. Through monochromated electron microscopy, nanostructures with optical or vibrational excitations in the infrared spectral regime can be examined, directly in their native length scales.

Here we use a Nion aberration-corrected high energy resolution monochromated EELS-STEM (HERMES^{TM}) to analyze infrared excitations. The monochromator improves the spectral resolution of the EELS from ~270 meV to ~20 meV, and more importantly reduces the background level throughout the mid-infrared (50-500) meV by nearly three orders of magnitude as shown in Figure 1 [1]. We utilize the combined spatial and spectral resolution of the microscope to analyze and map the localization of infrared excitations directly at the nanoscale [5].

References:
[1] JA Hachtel *et al*, *Sci. Rep.* **8** (2018), 5637
[2] A Agrawal *et al*, *Nano Lett.* **17** (2017), p. 2611
[3] C Dwyer *et al, Phys. Rev. Lett.* **117** (2016), p. 256101
[4] OL Krivanek *et al, Nature* **514** (2014), p. 13870
[5] Research supported by ORNL's Center for Nanophase Materials Sciences, which is a U.S. Department of Energy Office of Science User Facility and by ORNL's Laboratory Directed Research and Development Program, managed by UT-Battelle, LLC, for the U.S. Department of Energy.

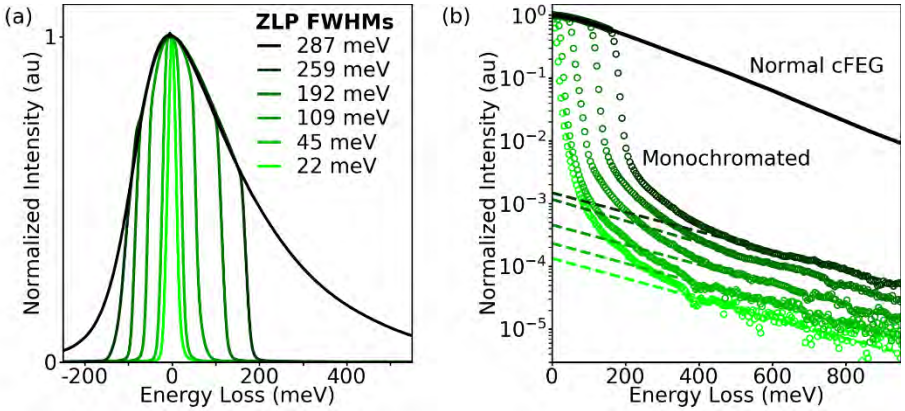

Figure 1. (a) Demonstration of energy spread in the zero-loss peak (ZLP) at different levels of monochromation. (b) Background reduction in the infrared as a function of monochromation.

The Possibility of an Integrated Electron Microscopy Toolset for Studying Superimposed Extreme Environments

Khalid Hattar[1], Samuel A. Briggs[1,2], and Katherine Jungjohann[1]

[1.] Center for Integrated Nanotechnologies, Sandia National Laboratories, Albuquerque, NM, USA
[2.] School of Nuclear Science and Engineering, Oregon State University, Corvallis, OR, USA

To fully grasp the response of materials to real world conditions, a fundamental understanding of the active mechanisms operating at the nanometer scale is needed. In-situ transmission electron microscopy (TEM) has been shown to be a valuable tool for elucidating these mechanisms in a broad variety of materials systems. Despite the success of this technique for exploring systems from batteries to structural metals, it has struggled in studying overlapping complex environments or providing complimentary micrographs and spectral maps during a single experiment. The increased automation associated with data collection for advanced electron microscopy techniques and subsequent ease of use has granted the ability to combine increasingly complex techniques in a single experiment. Although the concept of producing an integrated toolbox for exploring materials in the extreme is not new [1], the advent of improved processing and control systems has greatly advanced the discussion on the limits to which complex TEM techniques may be integrated [2].

This presentation will highlight some of the efforts underway at Sandia National Laboratories to perform in-situ electron microscopy studies utilizing overlapping environmental stressors. This will start with a description of the newly commissioned in-situ ion irradiation scanning electron microscope (I^3SEM), shown in Figure 1A. This facility combines a JEOL JSM-IT300HR/LV high-resolution SEM with low vacuum capabilities and the largest specimen chamber available with three mechanical testing and heating stages. The I^3SEM has been coupled to a 6 MV Tandem accelerator and will soon be connected to a 1.2 kV high-current ion source, to provide a variety of combined radiation plus straining environments. In a similar fashion, we have coupled a JEOL 200 kV LaB_6/Ta TEM to the same 6 MV Tandem and a 10 kV Colutron, which have been outfitted with a large range of in-situ and tomography stages, to create the in-situ ion irradiation transmission electron microscope (I^3TEM) [3]. This includes the recent addition of dynamic TEM (DTEM) capability for imaging with nanosecond time resolution during these extreme in-situ TEM experiments. Finally, this presentation will conclude with a discussion of what might be possible by coupling imaging techniques beyond the limits of current electron microscopy systems, by redesigning the electron optics and sample mounting techniques [4].

References:

[1] I. M. Robertson *et al.*, "Towards an integrated materials characterization toolbox," *Journal of Materials Research,* vol. 26, no. 11, pp. 1341-1383, 2011.

[2] M. L. Taheri *et al.*, "Current status and future directions for in situ transmission electron microscopy," *Ultramicroscopy,* vol. 170, pp. 86-95, 2016.

[3] K. Hattar, D. C. Bufford, and D. L. Buller, "Concurrent in situ ion irradiation transmission electron microscope," *Nuclear Instruments and Methods in Physics Research Section B: Beam Interactions with Materials and Atoms,* vol. 338, pp. 56-65, 2014.

[4] This work was performed, in part, at the Center for Integrated Nanotechnologies, an Office of Science User Facility operated for the U.S. Department of Energy (DOE) Office of Science. Sandia National Laboratories is a multi-

mission laboratory managed and operated by National Technology and Engineering Solutions of Sandia, LLC., a wholly owned subsidiary of Honeywell International, Inc., for the U.S. DOE's National Nuclear Security Administration under contract DE-NA-0003525. This paper describes objective technical results and analysis. Any subjective views or opinions that might be expressed in the paper do not necessarily represent the views of the U.S. Department of Energy or the United States Government.

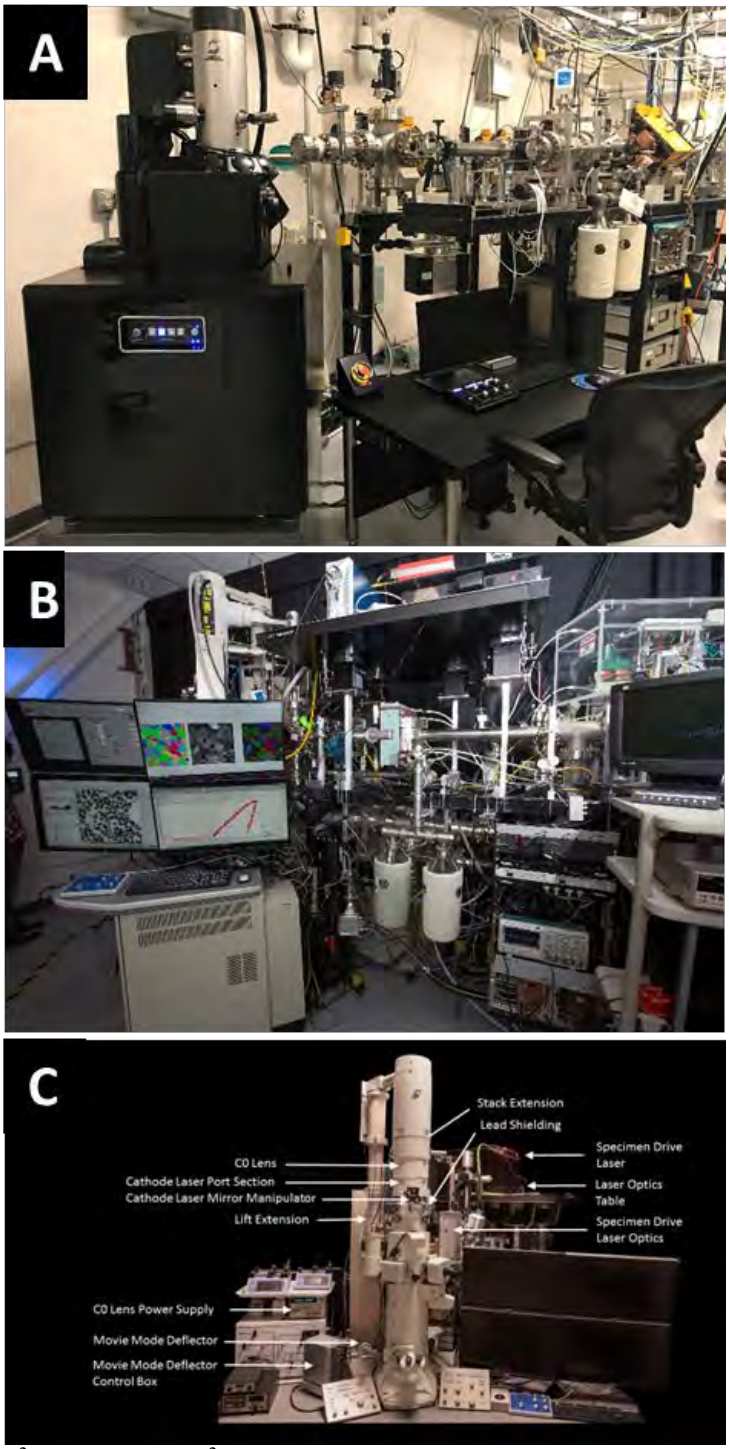

Figure 1. A) The I^{3}SEM and B) I^{3}TEM facility at Sandia National Laboratories. C) The DTEM components of the I^{3}TEM facility detailed.

Electron Microscopy for the Quantum Information Era

Juan Carlos Idrobo[1], Jordan A. Hachtel[1], Andrea Konečná[2], Jaume Gazquez[3], Tianli Feng[4], Hunter R. Sims[4], Jacob R. Jokisaari[5], Jingsong Huang[1,6], Ján Rusz[7], Nickolay V. Lavrik[1], Andrew R. Lupini[8], Miaofang Chi[1], Ilja Popovs[9], Santa Jansone-Popova[9], Jacek Jakowski[1,6], Raymond R. Unocic[1], Franklin S. Walden[10], Daniel S. Gardiner[10], Tracy C. Lovejoy[11], Niklas Dellby[11], David J. Masiello[12], Jon P. Camden[13], Robert F. Klie[5], Javier Aizpurua[3,14], Sokrates T. Pantelides[4], and Ondrej L. Krivanek[11]

[1.] Center for Nanophase Materials Sciences, Oak Ridge National Laboratory, Oak Ridge, TN 37831, USA
[2.] Materials Physics Center, CSIC-UPV/EHU, 20018 Donostia-San Sebastián, Spain
[3.] Institut de Ciència de Materials de Barcelona, Campus de la UAB, 08193 Bellaterra, Spain
[4.] Department of Physics and Astronomy and Department of Electrical Engineering and Computer Science, Vanderbilt University, Nashville, TN 37235, USA
[5.] Department of Physics, University of Illinois at Chicago, Chicago, IL 60607, USA
[6.] Computational Sciences and Engineering Division, Oak Ridge National Laboratory, Oak Ridge, TN 37831, USA
[7.] Department of Physics and Astronomy, Uppsala University, Box 516, S-751 20 Uppsala, Sweden
[8.] Materials Science and Technology Division, Oak Ridge National Laboratory, Oak Ridge, TN 37831, USA
[9.] Chemical Science Division, Oak Ridge National Laboratory, Oak Ridge, TN 37831, USA
[10.] Protochips Company, 3800 Gateway Centre Blvd, Suite 306, Morrisville, NC 27560, USA
[11.] Nion Company, 11511 NE 118th St, Kirkland, WA 98034, USA
[12.] Department of Physics, University of Washington, Seattle, Washington 98195, USA
[13.] Department of Chemistry and Biochemistry, University of Notre Dame, Notre Dame, Indiana 46556, USA
[14.] Donostia International Physics Center DIPC, 20018 Donostia-San Sebastián, Spain

Scanning and transmission electron microscopes (S/TEM) are now ubiquitous in materials and biological sciences laboratories. For decades these instruments have helped us to revolutionize our understanding of how materials and biological samples behave at the nanometer and atomic levels. However, it is only during the last twenty years, that S/TEM have had a truly a radical impact on materials and biological sciences with the successful development of aberration correctors [1,2], detectors with film-equivalent dynamical range [3], and more recently, with monochromators capable of achieving sub-10 meV energy resolution spectroscopy [4].

Here, I will present several examples demonstrating how we have exploited these capabilities and solved the pertinent experimental challenges to probe materials behavior at the nanometer and atomic scales. Specifically, I will show how by utilizing the phase of the electron probe one can reveal the magnetic order [5] and orbital polarization [6] of complex-oxide materials at the atomic level. Similarly, I will explain how using the new generation of monochromators combined with aberration correctors we can now reveal: (i) Fano resonances arising from the coherent interference between the phases of electromagnetic waves of small interacting gold nanostructures [7]; (ii) the anharmonicity and temperature of boron nitride nanoflakes using the principle of detailed balance, and electron energy gain and loss spectroscopy [8]; (iii) liquid

water vibrating slower when encapsulated inside nanovolumes [9]; (iv) isotopic labeling in water and in amino acids [9,10]. I will also show how one can detect the electric field of individual atomic columns of heavy and light elements, at the sub-Angstrom scale, by using an ultra-low noise SCMOS detector in the diffraction plane [11]. Finally, I will present a perspective reviewing the technical challenges already resolved, and on challenges electron microscopy will need to resolve as it enters the forthcoming quantum information era [12].

References:

[1] J. Zach and M. Haider, Optik **99** (1995), p. 112.
[2] O. L. Krivanek, *et al*, Institute of Physics Conference Series **153** (1997), p. 35.
[3] A. R. Faruqi, R. Henderson, Curr. Opin. Struc. Biol**. 17** (2007), p. 549.
[4] O. L. Krivanek, *et al*, Phil. Trans. R. Soc. A **367** (2009), p. 3683.
[5] J. C. Idrobo, *et al*, Adv. Struc. Chem. Img. **2** (2016), p. 5.
[6] J. Gazquez, *et al*, unpublished (2018).
[7] J. C. Idrobo, J. P. Camden, D. J. Masiello, *et al* unpublished (2018).
[8] J. C. Idrobo, *et al*, Phys. Rev. Lett. **120** (2016), p. 095901.
[9] J. R. Jokisaari, *et al*, Adv. Mater. *In press* (2018), DOI:10.1002/adma.201802702
[10] J. A. Hachtel, *et al*, unpublished (2018).
[11] J. A. Hachtel, *et al*, Adv. Struc. Chem. Img. *In press* (2018).
[12] This research was supported by the Center for Nanophase Materials Sciences, which is a Department of Energy Office of Science User Facility (J.C.I. J.A.H., J.H., N.V.L., M.C., J.J., R.R.U.), and by the Materials Sciences and Engineering Division Office of Basic Energy Sciences, U.S. Department of Energy (A.R.L., I.P., S.J.P.). This research used resources of the National Energy Research Scientific Computing Center, which is supported by the Office of Science of the U.S. Department of Energy under Contract No. DE-AC02-05CH11231, and instrumentation within ORNL's Materials Characterization Core provided by UT-Battelle, LLC under Contract No. DE-AC05-00OR22725 with the U.S. Department of Energy. This work used the Extreme Science and Engineering Discovery Environment (XSEDE). Theoretical work at Vanderbilt University was supported by DOE Award No. DE-FG02-09ER46554 and by the McMinn Endowment (T.L.F., H.R.S. and S.T.P.). Research of A.K. and J.A. was supported by the Spanish Ministry of Economy, Industry and Competitiveness (national projects MAT2015-65525-R, FIS2016-80174-P, and project MDM-2016-0618 of the Maria de Maetzu Units of Excellence Programme). This work was also supported by the University of Washington, the University of Notre Dame, the U.S. Department of Energy Basic Energy Sciences under Award Number DE-SC0018040 (D.J.M., J.P.C.), and the U.S. National Science Foundation under Grant Number DMR-1708189 (D.J.M., J.P.C.). This work was also facilitated though the use of advanced computational, storage, and networking infrastructure provided by the Hyak supercomputer system at the University of Washington.

Recent Developments and Current State of the STEM; A JEOL Perspective

Thomas C. Isabell[1], Patrick J. Phillips[1], Hidetaka Sawada[2] and Eiji Okunishi[2]
[1.] JEOL USA, Inc., 11 Dearborn Rd., Peabody, MA 01960
[2.] JEOL Ltd., 3-1-2 Musashino, Akishima, Tokyo 196-8558, Japan

Electron microscopy continues to play a vital role in materials science research. Specifically, given its ability to routinely yield directly-interpretable images, electron energy loss (EEL) and fine structure, and energy-dispersive X-ray spectroscopy (EDX) maps at the atomic scale, aberration-corrected (Cs) scanning transmission electron microscopy (STEM) is often the chosen method for advanced microscopy and analysis. The present contribution will focus on the current role and future direction of Cs-corrected STEM.

Over the last decade, JEOL Cs-corrected instruments have been at the forefront of worldwide research efforts in advanced microscopy. Elements such as a cold field emission gun (CFEG), higher-order aberration correctors, and large-area EDX silicon drift detectors (SDD) play a critical role across the JEOL platform. As JEOL recognizes a number of recent trends and desired outputs from within the microscopy community, significant discussion will center on improved and newly developed technology to address these factors.

For example, owed to its narrow energy spread, the CFEG enables fine structure and oxidation state analysis via EELS without sacrificing probe current. Its reduced ΔE mitigates the deleterious effects of chromatic aberrations, retaining spatial resolution at low accelerating voltages; *i.e.*, a regime where these effects are otherwise more pronounced. It is thus this combination of a CFEG with a higher-order aberration corrector that allows for the simultaneous acquisition of STEM images, EDX, and EELS/fine structure at atomic resolution, down to 30 kV.

Similarly, the replacement of SiLi detectors with SDDs has paved the way for routinely attaining atomic-resolution EDX maps in the STEM. Beyond this, in a sufficiently large pole piece gap, it is now possible to outfit two large-area SDDs, each with 158 mm^2 active area, yielding a solid angle of well over two steradians [1]. Corresponding data is shown in Figure 1. The 4DCanvas, a pixelated STEM detector from JEOL, marks the latest in hardware development [2]. This high frame rate, direct electron detector is ideal for applications such as magnetic domain imaging, ptychographic reconstruction, and differential phase contrast STEM; additional applications data will be presented.

The Monochromated ARM200F is the most recent Cs-corrected offering from JEOL [3]. Termed a “Spot-IN and Spot-OUT system”, this monochromator consists of a double Wien filter, resulting in a round, achromatic probe at the specimen plane. While detailed specifications and test data will be presented, an example EEL zero loss peak (ZLP) of FWHM 14 meV is shown in Figure 2. Briefly, the prospect of atomic-resolution Lorentz imaging will be addressed, as a newly-developed objective lens – nearly free of magnetic field at the specimen – has shown promising strides toward this end [4].

Looking forward, there exist many potential challenges associated with the design/manufacturing

of an "ideal" instrument and addressing the entire wish list of the modern day microscopist. Notably, however, much of the above is already targeting the needs of next-generation Cs-corrected STEM.
References:

[1] I Ohnishi *et al.*, Microsc. Microanal. **22** (2016), p. 318.
[2] R Sagawa, JEOL News **52** (2017), p. 53.
[3] www.jeol.co.jp/en
[4] Y Kohno *et al.*, Microsc. Microanal. **23** (2017), p. 456.

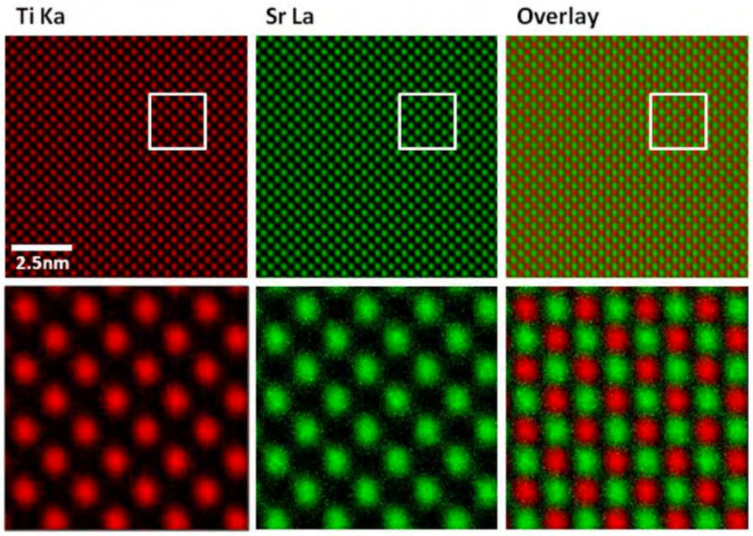

Figure 1. High resolution (1k x 1k pixels) EDX maps of $SrTiO_3$ acquired at 80 kV with 32 pA probe current; Wiener filter applied [1].

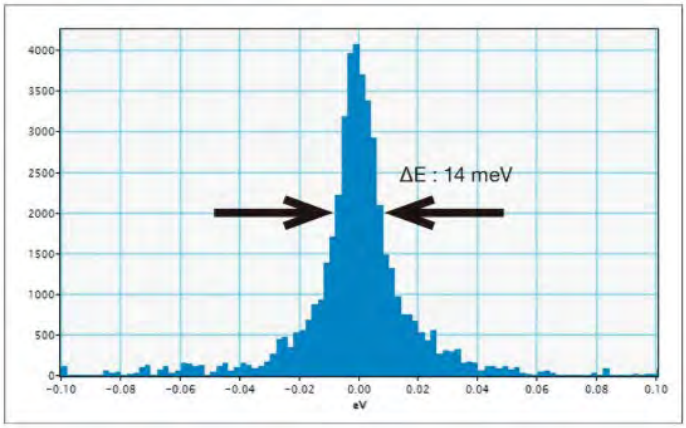

Figure 2. Zero-loss spectrum acquired at 30 kV with the Monochromated ARM200F [3].

Frame-series Imaging and Spectroscopy as a Flexible Experiment-design Dimension

Lewys Jones[1,2] , Annick DeBacker[3], Sandra VanAert[3]
[1.] Advanced Microscopy Laboratory, Centre for Research on Adaptive Nanostructures and Nanodevices (CRANN), Dublin, Ireland
[2.] School of Physics, Trinity College Dublin, Dublin Ireland
[3] EMAT, University of Antwerp, Belgium

While perhaps a seemingly obvious statement, the scanning transmission electron microscope (STEM) is a *scanned* probe instrument. Thus, any data obtained will always be a function of the size, shape, and intensity of the probe, as well as of the uniformity, reliability, and reproducibility of the scan-positioning. Lastly, the collection efficiency of spectrometers, as well as the behavior of imaging detectors with respect to time (not space like in conventional HRTEM) becomes important.

In this presentation, we will discuss these three key factors, highlighting how electron-dose, scan-distortion, and detector-afterglow artefacts affect STEM data respectively.

For robust specimens, it is rational to argue that larger beam-currents (resulting in larger electron doses) will yield data with a greater signal-to-noise ratio (SNR) and more usable detail. However, if we consider samples which damage under the electron beam, then clearly 'more beam is better' thinking will only extend so far. Instead, we should consider an analytical expression for the cumulative 'image imprecision' as a function of electron dose and minimize this function. This can be constructed by considering the uncertainty in quantitative measurements (such as atom-counts or spatial precision) as calculated from data spanning a range od dose-regimes (Figure 1).

The sensitivity of the STEM, which underpins its immense utility, is also a potential source of downfall. Any instabilities in the lab environment with respect to time, can become coupled into our data, appearing as scanning-distortions with respect to position [1,2]. However, there is a solution which is to fractionate the conventional image-scan into a series of faster individual frames. These collectively then contain (for no additional dose budget) additional redundant observations of the sample from which scan-distortion can be diagnosed and compensated.

What this does introduce then is a new dimension in experiment planning. Previously the operator had a one-dimensional tradeoff between SNR and sample-damage. Now we have separately control over beam-current and instantaneous pixel-charge, as well as over scan frame-rate, dose-per-frame, and separately the total series-dose. We now must evaluate many new factors; what is the optimum number of frames to record, is there some lower limit to useable beam current, and some upper limit to the reliable scan-speed (afterglow streaking) [3]. Fortunately these questions bear fruit which allows for improved experiment design and data capture for both image and spectra [4].

A reliable post-processing data alignment framework unlocks the possibility to wok at ultra-low-dose beam conditions by summing across very many frames. In these conditions it has been observed that annular dark-field (ADF) detectors are sensitive to single-electron signals [5].

Previous attempts to develop ultra-fast scanned ADF capture methods have been limited by afterglow and dynamic range limitations [3,6]. We will present some new results using pulse counting approaches on custom nanosecond-scale data-capture which solve these issues (Figure 2).

References:
[1] L. Jones, H. Yang, T. J. Pennycook, M. S. J. Marshall, S. Van Aert, N. D. Browning, M. R. Castell, and P. D. Nellist, Adv. Struct. Chem. Imaging **1**, 8 (2015).
[2] L. Jones, S. Wenner, M. Nord, P. H. Ninive, O. M. Løvvik, R. Holmestad, and P. D. Nellist, Ultramicroscopy **179**, 57 (2017).
[3] J. P. Buban, Q. Ramasse, B. Gipson, N. D. Browning, and H. Stahlberg, J. Electron Microsc. (Tokyo). **59**, 103 (2010).
[4] L. Jones, A. Varambhia, R. Beanland, D. Kepaptsoglou, I. Griffiths, A. Ishizuka, F. Azough, R. Freer, K. Ishizuka, D. Cherns, Q. M. Q. M. Ramasse, S. Lozano-Perez, and P. D. P. D. Nellist, Microscopy **67**, 98 (2018).
[5] R. Ishikawa, A. R. Lupini, S. D. Findlay, and S. J. Pennycook, Microsc. Microanal. **20**, 99 (2014).
[6] A. Mittelberger, C. Kramberger, and J. C. Meyer, Ultramicroscopy **188**, 1 (2018).
[7] The authors acknowledge funding from CRANN-AML and the SURE undergraduate programme.

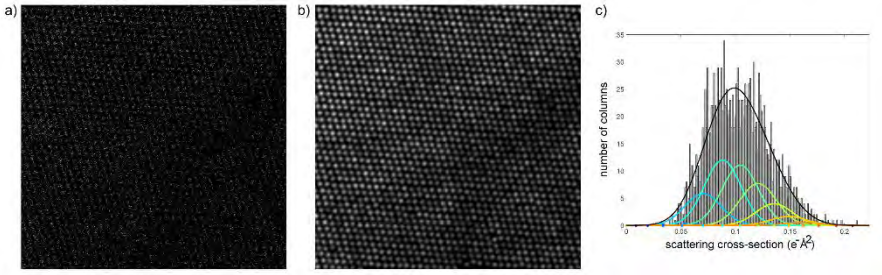

Figure 1. (a) Low-dose ADF image of a Pt wedge (770 e-Å^{-2}). (b) Refined parametric model using statistical parameter estimation theory. (c) Histogram of scattering cross-sections of all Pt columns.

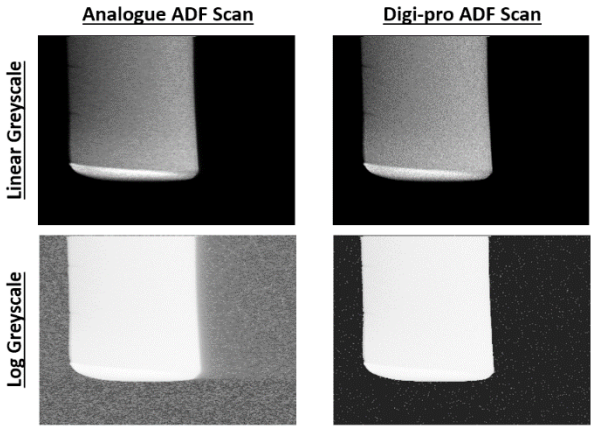

Figure 2. Proof of concept examples of conventional and proposed all-digital ADF readout methods.

The Lab on a Beam: Big Data and Artificial Intelligence in Scanning Transmission Electron Microscopy

Sergei V. Kalinin[1], Stephen Jesse[1], Chris T. Nelson[1], Maxim Ziatdinov[1], Rama K. Vasudevan[1], Ondrej Dyck[1], and Andrew R. Lupini[1]
[1.] Oak Ridge National Laboratory, Oak Ridge, TN 37831

Atomically-resolved imaging of materials has become the mainstay of modern materials science, as enabled by advent of aberration corrected scanning transmission electron microscopy (STEM). However, the wealth of quantitative information contained in the fine details of atomic structure, energy loss spectra, or CBED patterns, remains largely unexplored. In this talk, I will present the new opportunities enabled by physics-informed big data and machine learning to extract physical information from static and dynamic STEM images, ranging from statistical thermodynamics of alloys to kinetics of solid-state reactions on a single defect level, and extending this approach towards applications for e-beam based atom-by-atom assembly.

Generally, STEM data provides access to the structure of material, where the individual atomic positions become accessible with picometer-level precision. However, the natural question is what quantitative physical information can be extracted from this data, beyond phase or ferroic order parameter identification? One answer is based on mesoscopic model matching, where the material properties are described by the corresponding Ginzburg-Landau (GL) free energy. The corresponding analytical solutions for well-defined defects including domain boundaries, surfaces, or interfaces can then be fitted to STEM data, providing information on (poorly known) gradient terms and boundary conditions. This approach allowed us to systematically explore the shape of the ferroelectric vortices in multilayers and to develop a theory matching algorithm that allowed direct matching to phase field theory and extraction of the coefficients of the flexoelectric tensor. This approach is universally applicable for analysis of the mesoscopic physics of ferroic systems if the form of the corresponding GL expansion is known, or postulated, and sufficiently rich topological or structural defect populations are observed.

For discrete systems, we propose that by studying the characteristic structural and chemical fluctuations that exist within a single chemical composition, we can infer the relevant interactions and produce a generative model that can predict properties over a range of scales in a finite region of chemical and temperature space. We use the compositional and structural fluctuations in the quenched (static) system to build a generative model encoding the effective interactions in the system. Using the principles of statistical inference, we develop a framework for incorporating structural fluctuations into statistical mechanical models and use that to derive effective inter-atomic interactions driving segregation in a $La_{5/8}Ca_{3/8}MnO_3$ sample. A variational autoencoder further allows us to detect anomalous behaviors in the composition phase diagram. This study provides a framework for creating generative models from diverse data, including compositional fluctuation, structural distortions corresponding to frustrated and non-frustrated interactions, and their interactions.

Finally, we extend this machine learning approach to the mapping of solid state reaction mechanisms. The functionalities of solids are underpinned by the point defect, their clusters, and extended defects, linked through the networks of solid state reactions. Here we utilize the fact

that STEM of 2D materials allows visualization of (almost) all atomic species in real space, and that the electron beam can be used to induce complex atomic transformations in these materials, to open pathway to metastable defects states and allow exploration of reaction mechanisms. We developed a deep learning approach that allows fully automated identification of individual atoms in STEM images, using theoretical or labeled images as a training set. We show that the diffusion coefficient of S vacancies and transformation of the MoW – S-Vac complex can be explored quantitatively and mapped onto a Markov model, yielding transition probabilities on single defect level. We extend this approach to construct reaction pathways for point defects in 2D materials, trace the structural evolution of atomic species during electron beam manipulation, and create a library of defect configurations in Si- and vacancy doped graphene.

Finally, the synergy of deep learning image analytics and real-time feedback further allows harnessing beam-induced atomic and bond dynamics to enable direct atom-by-atom fabrication. Examples of direct atomic motion over mesoscopic distances, engineered doping at selected lattice sites, and assembly of multiatomic structures will be demonstrated. These advances position STEM to transition from a purely imaging tool towards a full atomic-scale laboratory of electronic, phonon, and quantum phenomena in atomically-engineered structures.

[1] This research is supported by the by the U.S. Department of Energy, Basic Energy Sciences, Materials Sciences and Engineering Division and the Center for Nanophase Materials Sciences, which is sponsored at Oak Ridge National Laboratory by the Scientific User Facilities Division, BES DOE.

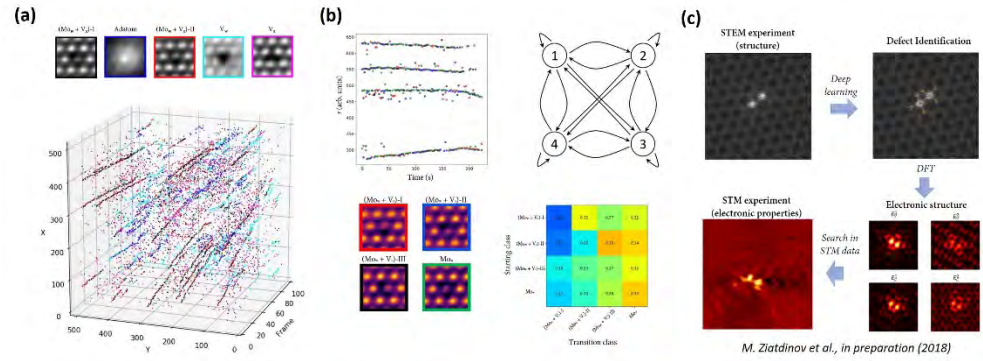

Figure 1. (a) Trajectories of single atomic defects in WS_2 material. (b) Markov analysis of transition probabilities for selected trajectories. (c) Construction of single defect libraries that allow to link together different atomically-resolved measurements.

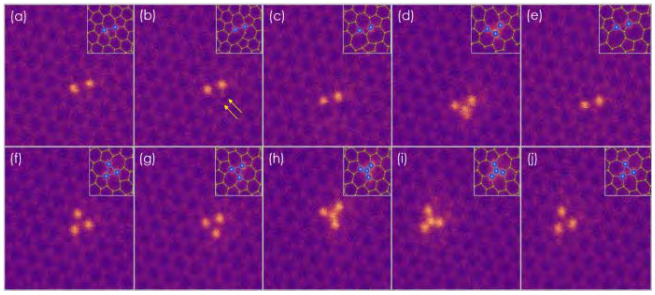

Figure 2. (a-j) Assembly of Si clusters on graphene via electron beam.

In-Situ STEM Characterization of 2-Dim Materials at High Energy and Spatial Resolution

Xuan Hu, Jacob R. Jokisaari, Liang Hong and Robert F. Klie

University of Illinois at Chicago, Department of Physics, Chicago, IL 60607

Two-dimensional materials, including graphene, BN and transition metal dichalcogenides (TMDs), exhibit great potential for a variety of applications, such as transistors, spintronics, photovoltaics, or even as window layers for in-situ microscopy holders.[1,2] When 2-dim materials are used in electronic devices, the potential for miniaturization offers remarkable improvements in electrical performance. Yet, the effects of heat dissipation can be a problem in designing electronic devices. Therefore, the thermal properties of 2-dim materials are an important subject of current research and new methods are being developed for temperature measurements at the nanometer scale.[3] In TEM in-situ liquid holders that utilized graphene as a window layer, it was demonstrated that the graphene layers interact strongly with the contained liquid, which can be beneficial in reducing electron beam induced damage.[4] However, the strong interaction between the reaction species with the graphene window layer can potentially alter the chemistry within the liquid cell and might yield effects not observed in more conventional reactor setups.

Over the last few years, we have developed a new approach that now enables us to measure the local temperature distribution and thermal expansion coefficient of 2-dim materials with nanometer resolution.[4] In addition, we have developed new, more inert window layers for liquid cells based on 2-dim materials that will enable in-situ characterization of fluids at unprecedented spatial and energy resolution. The electron-beam induced change in the pH of liquids, such as H_2O will be demonstrated using the dissolution and precipitation of calcium hydroxyapatite in a liquid cell based on 2-dim material. The experiments are carried out using the aberration-corrected, cold-field emission JEOL ARM200CF at the University of Illinois at Chicago. The benefits monochromated STEM, such as the NION HERMES, on the characterization liquids encapsulated by 2-dim materials will also be discussed.

Our nanoscale thermometry measurements are based on the principle that the plasma peak position is sensitive to the density of charge carriers, which changes as a materials expands/contracts as a function of temperature. For 2-dim materials, we have shown that the thermal expansion coefficient is also highly dependent on the number of layers, with monolayer materials exhibiting the higher expansion coefficient. We have also directly demonstrated that monolayer graphene has a negative thermal expansion coefficient, as previously suggested.[4] Figure 1 shows the thermal expansion coefficient for 2-dim MoS_2 and it can be directly seen that the spatial resolution of these measurements is close to the theoretical limit based on the delocalization of the plasmon peak signal. The spatial resolution of the HAADF images, obtained simultaneously with the low-loss EELS maps, remains close to 1 Å at elevated temperatures.

Up to now, window layers in in-situ liquid stages mostly consist of Si_3N_4, which is inert to most reactions within the liquid cell, and, more recently, graphene. While the strong interaction

between graphene and the radicals, formed as the results of electron-beam induced radiolysis, lowers the formation of hydrogen bubbles within the liquid, this interaction will also alter the chemical reactions within graphene liquid cells. Therefore, we have developed liquid cells based on 2-dim h-BN layers and will demonstrate that the sensitivity of the liquid to the electron beam is dramatically different (Figure 2). We will also discuss the possibility of using such cells for novel EELS experiments including ultra-high resolution vibrational EELS using monochromated electron sources.[5]

References:

[1] B. Standley *et al.*, Nano Lett. **8** (2008), p. 3345–3349.
[2] C. Wang *et al.*, Appl. Mat. **26** (2014), 3410-14.
[3] X. Hu *et al.*. Phys. Rev. Lett. **120(5)** (2018), 055902.
[4] C. Wang *et al.*, Adv. Mat, **28(35)** (2016), 7716.

[5] This work was in part supported *by the National Science Foundation (EFMA-1542864 (EFRI))*

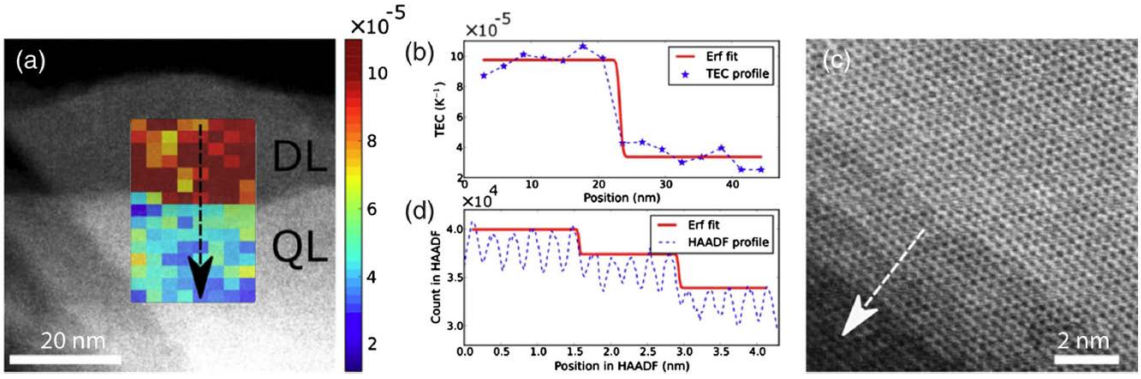

Figure 1. (a) HAADF image of $MoSe_2$ at 623 K and the spatially resolved map of the local thermal expansion coefficient at the edge a between double-layer (DL) and four-layer (QL) area. (b) Line profile of the thermal expansion coefficient of the interface indicated by the black line in (a). (c) Representative atomic-resolution HAADF image of MoS_2 taken at 573 K. (d) Line profile of image contrast across several layers of MoS_2 at 573 K.

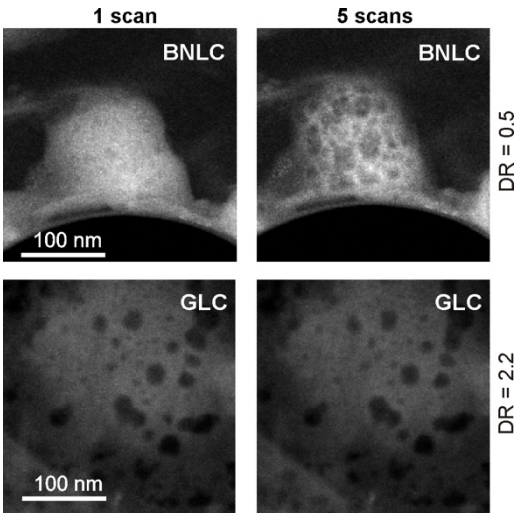

Figure 2. Comparison of the dose rate damage threshold for boron nitride liquid cells (BNLC) and graphene liquid cells (GLC). For the same electron dose-rate (flux) is the same for both liquid cells. The liquid contained in the BNLC show a higher sensitivity towards the electron beam compared to GLC.

Environmental TEM Study of Catalytic Nanoparticles in Reactive Gas Environment

L. Kovarik[1], Z. Wei[2], J. Szanyi[2], J.H. Kwak[2], C.H.F. Peden[2]
[1] Environmental Molecular Science Laboratory, Pacific Northwest National Laboratory, P.O. Box 999, Richland, Washington 99352
[2] Institute for Integrated Catalysis, Pacific Northwest National Laboratory, P.O. Box 999, Richland, Washington 99352

Supported transition metal nanoparticles are important class of materials used extensively in catalytic applications due to their high surface to volume ratio and high concentration of low coordinated atomic sites. When exposed to elevated temperatures and gas environment, a range of thermally activated processes can lead to morphological, structural and surface transformation, which have an effect on catalytic properties. Characterization of these transformations under in-situ conditions is critical for rationalization of structure-property relationship, and essential for future advancement of catalytic technologies. In the current talk, we will present atomic level in-situ TEM observations of Pd nanoparticles during exposure to elevated temperature and oxidizing environment. The *in-situ* observations were performed with environmental FEI Titan 80-300 equipped with a CEOS C_s–image corrector operated at 80kV and 300kV. In particular, the work will focus on the characterization of oxide nucleation and growth, and identifying the crystallographic features of Pd metal-oxide transformation. We will also show how coherency strains from the substrate play role in inhibiting phase transformations, and show that a distinct chemical interaction with the substrate can lead to significant changes in the initial stages of oxide formation. As a part of this presentation, we will also describe a gas control unit that enabled us to carry out switching between well-controlled mixtures of gasses, and demonstrate the use of this system to study gas-induced transformations at the atomic scale.

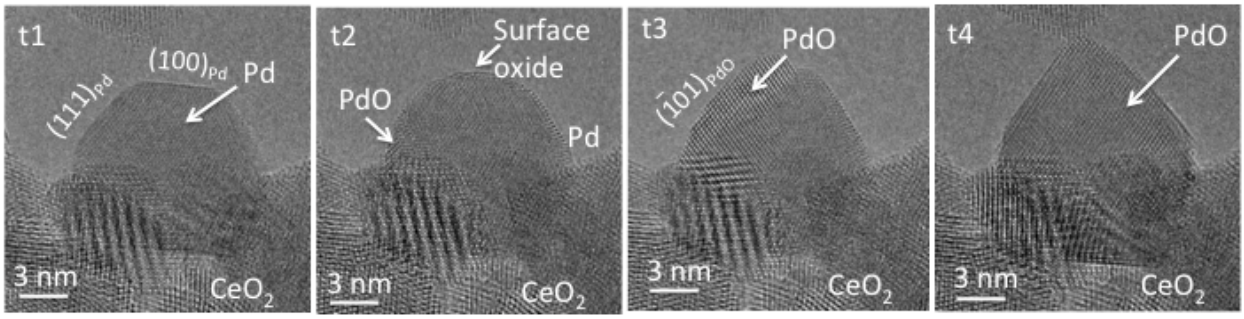

Figure: High resolution ETEM observation of Pd to PdO transformation at oxygen partial pressure of ~1 mbar and temperature of 400°C (a) Initial Pd nanoparticle supported on CeO_2. (b) Transition period corresponding to the formation of surface oxide (c) Transition period corresponding to growth PdO (d) Final stage of transformation corresponding to the formation of PdO.

References:

[1] This research was part of the Chemical Imaging Initiative at Pacific Northwest National Laboratory. The work was conducted in the William R. Wiley Environmental Molecular Sciences Laboratory (EMSL), a national scientific user facility sponsored by DOE's Office of Biological and Environmental Research and located at PNNL.

Ultra-high Energy Resolution EELS

O.L. Krivanek[1,2], A.L. Bleloch[1], G. Corbin[1], N. Dellby[1], M.V. Hoffman[1], B. Plotkin-Swing[1], and T.C. Lovejoy[1]
[1.] Nion R&D, 11511 NE 118th St, Kirkland, WA 98034, USA
[2.] Department of Physics, Arizona State University, Tempe, AZ 85287, USA

EELS in the electron microscope has progressed greatly in recent years. The best energy resolution reached prior to 2013 was 40 meV in a 30 msec exposure (full-width at half-maximum of the zero loss peak (FWHM of ZLP) at 200 kV) and the ZLP "tail" intensity was about 1/1000 of the ZLP maximum at an energy loss of 300 meV [1]. The introduction of the Nion ground-potential monochromator in 2013 improved the energy resolution to 16 meV in a 55 msec exposure (at 60 kV) [2], and allowed the exploration of vibrational (phonon) signals in the electron microscope to begin [3]. The introduction of the Nion EEL spectrometer in 2017 improved the resolution to 5.9 meV at 60 keV (in a 100 msec exposure), and 4.2 meV at 30 keV (Fig. 1), and reduced the ZLP tail to the 1/1000 level at 40 meV loss [4]. The new spectrometer achieves <1 meV r.m.s. jitter of the ZLP, and <5 meV energy drift per minute.

The key design features of our system are:

a) Putting the monochromator (MC) at ground potential, so that the monochromated energy is determined by the prism current and does not depend on the high tension (HT).
b) Eliminating instability effects due to small variations in the prism current, by connecting the three MC prisms plus the spectrometer prism in series.
c) Improving the stability of the HT by sensing the beam intensity falling on each half of the MC's energy-selecting slit, and using the difference signal for HT stabilization.
d) Optimizing the MC, corrector, and EELS multipole design for the best possible energy stability.
e) Using quadruple mu-metal shielding around the monochromator and triple shielding around the EELS so as to minimize the effect of stray magnetic fields.
f) Strengthening the EELS with robust anti-vibration bracing, to improve the system energy stability.
j) Optimizing spectrum detection by using an ultra-low noise SCMOS camera that gives a wide dynamic range as well as DQE>0.5 when detecting single electrons, with further improvements planned for the future through the use of direct electron detection.

Great attention has also been paid to aberration correction in the entire optical system. As shown by Fig. 2, small crossovers containing images of the electron source occur in many planes in the microscope, including the MC slit, the sample, and the EELS detector. At each of these places, higher performance (better energy or spatial resolution) becomes possible by minimizing the size of the crossover image. This is achieved by thorough aberration correction: up to 3rd order in the monochromator, and up to 5th order in the probe corrector and the spectrometer. The correction improves the energy resolution and the collection efficiency of the EELS, and it has an important side benefit: improved STEM spatial resolution when moderate monochromation is used to improve the C_c res. limit, to 1.07 Å at 30 keV.

Examples of recent applications include momentum-resolved vibrational spectroscopy that provides similar information to neutron scattering and inelastic X-ray spectroscopy, but from much smaller volumes [5], measuring the temperature of small sample areas by energy gain/energy loss spectroscopy [6,7], and damage-free vibrational spectroscopy of ice (Fig. 3) and liquid water, combined with the ability to detect isotopic substitution [8]. These and other examples will be presented in the talk.

References:
[1] E Essers et al., Ultramicroscopy 110 (2010) 971–980.
[2] OL Krivanek et al., Microscopy 62 (2013) 3–21.
[3] OL Krivanek et al., Nature 514 (2014) 209-213.
[4] https://www.stem.lps.u-psud.fr/chromatem-delivers-site-sub-5-mev-30-kev
[5] FS Hage et al., Science Advances (2018) 7495 (DOI: 10.1126/sciadv.aar7495).
[6] J-C Idrobo et al., Phys. Rev. Lett. 120 (2018) 095901.
[7] M Lagos and PE Batson, Nano Lett., 18 (2018) 4556–4563.
[8] JR Jokisaari et al., Adv. Mater. (2018) 1802702.

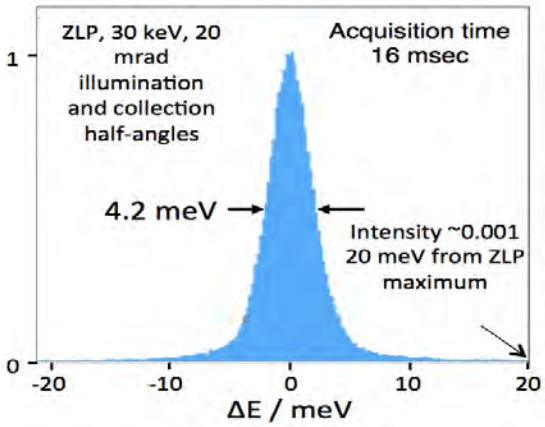

Figure 1. Zero loss peak (ZLP) obtained at 30 keV.

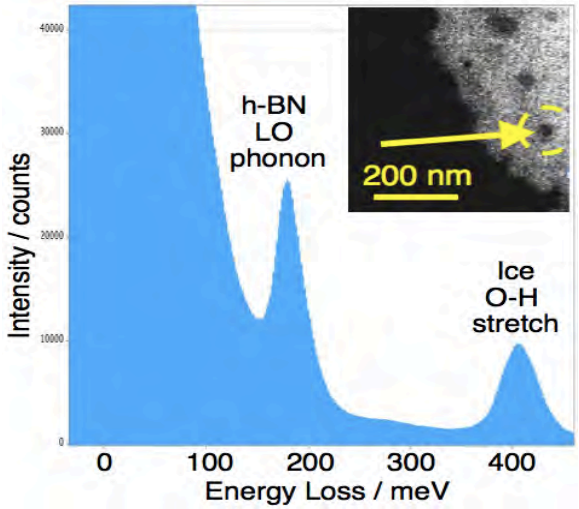

Figure 3. Vibrational spectrum of ice adsorbed onto an h-BN flake. Insert shows the h-BN flake, coated with about 30 nm of ice, with a hole made by the beam (arrowed). The probed area is indicated by the dashed yellow circle.

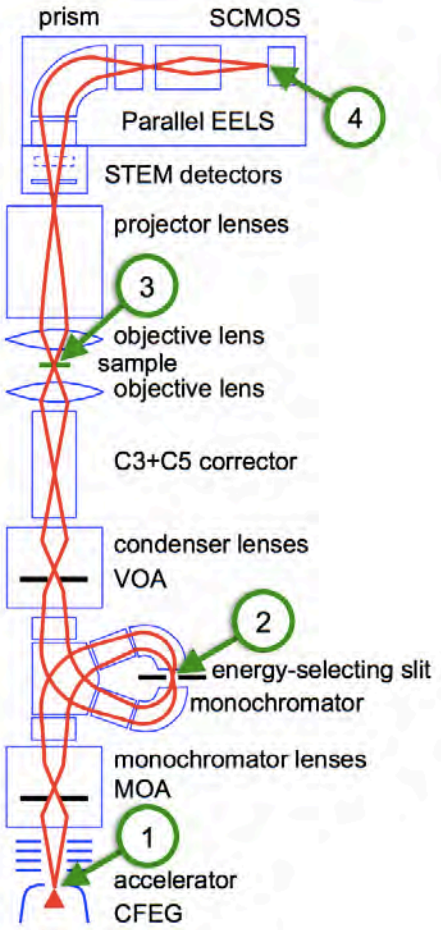

Figure 2. Schematic diagram of the electron trajectories through the Nion Ultra-High Energy Resolution Monochromated EELS-STEM (U-HERMES). Beam crossovers containing images of the electron source include:
1 = CFEG virtual crossover
2 = monochromator slit crossover
3 = sample-level crossover
4 = EEL spectrum crossover

Accelerating the Pace of Discovery with In Situ 4D STEM

James M. LeBeau
[1.] Department of Materials Science & Engineering, North Carolina State University, Raleigh NC USA.

With the introduction of 4D STEM detectors, such as the Cornell EMPAD [1], new methods to directly connect structure and properties have been made possible. For example, quantitative measurement of electric/magnetic fields, high S/N ratio imaging of light elements, and phase retrieval are on their way to becoming routine with STEM. While the speeds to capture 4D STEM data (~1 ms/probe position) is still slower than conventional imaging (~1 μs/probe position), in situ experiments significantly benefit from this 4D data. Beyond acquisition, the size of this data also presents challenges in terms of rapid analysis.

In this talk, I will present our recent in situ 4D STEM studies using an electric field applied to the relaxor ferroelectric PMN-PT. The unique dielectric properties of these materials are thought to be due to nanoscale polar regions that can be difficult to probe due to their size and overlap in projection [2]. While in-situ microscopy offers the ideal approach to study the response of such polar materials to external electric fields, efforts in this direction are often plagued by challenges of sample preparation with FIB. As a first step, I will discuss our approach that overcomes these limitations by combining microfabrication techniques with conventional TEM sample preparation (Figure 1). The most important consequence of this scheme is the high degree of uniformity of the resulting electric field distribution between wired electrodes and allows us to extract representative device characteristics, i.e. polarization-voltage curves as also shown in Figure 1. As a demonstration of the approach, I will show how 4D STEM analysis of field-induced changes to the atomic structure and domain orientation provide rapid insights into the behavior of relaxor ferroelectric materials as the applied field is varied.

From our experience with in situ 4D STEM studies, I will also discuss how fast analysis tools can help accelerate discovery, particularly when real-time, quantitative feedback is provided at the microscope. As a somewhat simple, yet non-trivial example, I will highlight real-time feedback of sample thickness and tilt with PACBED. Conventionally, such patterns are usually matched with least squares fitting after acquisition or by an experienced operator at the microscope. Either approach is slow (and potentially inaccurate), since only slight contrast feature changes are used be distinguish patterns that are within a few nm. To this end, I will discuss how we use convolutional neural networks (CNN) to automatically extract local sample features from 4D STEM datasets in real-time, examples results of which are shown in Figure 2 [3]. With a trained network (an automatic process), the CNN approach is very fast with average quantification of tilt and thickness achieved within 0.025 s per pattern (> 40 fps), vastly outperforming least squares [4].

References:

[1] MW Tate, et al., Microscopy and Microanalysis **22** (2016) p.237
[2] MJ Cabral, et al., Applied Physics Letters **112** (2018) p.082901
[3] W Xu and JM LeBeau, Ultramicroscopy **188** (2018) p.59

[4] The authors acknowledge the support from the National Science Foundation (NSF) (DMR-1350273, IIP-1361571, IIP-1361503) and Air Force Office of Scientific Research (FA9550-14-1-0182). We thank analytical Instrumentation Facility (AIF) at North Carolina State University supported by the State of North Carolina, the National Science Foundation (ECCS-1542015) and the North Carolina Research Triangle Nanotechnology Network from the National Nanotechnology Coordinated Infrastructure.

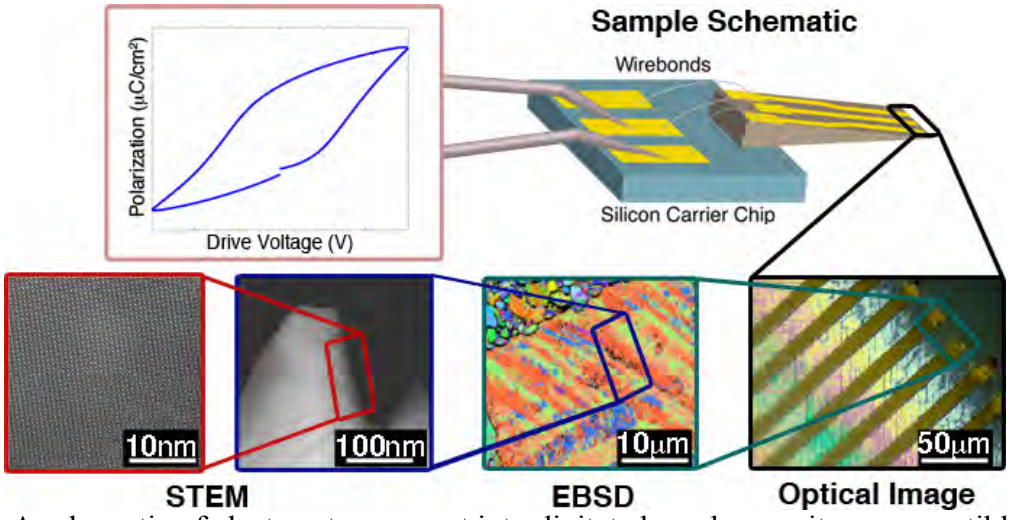

Figure 1. A schematic of electron-transparent interdigitated comb capacitors, compatible with various complementary imaging methods such as polarized optical microscopy, electron backscatter diffraction, and even atomic resolution scanning transmission electron microscopy, including 4D STEM.

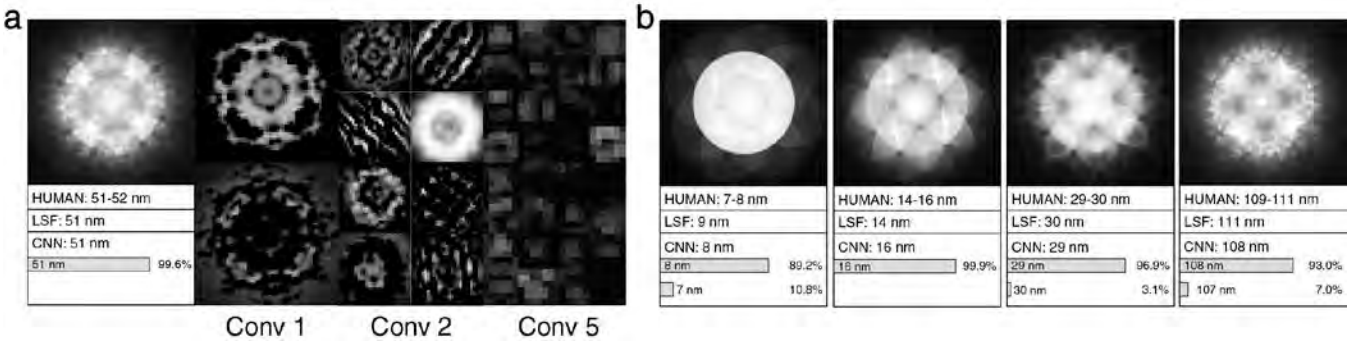

Figure 2. Example of experimental PACBEDs and their thickness identification by the operator, least square fitting (LSF) and the convolutional neural network (CNN). Selected network activations in the first, second and fifth convolutional layers after ReLU are illustrated in (a).

Mechanistic Understanding of the Growth Kinetics and Dynamics of Nanoparticle Superlattices by Coupling Inter-particle Forces from Real-time Measurements

Jaewon Lee[1], Elias Nakouzi[1], Miao Song[1], Jaehun Chun[1], and Dongsheng Li[1]
[1.] Physical and Computational Sciences Directorate, Pacific Northwest National Laboratory, Richland, WA 99352

Superlattice structures formed by nanoparticle (NP) self-assembly have attracted increasing attention due to their potential as a novel class of nanomaterials with enhanced physicochemical properties tailored by the assembly structure.[1] However, many key questions remain regarding the correlation between the dynamics of individual NPs and the emerging superlattice patterns. Here we investigated the self-assembly of gold NPs by employing in situ transmission electron microscopy equipped with direct detection camera capabilities, which enabled us to track the rapid motion of individual nanoparticles in real time.[2]

To gain insights into the self-assembly process, we conducted in situ liquid cell TEM (LCTEM) experiments and monitored the monodispersed gold NPs (average diameter of ~4 nm, average inter-particle separation of 1.6 ± 0.6 nm) dynamics in real time. Initially, individual gold NPs were dispersed randomly across the viewing area (red circles, Fig. 1a) with a few clusters of dimers and trimers (white circle, Fig. 1a). The particles moved in random directions as represented by particle i and ii (white arrows, Fig. 1a and 1d). (Fig. 1d). As the experiment progressed, the gold NPs gradually aggregated into clusters (Fig. 1b). Eventually, the gold NPs self-assembled into a relatively ordered hexagonal superlattice structure after ~650 s (Fig. 1c, and 1e).

To understand kinetic details of the process, the self-assembly of gold NPs can be further analyzed by calculating the contributions of Brownian (F_{Br}), van der Waals (F_{vdW}), Hydrodynamic drag (F_D) and steric hindrance forces (F_{Sh}).[3-4] During the initial ~200 s, the average magnitude of F_{vdW} was ~ 10^{-15} N (Fig. 2a), i.e. 2-5 orders of magnitude smaller than the theoretical F_{Br} (Fig. 2b). As the average h decreased, the average F_{vdW} steadily increased to ~10^{-13} N; which is comparable to the lower end of the F_{Br} distribution at ~470 s (Fig. 2a). Accordingly, F_{Br} was the dominant force in the early stages of the assembly process before ~470 s. After ~470 s, F_{vdW} measured ~10^{-11} N which was comparable to the magnitude of F_{Br} (Fig. 2a). At this point, F_{vdW} overrode F_{Br} statistically. For example, F_{vdW} on individual particle 5-8 (Fig. 2c) had comparable magnitude with F_{Br}. Similarly, F_{vdW} on particle 10-12 at 780 s (Fig. 2d) exceeded the magnitude of F_{Br} and the net force was directed towards the center of the cluster. For a given particle pair, the repulsive F_{sh} increases with decreasing h and balances with attractive F_{vdW} at an equilibrium separation, here measured as h_{eq}, = 2.8 nm, where $F_{vdW} = F_{Sh} \sim 3.00\times10^{-12}$ N. This prediction is validated by our experimental observations; the particles assembled into a superlattice with an average h of 2~3 nm after ~700 s. The cluster after assembling has an interesting dynamic nature due to the competition between F_{vdW} and F_{sh} along with the random F_{Br} on the particles.

We obtained a quantitative evaluation of the competitive interactions that drive the assembly process. Such competition between forces over various separations is critical for the kinetics of

cluster growth, as well as the superlattice formation. In the close proximity, a delicate balance between van der Waals and steric hindrance forces surprisingly led to a unique dynamic nature of the assembled superlattice. Our study provides a fundamental understanding of coupling energetics and dynamics of NPs involved in the assembly process, enabling the control and design of the structure of nanoparticle superlattices.

References

[1] M Boles, M Engel, and D. V. Talapin. Chemical reviews 116, (2016), p11220-11289.
[2] J. M. Yuk, J. Park, P.Ercius, K. Kim, D. J. Hellebusch, M. F. Crommie, J. Y. Lee, A. Zettl,; A. P. Alivisatos, , Science 336, (2012), p61-64.
[3] W.B. Russel, W B. Russel, D. A Saville and W. R. Schowalter, in "Colloidal dispersions", ed G.K. Batchelor (Cambridge university press, New York)
[4] J. N. Israelachvili, in "Intermolecular and surface forces", ed Academic press, (Elsevier, Santa Barbara)

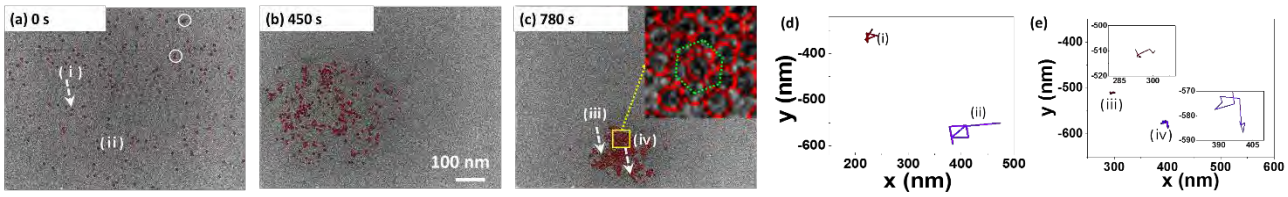

Figure 1 (a-c) Snapshots of LCTEM movie of the Gold NP self-assembly, insets of c is zoomed in images showing hexagonal pattern; (d-e) particle (i-iv in Fig. a, and c) movement tracks within 1 s and time interval is 0.1 s;

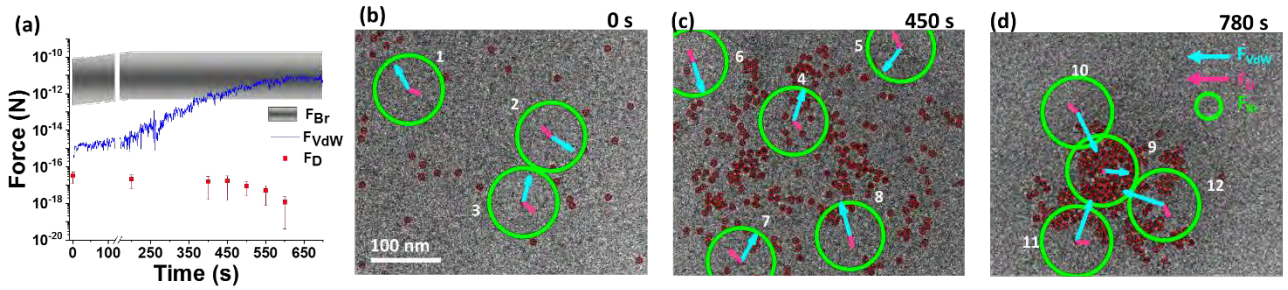

Figure 2 F_{Br}, F_D and F_{vdW} analysis during gold NPs self-assembly process. (a) theoretically calculated average F_{vdW}, F_D, and F_{Br}; (d-f) Snapshots of LCTEM movie of the Gold NP self-assembly showing F_{vdW} (blue arrow), F_D (red arrow), and F_{Br} (green circle) The magnitude of blue and red arrows are scaled logarithmically.

Understanding Nanorod Dissolution Mechanisms by Liquid Phase Electron Microscopy: The Case of β-FeOOH

Lili Liu,[1] Xin Zhang,[1] Elias Nakouzi,[1] Libor Kovarik,[2] Jennifer Soltis,[1] Kevin Rosso[1] and James J De Yoreo [1, 3]
Corresponding Author: James.DeYoreo@pnnl.gov

1. Physical and Computational Sciences Directorate, Pacific Northwest National Laboratory, Richland, Washington 99354, United States.
2. Environmental Molecular Sciences Laboratory Pacific Northwest National Laboratory, Richland, Washington 99354, United States.
3. Department of Materials Science and Engineering, University of Washington, Seattle, Washington 98185, United States.

Nanoparticle dissolution is a common process in synthetic procedures where primary particles are replaced by more stable phases, as well as in environmental settings where they both serve as electron sinks or sources for microbes and are responsible for release of nutrients or contaminants. Iron oxides and iron oxyhydroxides, which are widespread in technological applications and environmental settings, are a prime example. To decipher the pathways that underlie dissolution and quantify the kinetic parameters controlling rates, we investigated dissolution of β-ferric oxyhydroxide (β-FeOOH) nanorods via *in situ* liquid phase (LP)-TEM. Previous ex situ studies that investigated dissolution of iron (III) hydroxides by proton or photoreductive attack found that photoreductive dissolution of is faster than by nonreductive dissolution (e.g. proton-promoted or ligand promoted thermal dissolution). Other studies concluded that the rate-determining step during dissolution in HCl is protonation of the surface together with formation of a chloride-Fe surface complex. Generally, dissolution of β-FeOOH nanorods in strong acids occurs end-to-end along the [010] direction and has been attributed to proton penetration and destabilization of so-called "tunnel structures" by removal of Cl ions. In our work, we find dissolution of β-FeOOH nanorods occurs both end-to-end (along [010]) and side-to-side (along [100]) directions under the electron beam, even at extremely low electron dose rates. Dissolution involves two reaction steps: (i) beam radiolysis of the water to release H^+ that promotes end-to-end dissolution; (ii) beam induced reduction of Fe(III) at the nanorod surface with subsequent release of Fe(II) into the solution, which drives side-to-side dissolution. To further understand the role of protons on dissolution, we investigated the effect of pH. The results show low concentration pH buffers reduce and even stop end-to-end dissolution, but side-to-side dissolution was still observed, leading to formation of dumbbell-shaped nanopartcles that eventually dissolve completely. Nanorods dissolution was totally inhibited for pH buffer concentrations higher than 100 mM. In addition, we found that chloride ions can inhibit end-to-end dissolution of β–FeOOH nanorods while promoting side-to-side dissolution at low concentration pH. The results provide strong evidence that radiolysis contributes to the reduction of Fe(III) to release of Fe(II) even at neutral pH, thus promoting dissolution of iron oxyhydroxides. Because, photolysis is a naturally occurring process in the environment that is similar to radiolysis, the findings of this *in situ* study may help to understand dissolution and transformation of iron oxides and iron oxyhydroxides in Nature.

Advantages of Direct Detection and Electron Counting for Electron Energy Loss Spectroscopy Data Acquisition

Paolo Longo[1], Jamie L. Hart[2], Andrew C. Lang[2], Ray D. Twesten[1] and Mitra L. Taheri[2]

[1]Gatan Inc., 5794 W Las Positas Blvd, Pleasanton CA, 94588, USA
[2]Department of Materials Science and Engineering, Drexel University, Philadelphia PA, 19104, USA

Transmission electron microscopes primarily employ indirect cameras (IDC) for electron detection in imaging, diffraction and EELS modes. Such cameras convert incident electrons to photons which, through a fiber optic network or lens, are coupled to a light sensitive camera. This indirect detection method typically has a negative impact on the point spread function (PSF) and detective quantum efficiency (DQE) of the camera. Over the last decade, radiation tolerant CMOS active pixel sensors, which directly detect high-energy incident electrons and have the speed to count individual electrons events, have been developed. These detectors result in greatly improved PSF and DQE in comparison to conventional IDCs. Such direct detection cameras (DDCs) have revolutionized the cryo-TEM field as well as have strong advantages for in-situ TEM in both imaging and diffraction applications. EELS applications can benefit from the improved PSF and the ability to count electrons. The improved PSF allows spectra to be acquired over larger energy ranges while maintaining sharp features and greatly reduced spectral tails. The ability to count electrons nearly eliminates the noise associated with detector readout and greatly reduces the proportional noise associated with detector gain variations. This effectively leaves the shot noise as the limiting noise source present. The implication for EELS acquisition is that fine structure analysis becomes more straightforward for typical conditions and even possible for the case of low signal levels.

As example of the advantages due the reduced noise and PSF, Figures 1 show the EELS spectra extracted from the Ti $L_{2,3}$-edges at 456eV and Sr $L_{2,3}$-edges at 1940eV. Here both the DD and IDC detectors were set in such way that the resulting energy range is about 2000eV and this can be achieved specifically with a dispersion of 1eV/channel in the case of IDC and 0.5eV/channel for DD. The DD detector is made of 4k x 4k pixels, hence the use of dispersion 0.5eV/channel to generate a spectrum with an energy range of 2000eV. With such high energy range both the Ti L- and Sr L-edges can be collected in the same spectrum. In the case of DD, given the much reduced PSF, the energy resolution is such that the eg and t2g peaks in both L2 and L3 edges can be easily resolved and show that the Ti is in 4+ oxidation state. In the case of IDC, dispersion 1eV/channel does not allow enough energy resolution to resolve all the features in the Ti L and identify the oxidation state. Higher dispersion would be needed in order to cope with the high PSF and give enough energy resolution for chemical analysis. The much lower noise of the DD allows the collection of a spectrum where both the L2 and L3 edges of the Sr L can be easily resolved. In the case of the spectrum extracted using the IDC detector, the amount of noise is such that L2 and L3 edges cannot be resolved as nicely as in the DD case. All these data was acquired using exactly the same experimental conditions across similar areas in the same specimen.

Very high-energy edges have always been very hard or almost impossible to acquire using EELS due to the very limited amount of signal. With the introduction of DD detectors the amount of noise has been enormously reduced and as result low intensity signals can now be observed and

detected. Figures 2 show EELS spectra of Cu K and N K-edges at about 9keV and 8.3keV. The spectra can be easily observed and the quality is such that high contrast elemental maps can be generated as shown in Figure 2c. Until now, such high energy edges have been collected using synchrotron based techniques such as XAS with very limited spatial resolution. Now, by acquiring EELS data in counting mode using DD detectors, high energy edges can be collected and their signal mapped out with high spatial resolution. A new world is about to open up.

In this presentation, we will review the current state of electrons counting detectors for electron microscopy with an emphasis on system for EELS measurements.

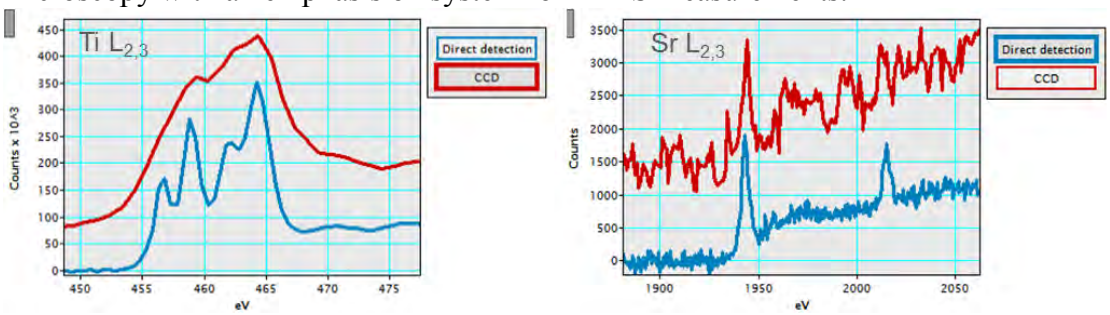

Figures 1a,b EELS spectra of Ti L- and Sr-edges at 456eV and 1940eV extracted from the same area in the specimen under the same experimental conditions using both the DD and IDC detectors. Both the Ti and Sr L signals are extracted from the same spectrum. The spectra extracted using the DD detector show higher energy resolution as well as much reduced noise that allows the clear observation all the main features in the near edge fine structure

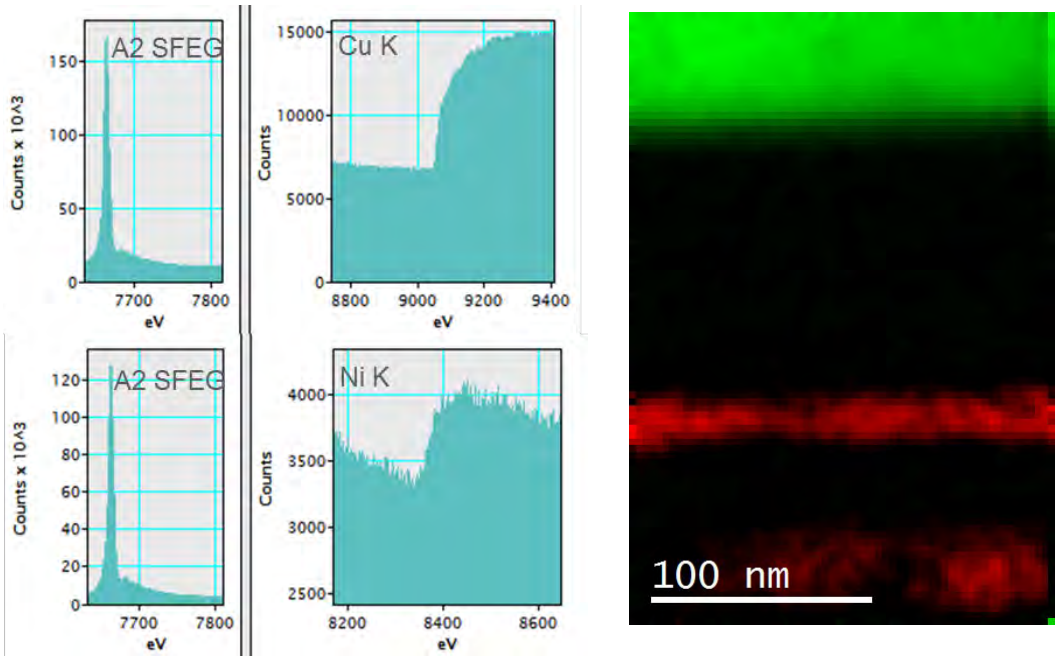

Figures 2: a,b) EELS spectra of Cu K and Ni K at 9keV and 8.3keV acquired in STEM mode using the DD detector in counting mode. The signal-to-noise ratio is quite and allows the clear observation. C) EELS elemental maps of Ni K in red and Cu K in green. This proves that such high energy edges can be collected, observed and the signals extracted generating high-contrast elemental maps in STEM mode.

Seeing is Believing – New Horizons for In Situ Microscopy

Jordan Moering[1], Kate Marusak[1]
[1.] Protochips, Morrisville, USA.

New innovations are transforming the Transmission Electron Microscope (TEM) from a simple high-resolution image acquisition tool into a nanoscale materials research and development laboratory. Researchers can now better understand material behavior by analyzing samples in real-world gas or liquid environments, at high temperature and with ultra-low noise electrochemical and electrical characterization techniques. With the new *in situ* tools from Protochips, materials research occurs in highly controlled environments at high resolution without sacrificing the analytical capabilities of the TEM such as EDS. Applications for these tools include heterogeneous catalysis, semiconductor fabrication, lithium-ion batteries, energy materials, memory storage, and more. In this presentation, we show some of the most recent in situ results and findings from leading researchers in fields spanning the entire scientific discipline from life science to material science.

The recently released Atmosphere 210 gas cell delivers in situ sample heating up to 1000ºC with comprehensive environmental control of the gas environment. Arbitrary gas mixtures can be created at pressures ranging from 0.3 – 760.0 Torr and can be controlled at flow rates ranging from 0.005 – 1.000 mL/min, allowing realistic application conditions to be reproduced within the EM. Coupled with Mass Spectrometry (MS) compatibility, Atmosphere 210 enables comprehensive analysis of catalyst materials undergoing complex reactions with their surrounding environment [1]. Results featuring these and other analytical capabilities will be presented.

Fusion offers accurate and precise thermal and electrical characterization of samples ranging from nanowires and thin films to FIB Lamellae and 2D materials. FIB-optimized E-chips utilize a unique design that complements the conventional liftout workflow to streamline and improve sample preparation for samples ranging from metals to semiconductors. The chemically inert silicon carbide heating membrane delivers accurate, uniform heating which enables atomic resolution imaging of nucleation and growth phenomenon of nanoscale materials and much more.

The Poseidon Select liquid cell surrounds samples in a self-contained, fully hydrated, hermetically sealed chamber directly within the TEM. It features in situ electrochemistry capabilities, which enables the observation and characterization of electrochemical reactions in realistic reaction environments in real-time, and now offers liquid heating, for experiments in growth and reaction kinetics and temperature sensitive samples. Recently released EDS-optimized E-chips, which when combined with a low penumbra in situ results in a six-fold improvement in the counts per second obtained by the EDS detector and enables EDS maps to be obtained without tilting the specimen and/or at low beam currents [2].

References:

[1] K.A. Unocic *et al*, Microsc. Microanal. (2018) p. 286-287.
[2] J Moering *et al*, Microsc. Microanal. (2018) p. 304-305.

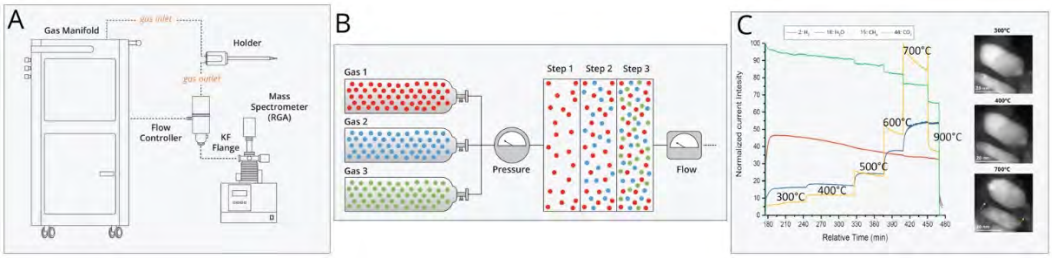

Figure 1. *A)* Schematic showing how a MS can be connected to the Atmosphere 210 system. B) Schematic of a three-component mixture being created with Atmosphere 210. C) MS monitoring of a NiO catalyst showing the consumption of CO_2 and H_2 in the production of CH_4 and H_2O at various temperatures. Courtesy Mounib Bahr institut de Physique et Chimie des Materiaux de Strasbourg.

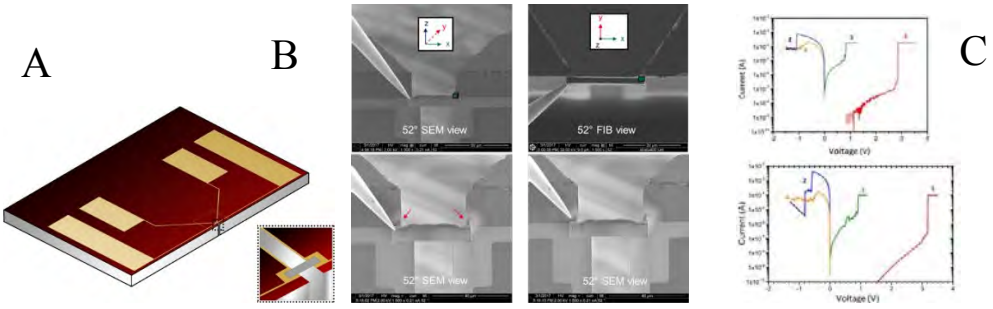

Figure 2. *A) Overview of FIB-Optimized E-chip with inset showing lamellae placement. B) Attaching lamellae to the electrical contacts similar to traditional FIB sample preparation. C) In Situ electrical characterization of semiconductor lamellae (top) aligning well with test results on a bulk sample (bottom).*

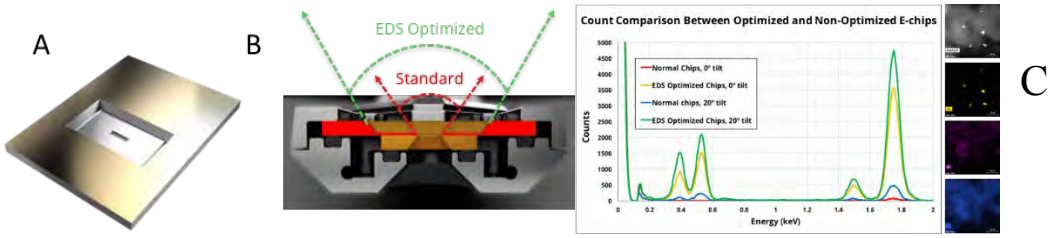

Figure 3. *A) Back view of the optimized EDS E-chip for the Poseidon Select liquid cell. B) Cross section of the x-ray exit angle for the EDS optimized E-chip (green) and standard E-chip (red). C) EDS spectra of gold nanoparticles and aluminum obtained using both standard and EDS optimized E-chips, taken at 0° and 20° holder tilt, at a beam current of 60pA, and with a 5 minute acquisition time.*

Pushing the Limits of Materials Science TEM with Direct Detection Cameras

Direct Electron, LP (San Diego, CA USA)

Direct Electron introduced the first large-format Direct Detection Device (DDD®) TEM camera in 2008, originally targeted for low-dose life science applications. Since this introduction of direct detection camera technology, biological electron cryo-microscopy (cryo-EM) has experienced a "resolution revolution," achieving unprecedented results and a rapid growth in popularity.

Materials science TEM is on the cusp of a similar "revolution" due to the next generation of direct detection technology. While the original direct detectors designed for life sciences had limited dynamic range and framerate, our new DE-16 Camera is designed and optimized to introduce significantly improved capabilities to a range of materials science TEM experiments—most notably for the fast-growing techniques of in situ TEM, imaging of radiation-sensitive materials, and 4D-STEM.

First, in situ TEM is a powerful technique for studying dynamics of materials at medium or atomic resolution. For example, structural changes in materials can be studied during compression, heating, crystal growth, electrical stimulation, etc. Direct detection cameras designed and optimized for materials science significantly expand the capabilities of in situ TEM by delivering a larger field-of-view, a significantly faster frame rate, and much better image quality.

Second, the electron beam in a TEM often produces unwanted effects on specimens, which can significantly alter the interpretation of experimental results. Many materials are radiation sensitive, requiring very low-dose imaging in order to elucidate the native structure of the specimen. Because direct detection cameras are sensitive to single electrons with a very high signal-to-noise ratio (SNR), these cameras can be operated in electron counting mode, which can provide SNR approaching the theoretical maximum for pixelated detectors, and thus enable visualization of structural features at much lower doses than ever before possible.

Third, STEM is the standard materials science technique for atomic resolution imaging, using single-value detectors to integrate all the bright-field or high-angle dark field signal, as the STEM probe scans across the specimen. However, it is clear that the bright-field disc (and likely also the surrounding dark field area) contains useful structural information encoded in intensity variations across its area. Capturing and analyzing this data, requires a pixelated detector that has very high speed and very high sensitivity. While several new detectors have recently been introduced for this purpose, all of these detectors are still significantly slower than conventional STEM requires, which limits the specimen field-of-view that can be captured without noticeable specimen drift. The DE-16 Camera provides the high sensitivity required, but with more than four-times faster speed than many of the other pixelated detectors that are currently available.

An Attempt to Integrate Electron Tomography and in-situ Deformation for 3D Dislocation Dynamics

M. Murayama[1,2,3] and S. Hata[4,5]
[1.] Department of Materials Science and Engineering, Virginia Tech, Blacksburg, VA, USA.
[2.] Energy and Environmental Directorate, Pacific Northwest National Laboratory, Richland, WA, USA.
[3.] The Virginia Tech National Center for Earth and Environmental Nanotechnology Infrastructure, Virginia Tech, Blacksburg, VA, USA.
[4.] Faculty of Engineering Sciences, Kyushu University, Fukuoka, Japan.
[5.] The Ultramicroscopy Research Center, Kyushu University, Fukuoka, Japan.

Staring from 1980's, in-situ TEM deformation technique has been deployed to investigate material's microstructure response to external stimuli such as elastic/plastic deformation and fracture, and has been applied to various size and type of materials including but not limited to metallic, semiconductor, nanostructured, polymer, and carbonations materials. The technique is also applicable to observe morphological changes of nanostructured materials under various types of stresses. Now, one major drawback of this technique is that this could not be ruled out of the image-projection problem like many other TEM based techniques, thus the observation could not maintain the spatial resolution in the depth (sample thickness) direction.

Electron tomography is an adequate technique to retrieve the depth scale information, and thus allows us to investigate and visualize dislocation interactions three-dimensionally. Inspired by several initial successful demonstrations (for example [1]), we have further developed the idea of integrating electron tomography with in-situ deformation for expanding the capability and versatility of the 3D electron microscopy technique. The technique could be more effective by overcoming several technical roadblocks such as (1) installing deformation mechanism into a TEM sample holder introduces additional experimental constraints such as narrower tilt angular range and smaller field of view compared with standard tomography holders, and those could influence the accuracy of three-dimensional reconstruction in various different ways; (2) tensile is common but compression is appears to be hardly executable based on the generally used liner-motion mechanism, thus it is often altered by nanoindentation; (3) deformation test must be interrupted for at least few ten minutes for every acquisition of a series of images by tilting a specimen over a wide angular range to reconstruct three dimensional microstructure.

The specimen deformation mechanism we developed for this project employs a unique cartridge-type blade system that allows to pursue both tensile and compression testing in the rate between 1.5×10^{-6} and 5.2×10^{-3} s^{-1} (Fig. 1) [2]. First, we have also confirmed that the maximum tilt angle of the specimen holder reaches ±60° with a standard 3mm diameter disc shape sample. Second, we have observed a morphological change of a commercial Pb-Sn solder wire during an interrupted tensile test. Twelve tilt series were acquired with gradually deforming the solder wire sample, and the results demonstrates a complex three-dimensional morphological change due to a share component likely introduced by a combination of small misorientation from the main loading axis and non-uniformity of material's microstructure response (Fig. 2) [3].

An additional advantage of this cartridge system is that the mechanical drift of the field of view or the region of interest under stress, i.e., imaging both during and between the interruption, is noticeably smaller than the conventional liner-motion tensile stage. This allows to perform atomic resolution imaging and sub-nanometer spectroscopy near a crack tip or freshly opened crack area without unloading, thus observing a time dependent microstructure evolution under stress is possible. The presentation will cover several different applications including nano-porous gold thin film and bulk metallic and mineralogical materials.

[1] Josh Kacher and I.M. Robertson, Acta mater., 60 (2012) 6657-6672.
[2] K. Sato, H. Miyazaki, T. Gondo, S. Miyazaki, M. Murayama and S. Hata, Microscopy, 64, (2015) 369-375.
[3] S. Hata, S. Miyazaki, T. Gondo, K. Kawamoto, N. Horii, K. Sato, H. Furukawa, H. Kudo, H. Miyazaki and M. Murayama, Microscopy, 66, (2017) 143-153.

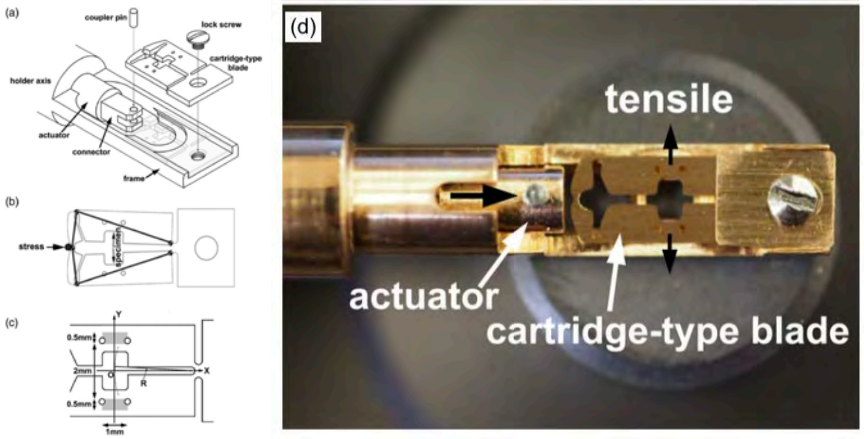

Figure 1. *The appearance of the newly develop in-situ deformation high tilt angle specimen holder having the cartridge-type blade design. [2]*

4D-STEM Experimental and Simulation Methods

Colin Ophus, *NCEM, Molecular Foundry, Lawrence Berkeley National Laboratory, Berkeley USA.*

By converging an electron probe to small dimensions and measuring the diffracted signal, we can measure atomic-scale information about a sample's structure, orientation, deformation, composition, three-dimensional defect crystallography and more. Conventional STEM imaging experiments sum up electron counts for 1 or 2 large regions of the diffraction pattern, throwing away a lot of information. With the introduction of high speed, pixelated electron detectors, we can now record a full image (2D data) of the diffracted electron probe scanned over the sample (2D grid of positions), producing a four-dimensional dataset we refer to as a 4D-STEM experiment. In this talk, I will demonstrate various imaging and property measurement modalities possible with 4D-STEM, including diffractive imaging. I will also cover modern electron scattering simulation methods, appropriate for 4D-STEM simulations.

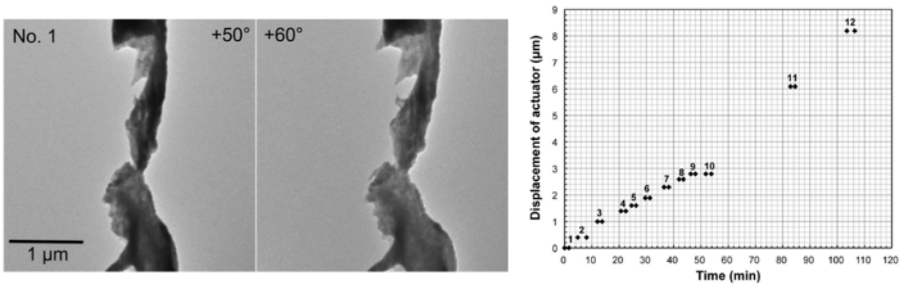

Figure 2. (Left) TEM BF images acquired at sample-tilt angles of +50° and +60°. Stereographic observation of the two TEM images shows that the sample morphology in this FOV is like a partly curled ribbon rather than like a rod. **(Right)** Displacement of the actuator for sample deformation as a function of time. Neighboring plots at the same displacement value correspond respectively to the starting time and ending time of a tilt-series data set acquisition. The sample straining and subsequent tilt-series data set acquisition were repeated 12 times. [3]

Figure 1**a** shows the basic geometry of a 4D-STEM experiment, where diffraction patterns are measured from converged electron probes after interaction with a sample. Electrons scattered to higher angles are typically also recorded using an annular detector, generating another signal channel typically referred to as a high angle annular dark field (HAADF) image. Figures 1**b**, **c**, and **d** show typical 4D-STEM experiments. The sample imaged in Figure 1**b** is a semi-crystalline soft-matter beam-sensitive sample, where overlapping crystalline domains produce diffraction spots perpendicular to the backbone of the structure, allowing for mapping of the sample's local orientation. Figure 1**c** shows strain mapping from a crystalline stainless-steel sample, adapted from [1]. While Figure 1**d** shows *in situ* strain mapping from an amorphous metallic glass sample during mechanical deformation, adapted from [2]. Another important application of 4D-STEM is diffractive imaging, including differential phase contrast (DPC), ptychography, and phase contrast generated by using phase plates in the probe-forming aperture. I will show results from our group and others, including the experiment shown in Figure 1**e** where multiple STEM beams are used to perform holographic measurements of long-range, weak phase shifts such as those generated by electrostatic or magnetic fields, adapted from [3].

Figure 1**f** shows the algorithmic steps required for a STEM simulation, using either the multislice method or the newly developed PRISM algorithm [4, 5]. Simulations are essential for validating or interpreting many 4D-STEM experiments, especially complex phase contrast imaging experiments. For example, Figure 1**e** shows a study where simulated diffraction patterns were matched to experimental measurements to determine the best fit for sample thickness and composition in an STO-LMO multi-layer sample [6]. I will discuss the advantages and disadvantages of various STEM simulation codes [7].

References

[1] TC Pekin, C Gammer, J Ciston, AM Minor and C Ophus **176**, 170 (2017).
[2] C Gammer, C Ophus, TC Pekin et al., Applied Physics 112, 171905 (2018).
[3] T Harvey, FS Yasin, JJ Chess et al., arXiv:1808.00370 (2018).
[4] C Ophus, Advanced Structural and Chemical Imaging **2**, 11 (2017).
[5] AJ Pryor Jr., C Ophus and Jianwei Miao, Advanced Structural Imaging **3**, 15 (2017).
[6] C Ophus, P Ercius, M Huijben and J Ciston, Applied Physics Letters **110**, 063102 (2017).

[7] Work at the Molecular Foundry was supported by the Office of Science, Office of Basic Energy Sciences, of the U.S. Department of Energy under Contract No. DE-AC02-05CH11231. We thank the NVIDIA Corporation for donation of GPU resources.

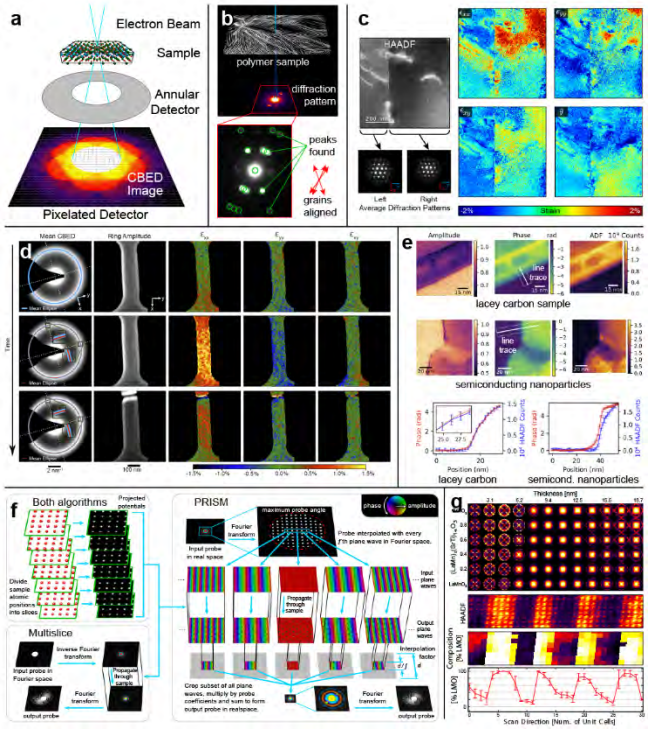

Figure 1. (a) Experimental geometry of a 4D-STEM experiment measuring a convergent beam electron diffraction pattern, also known as pixelated STEM or scanning electron nanodiffraction (SEND). **(b)** Experimental diffraction pattern from a weakly scattering polymer material, where diffraction peaks are automatically detected and classified to measure orientation. **(c)** Strain of local lattice displacements across a twin boundary in a crystal, measured from slight shifts in the diffracted disk positions, and (**d**) local strain measured from a metallic glass during an *in situ* experiment. (**e**) STEM holography phase contrast measurements comparing a conducting lacey carbon film to semiconducting nanoparticles. Line traces inset in (**e**) show that STEM holography can measure the electrostatic fields extending from the particle due to charging. **(f)** Simulation steps for two algorithms for computing 4D-STEM patterns: multislice and PRISM. **(f)** Diffraction pattern library computed for different sample compositions and thicknesses, used the classify composition of each unit cell in the experimental 4D-STEM dataset below.

Characterizing Formation, Growth, Dissolution, and Transformation of Nanoscale Objects in Aqueous and Non-Aqueous Suspensions

Jennifer Soltis
Nathan Burrows
Virany Yuwono
Sandeep Kumar
Amanda M. Vindedahl
Kairat Sabyrov
Louis Corcoran
Alon McCormick
Department of Chemical Engineering and Materials Science, University of Minnesota, Minneapolis, MN 55455
R.Lee Penn
Department of Chemistry, University of Minnesota, Minneapolis, MN 55455

Electron microscopy is a powerful technique for elucidating the mechanisms of the formation, growth, dissolution, and transformation of nanoscale objects. We employ cryogenic transmission electron microscopy (TEM) and in situ TEM; in combination with conventional TEM, dynamic light scattering, X-ray diffraction and scattering, UV-visible spectroscopy, as well as kinetic modeling; to elucidate the fundamental processes that govern the kinetics of these processes. Each of these techniques has advantages and limitations, and a combination of methods is essential.

Advanced Compositional and Structural Mapping of Nanoscale Environmental and Energy Materials Enabled by Correlative APT and TEM

Daniel E. Perea[1], Libor Kovaik[1] and Steven R. Spurgeon[2]
[1.] Earth and Biological Sciences Directorate, Pacific Northwest National Laboratory, Richland USA.
[2.] Energy and Environment Directorate, Pacific Northwest National Laboratory, Richland USA.

The ability to map composition and structure of complex buried interfaces over nanometer to micrometer length scales is fundamental to correlating structure properties relationships in energy and environmental materials and is aided by a multimodal approach using advanced complementary microscopic and spectroscopic characterization techniques. Atom Probe Tomography (APT) is a 3-dimensional compositional mapping technique that relies on the thermally-assisted field evaporation of individual atoms and/or molecules as positive ions from the tip of a cryogenically-cooled needle-shaped specimen [1]. The chemical identity of each ion is determined from time-of-flight mass spectrometry while the 3-dimensional position is determined from the relative position on the detector and the time sequence of evaporation events. From this information, a unique 3-dimensional atom-by-atom reconstruction can be formed revealing the atomic scale composition along with impurity distributions up to a part-per-million sensitivity and sub-nanometer spatial resolution [2]. Although unique tomographic compositional maps are obtained with APT, it is unable to provide crystallographic or chemical information. The powerful complementary imaging technique of High Angle Annular dark-field Scanning Transmission Electron Microscopy (HAADF-STEM) combined with simultaneous spectroscopic mapping by energy dispersive X-ray (EDX) or Electron Energy Loss Spectroscopy (EELS) [3] can supplement these deficiencies in APT [4].

Using a Focused Ion Beam/Scanning Electron Microscope (FIB/SEM) to site-specific target regions of interest for specimen fabrication within a bulk or low dimensional material, we are able to create needle-shaped specimens from environmental and energy materials that are compatible with both APT and STEM techniques to provide powerful correlative multimodal imaging. Two examples will be discussed in detail that demonstrate the complementary nature of the two techniques. In Figure 1 and 2, STEM and complementary APT analysis is performed on a multiferroic NiFe2O4-LaFeO3 (NFO-LFO) nanocomposite revealing a highly complex interface morphology [5] and a natural ancient biogeological FeS2 mineral revealing nanoscale water-filled inclusions, respectively.

[1] Miller, M. K.; Forbes, R. G. Atom Probe Tomography. *Materials Characterization* **2009**, *60* (6), 461–469.
[2] Larson, D. J.; Prosa, T. J.; Ulfig, R. M.; Geiser, B. P.; Kelly, T. F.; Humphreys, P. S. C. J. *Local Electrode Atom Probe Tomography: A User's Guide*; Springer New York, 2016.
[3] *Scanning Transmission Electron Microscopy: Imaging and Analysis*, 2011 edition.; Pennycook, S. J., Nellist, P. D., Eds.; Springer: New York, NY, 2011.
[4] Devaraj, A.; Perea, D. E.; Liu, J.; Gordon, L. M.; Prosa, T. J.; Parikh, P.; Diercks, D. R.; Meher, S.; Kolli, R. P.; Meng, Y. S.; et al. Three-Dimensional Nanoscale Characterisation of Materials by Atom Probe Tomography. *International Materials Reviews* **2017**, *10.1080/09506608.2016.1270728* (0), 68–101.

[5] Comes, R. B.; Perea, D. E.; Spurgeon, S. R. Heterogeneous Two-Phase Pillars in Epitaxial NiFe2O4-LaFeO3 Nanocomposites. *Adv. Mater. Interfaces* **2017**, *4* (16), 1700396.

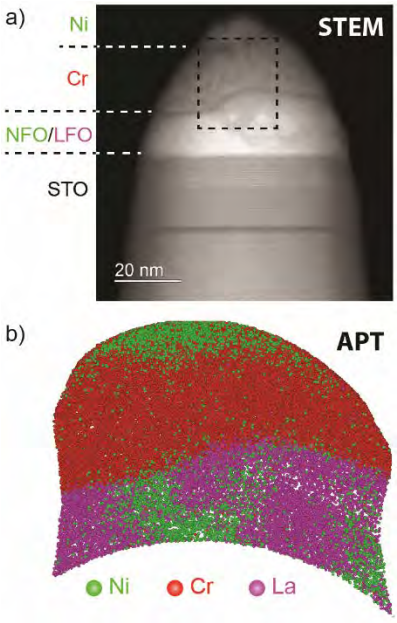

Figure 1: a) STEM micrograph of NFO-LFO nanocomposite material. b) APT reconstruction of same volume highlighted by dashed-line bounding box in panel a. Note the clear

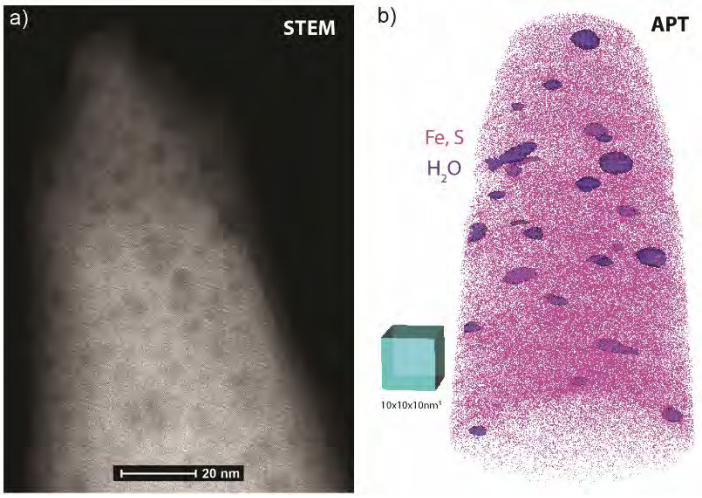

Figure 2: a) STEM image of a natural framboidal pyrite (FeS_2) obtained from sediment dated to the Devonian time period (4.2-3.6 million years ago). b) APT reconstruction of same volume with Fe and S shown as pink. Detected water is spatially segregated into nanoscale volumes (blue surfaces) and corresponds to the dark colored (low density) regions in the STEM image.

Exploring the Local behavior of Magnetic Nanostructures via In-situ Lorentz TEM

Amanda K. Petford-Long[1], Saidur Bakaul[1], Frank Barrows[1], Vuk Brajuskovic[1], Marc De Graef[2], Olle Heinonen[1], Charudatta Phatak[1], Sheng Zhang[1]
[1.] Materials Science Division, Argonne National Laboratory, Lemont, IL, USA
[2.] Department of Materials Science and Engineering, Carnegie Mellon University, Pittsburgh, PA, USA

As the dimensions of magnetic materials decrease to the nanoscale, novel distributions of spin can be created. In order to understand how these novel spin distributions form and how they behave, it is necessary to gain an understanding of the local energy landscape of the nanostructures and how this can be controlled through parameters such as confinement, the presence of adjacent layers and in response to external stimuli such as applied magnetic fields and temperature.

Lorentz transmission electron microscopy (LTEM), combined with in-situ magnetizing and heating experiments, is an ideal technique to explore the behavior of magnetic nanostructures, as the spatial resolution that can be achieved is of the order of a few nanometers [1]. In addition, it is easy to correlate the spin distribution with the microstructure since both are accessible within the same instrument. Although we can gain a good understanding of the magnetic behavior simply from Fresnel mode (out-of-focus) LTEM images, we have also used the transport of intensity equation (TIE) approach [2] to obtain quantitative maps of the in-plane magnetic induction, enabling us to visualize the magnetic structure in two dimensions, or in three dimensions [3], and we carry out our experiments in a dedicated LTEM instrument equipped with a spherical aberration corrector. By comparing these data with the results of micromagnetic simulations, we are able to gain a fuller understanding of the various energy terms that contribute to the behavior that we observe.

Magnetic skyrmions are topologically non-trivial chiral spin structures that have attracted considerable attention both because of their fundamental behavior and because of their potential for use as low-power information carriers [4]. We have applied LTEM to a number of skyrmion systems and we will discuss two of these here. Ni_2MnGa is a Heusler alloy that is ferromagnetic and ferroelastic and we have explored the magnetic structure and the formation of naturally-occurring skyrmions in the martensitic phase, together with the stability of the skyrmion lattices that form [4]. Figure 1 shows a Fresnel mode LTEM image of a skyrmion lattice that forms spontaneously in alternating twins in Ni_2MnGa, together with the in-plane magnetic induction map reconstructed from the LTEM data (the inset color wheel indicates the magnetization directions). The schematic in Fig. 1(c) shows the arrangement of the skyrmions. Secondly, we will discuss the creation of 'artificial' skyrmions and antiskyrmions in Co/Pt multilayer films [5].

Artificial spin ices (ASIs) are nanoscale geometrically-engineered arrays of nanoscale magnetic bars or islands patterned on a geometric lattice [6]. There is considerable interest in these systems because they display room-temperature magnetic frustration. We have explored ASIs patterned on both periodic and aperiodic lattices, and in this presentation we will focus on the behavior of Permalloy ASIs patterned in P2 [6] and P3 Penrose tilings. These quasicrystalline

ASIs lack translational symmetry and are composed of vertices with a varying number of interacting elements. An example of the magnetic domain structure of a P2 QC-ASI, reconstructed from our LTEM data, is shown in Figure 2. We will present LTEM studies of the way in which the underlying lattice geometry influences the energy landscape, and thus the emergent magnetic order that emerges during magnetization reversal and thermalization of the QC-ASIs, using a novel graph-analytical approach to explore topology. Acknowledgements to the funding provided for this research are included in reference [7].

References:

[1] C Phatak, AK Petford-Long and M De Graef, Curr. Opin. Solid State Mater. Sci. **20** (2016), p. 107.
[2] E Humphrey, C Phatak, AK Petford-Long and M De Graef, Ultramicroscopy **139** (2014), p. 5.
[3] C Phatak, M Beleggia and M De Graef, Ultramicroscopy **108(6)** (2008), p. 503.
[4] C Phatak, OG Heinonen, M De Graef and AK Petford-Long, Nano Lett. **16(7)** (2016), 4141.
[5] S Zhang, AK Petford-Long and C Phatak, Sci. Rep. **6** (2016), 31248.
[6] V Brajuskovic, F Barrows, C Phatak and AK Petford-Long, Sci. Rep. 6, 34384 (2016).
[7] This work was supported by the US Department of Energy, Office of Science, Office of Basic Energy Sciences, Materials Science and Engineering Division. Use of the Center for Nanoscale Materials was supported by the US Department of Energy, Office of Science, Office of Basic Energy Sciences, under contract no. DE-AC02-06CH11357.

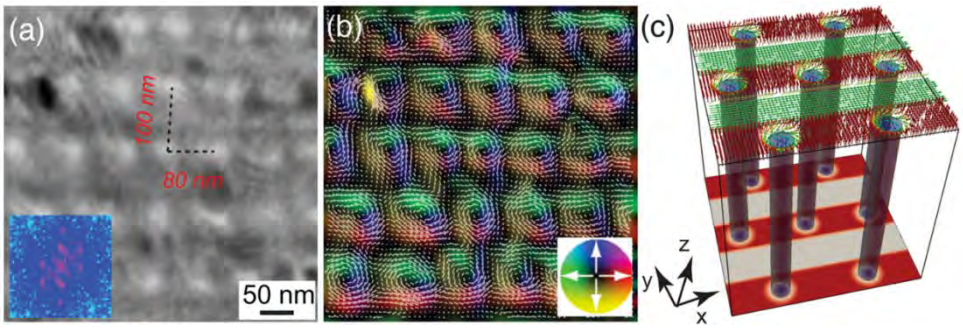

Figure 1. (a) High resolution under-focused LTEM image of Ni_2MnGa: bright spots correspond to the cores of Bloch skyrmions; (b) corresponding color magnetization map reconstructed from the LTEM data: inset color wheel shows the magnetization directions; (c) 3D schematic of the skyrmion lattice. Reproduced from Phatak et al., Nano Lett. 16(7) (2016), 4141. © 2016 Amer. Chem. Soc.

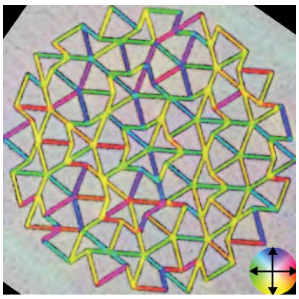

Figure 2. Color magnetization map of P2-tiled quasicrystalline artificial spin ice patterned in thin film Permalloy. Bar lengths are ~ 2 μm. Inset color wheel shows the magnetization directions. Brajuskovic et al., Sci. Rep. 6 (2016) 34384. Licence: Creative Commons 4.0

Recent Advances in Electron Microscopy Developments

Jan Ringnalda[1]
[1] Thermo Fisher Scientific, Hillsboro, OR, USA 97124

State-of-the-Art materials research is a rapidly moving field, with more and more requirements in terms of resolution, both in imaging as well as analytical performance. Sometimes these do not require the same optimization. Detectors and their efficiency/cleanliness play a very large role in how these systems perform. In this presentation we will show some of the recent developments to allow users to get the best imaging and analytical resolutions from both ideal and non-ideal samples, while minimizing the dose requirements. These developments will include performance at low-kV using a monochromator and new probe corrector, some new energy resolution capabilities and a unique diffraction camera development.

Tools for *In Situ* and *Operando* TEM and other Imaging Platforms

Julio A. Rodriguez Manzo[1], Khim Karki[1], Daan Hein Alsem[1], and Norman Salmon[1]
[1.] Hummingbird Scientific, Lacey, USA

I will present an overview of sample holders that broaden the stimuli "knobs"—environment, temperature, electric potential, etc.—that can be used to observe, with high-spatial resolution, a specimen or device in an electron or x-ray microscope under operating conditions.

For example, with a standard transmission electron microscopy (TEM) sample holder specimens are observed at low pressures (~ 10-7 mbar) that are incompatible with liquid or gaseous environments. Now, however, with micro-sized environmental cells we can observe samples submerged in a thin liquid layer routinely in a TEM. I will present this approach, where different sample holders have been used to study, for example, the diffusion rates of two metal atoms (Kirkendall effect) in nanoparticles submerged in liquid at different temperatures [1] (figure 1); the electrical transport of graphene-nanoribbons (GNR) patterned inside a TEM column with the converged electron beam [2] (figure 2); the kinetics of Li-ion insertion and extraction in particles under an electrochemistry reaction [3] (figure 3); etc.

Finally, I will discuss recent efforts to bridge bulk-size sample analysis with results obtain from *in situ* TEM experiments, with examples from mobile nanoprobes and electrochemistry.

References:

[1] SW Chee *et al*, Nature Communications **8** (2017), p. 1224.
[2] JA Rodriguez-Manzo *et al*, ACS Nano **10** (2016), p. 4004.
[3] J Lim *et al*, Science **353** (2016), p. 566.

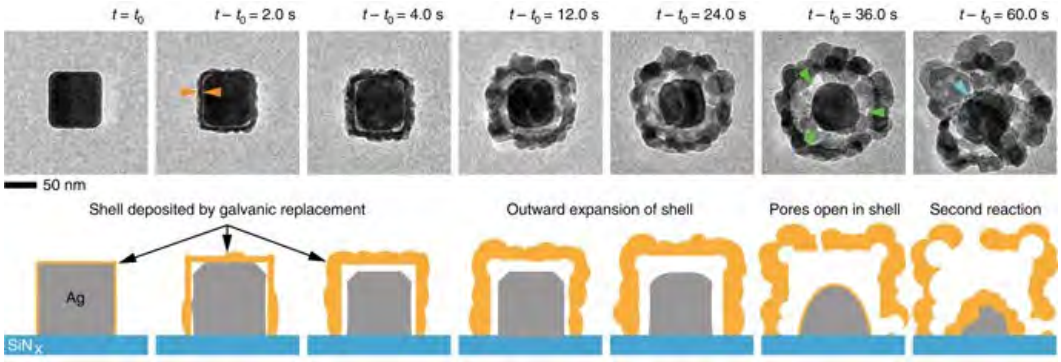

Figure 1. Observation of the Kirkendall effect at the nanoscale. TEM images of metal nanocubes in liquid as they undergo a chemical transformation. Adapted from Reference 1.

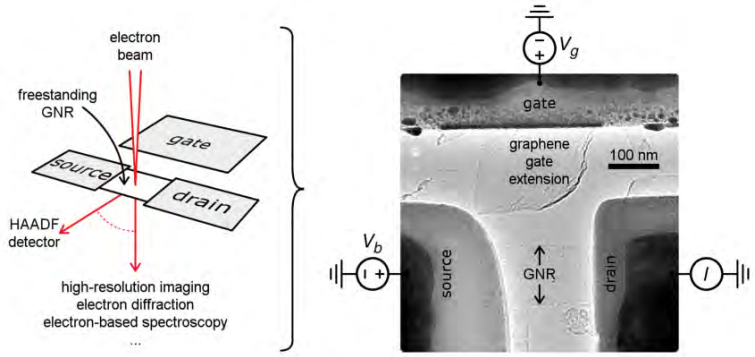

Figure 2. Setup to pattern GNR-based devices inside a TEM column and measure their transport properties. Adapted from Reference 2.

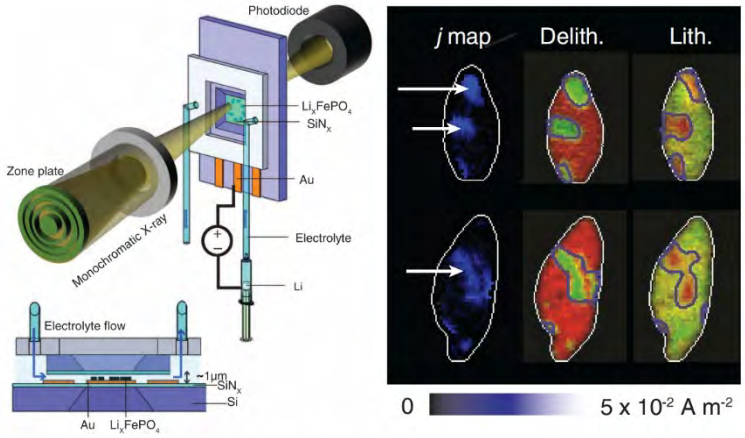

Figure 3. Schematic of the operando environmental liquid cell liquid imaging platform to image Li-ion insertion and extraction mechanisms. Adapted from Reference 3.

Multimodal Methods for *In-Situ* Transmission Electron Microscopy

Renu Sharma[1], Wei-Chang (David) Yang[1,2], Canhui Wang[1,2] and Alina Bruma[1,2]
[1.] Center for Nanoscale Science and Technology, National Institute of Standards and Technology, Gaithersburg, MD 20899-6203, USA
[2.] Maryland NanoCenter, University of Maryland, College Park, USA.

In recent years the environmental scanning transmission electron microscope (ESTEM) has been successfully employed to reveal and understand the structural and chemical changes occurring in the nanoparticles under reactive environments [1,2]. However, quantitative measurements of reaction rates and chemical changes are limited by (a) the nanoscale regions used for atomic-resolution imaging, (b) uncertainty in the temperature of the imaged region and (c) difficulty in analyzing the large quantities of data generated. We present various technical and analytical techniques that have been incorporated in an ESTEM to address these issues.

First, we have incorporated a free-standing, broad-band, light focusing system (Figure 1) in the ESTEM to excite and collect vibrational and optical spectroscopies under reactive environments [3]. This bimodal data collection enables not only the acquisition of vibrational spectroscopy (Raman) data concurrently with other electron microscopy data, such as imaging, diffraction and electron energy-loss spectroscopy under identical chemical environment, it expands the spatial resolution from nanoscale to microscale. This set-up also extends our capabilities from high-resolution imaging (Figure 2a) to cathodoluminescence (CL) measurements (Figure 2b), reaction kinetics (Figure 2c), and pulse heating (Figure 2d), etc.

In order to obtain quantitative information from the large data sets of atomic resolution images generated during in situ measurements, we have developed an automated image processing system (AIPS) that utilizes a combination of home-built and publicly available algorithms for image drift correction, noise reduction, and intensity peak location to accurately and automatically determine the position of atomic columns [4]. Average nearest neighbor for each frame is calculated to identify phases and thus phase transformations at the atomic-scale. A color-coded image (Figure 3a), extracted from a video, shows the distribution of Co (blue) and Co_2C (magenta) phases within the 3nm catalyst particle as determined by measuring nearest neighbor distances. The measurement error is estimates from the histogram as shown in Figure 3b.

Recently, we have also employed the ESTEM, operated at 80 kV, equipped with monochromated field emission electron source and image corrector, to reveal the gas adsorption sites and room temperature chemical reactions assisted by plasmonic Au nanoparticles. We utilize a combination of ESTEM based techniques such as low-loss and core-loss electron energy spectrum (EELS) maps, high-resolution TEM and STEM images, and electron diffraction, to identify the gas adsorption sites, morphological changes, structural modifications and reaction products. While the low-loss EELS provided the information about the local surface plasmon resonance energies in vacuum and gas environment, core-loss EELS data showed the CO adsorption site on Au nanoparticle (Figure 3c) and the location of amorphous carbon (reaction site) formed as result of CO disproportionation reaction (Figure 3d).

References:

[1] Sharma, R., J. Mat. Res. 2005, 20, 1695
[2] Hansen et al., Science 2001, 294, 1508.
[3] Picher et al., Ultramicroscopy, 2015, 150, 10.
[4] Hussaini et al. Ultramicroscopy 2018, 186, 139.

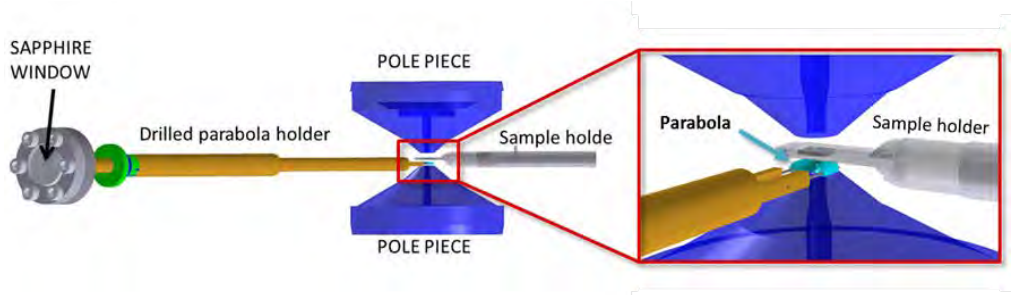

Figure 1. *Schematic representation of the Raman data collection system: the laser travels through the hole drilled in the parabola holder, then hits the parabola, is focused on the sample, and the collected Raman signal is finally sent back to the spectrometer through the parabola holder.*

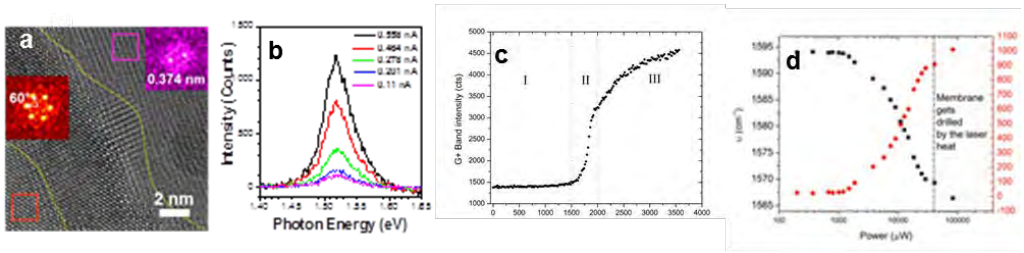

Figure 2. *(a) High-resolution image of CdTe showing the grain structure and grain boundary (b) CL intensities measured as a function of electron beam current. (c) Time resolved Raman spectra is used to obtain growth kinetics of carbon nanotubes in ESTEM. (d) temperature versus laser power showing no heating effect up to 1 μW power. It can also be used for local pulse heating of the TEM sample.*

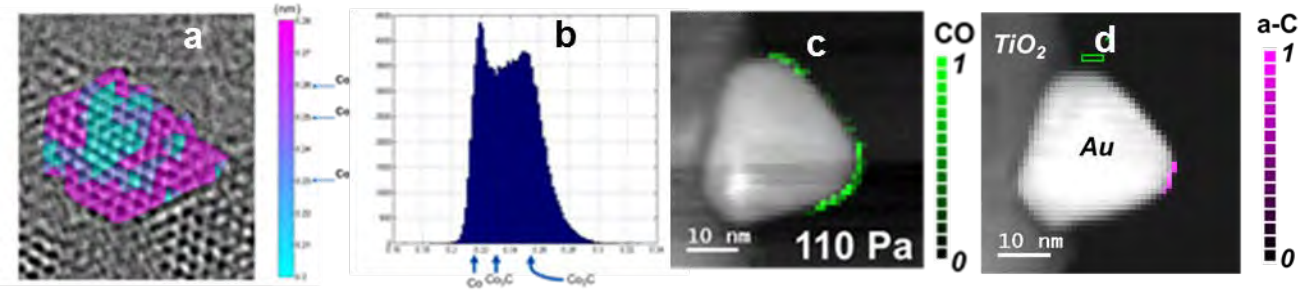

Figure 3. (a) Color coded high-resolution image extracted from a video recorded during carbon nanotube growth showing the existence of Co metal and carbide (mostly Co_2C) phase in the same catalyst particle. (b) Automated measurements of 100 frames shows that nearest neighbor distances can be measured with 0.07 nm accuracy while our inability to distinguish between Co_2C and Co_3C phase results in higher error (0.15 nm). (c) C K-edge map, obtained after subtracting environmental CO contribution, showing CO absorption locations on Au triangular biprism loaded on TiO_2. (d) C K-edge map of the same particle acquired after CO evacuation showing the carbon deposit formed due to CO disproportionation reaction at cantilevered corner of the particle.

Applications of Cryogenic Transmission Electron Microscopy for Hard Materials

Jennifer A. Soltis,[1] R. Lee Penn,[2] Benjamin Gilbert,[3] and Edgar C. Buck[1]
[1.] Pacific Northwest National Lab, Richland, WA
[2.] University of Minnesota Department of Chemistry, Minneapolis, MN
[3.] Lawrence Berkeley National Lab, Berkeley, CA

The advent of cryogenic transmission electron microscopy (cryo-TEM) transformed the way electron microscopists looked at hydrated specimens. The technique was brought to the public eye in 2017 when the Nobel Prize in chemistry was awarded for work on biomolecules and is commonly known in structural biology, virology, and for the study of polymers and micelles. However, its use in characterizing hard materials is ever-increasing.

One of the strengths of cryo-TEM is the ability to look at hydrated specimens in a high vacuum environment. Unlike conventional TEM, in which samples must be dried, cryo-TEM samples are prepared by vitrifying a small amount of specimen via rapid cooling in a cryogen, typically liquid ethane. The specimen of interest, such as an assembly of nanoparticles, is then preserved in its hydrated state within an electron-transparent amorphous solid. Through the preservation of *in aqua* conformation, details about materials structure can be seen that would otherwise be lost upon drying. This poster presents several uses of cryo-TEM to elucidate *in aqua* structures of hard materials.

The uranyl peroxide nanocluster U60 is a cage-like polyoxometallate (POM) with fullerene topology. Upon mixing solutions of U60 with metal nitrate salts, the clusters assemble into secondary and tertiary structures. When imaged with an electron beam, U60 is rapidly reduced to crystalline U_3O_8. Further, it is unknown if these secondary and tertiary structures accurately retain their shape upon drying. Figure 1 shows cryo-TEM images of (a) a hollow sphere of U60 clusters and (b) a tertiary assemblage of blackberry-like structures. The vitrified water preserves the original conformation of the U60 structures and sufficiently prevents the migration of the clusters and reduction into a larger crystal of U_3O_8 [1].

Mesocrystals, the kinetically stable intermediate structure of the non-classical crystal growth mechanism oriented attachment (OA), are another excellent candidate for imaging via cryo-TEM. During OA, crystalline primary particles form a crystallographically-aligned array with no direct contact of the mineral surfaces before forming mineral-mineral bonds to produce a single crystal. The intermediate mesocrystal structure often exists only *in aqua* and is destabilized by drying, rendering them difficult to image with conventional TEM. Figure 1c shows cryo-TEM images of a goethite (α-FeOOH) mesocrystal at sufficient resolution to demonstrate that lattice fringes (an indicator of crystal structure) extend across primary particles that are separated by a vitrified water layer [2].

Cryo-TEM can also be used as a correlative technique to support the findings of liquid cell electron microscopy (LCEM). Analysis of LCEM must take into consideration the effects of the electron beam on the specimen and the solvent. The electron beam may have charging effects on the membranes of the liquid cell or the specimen itself that move, dissolve, or promote the formation

of the specimen being studied. Solvent radiolysis can also complicate analysis of results. Cryo-TEM can be used to verify that the sample conformation has not been affected by the electron beam by comparing images of a vitrified aliquot of the same specimen to the results seen in LCEM, such as in Figure 2, which compares a) a LCEM image of boehmite (γ-AlOOH) nanoparticles in water with b) a cryo-TEM image of a vitrified portion of the same suspension [3,4].

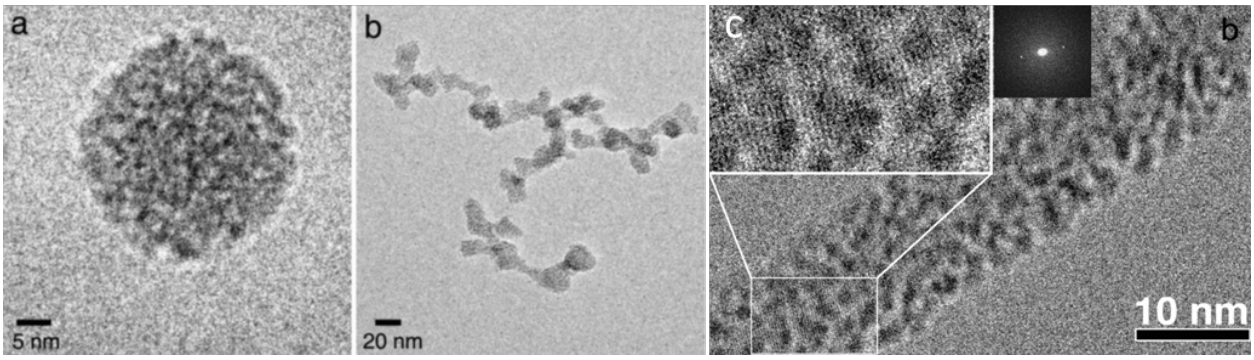

Figure 1: Cryo-TEM images of U60 uranyl peroxide clusters (~2.5 nm) assembled into secondary and tertiary structures when vitrified a) 20 min after treatment with $CaNO_3$ and b) 15 min after treatment with $K_2(NO_3)_3$ from [1]. c) Cryo-TEM images of a goethite mesocrystal in which lattice fringes extend continuously across the mesocrystal. Insets: higher magnification image of indicated region and fast Fourier transform showing crystalline structure from [2].

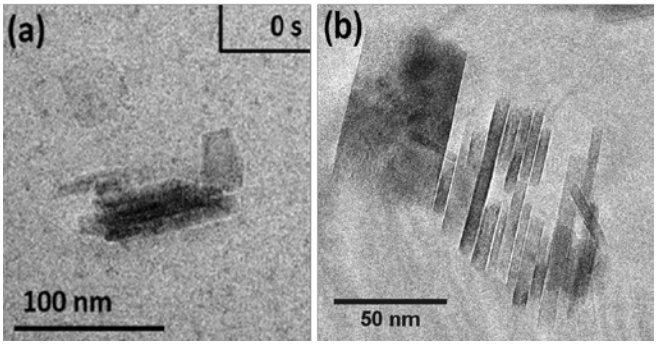

Figure 2: (a) TEM image of an aqueous suspension of boehmite nanoparticles in a liquid cell holder from [3]. (b) Cryo-TEM image of a vitrified suspension of boehmite nanoparticles.

[1] Soltis, J. A. *et al*, J. Am. Chem. Soc. **138** (2016), p. 191-198.

[2] Yuwono, V. M. *et al*, J. Am. Chem. Soc. **132** (2010), p. 2163-2165.

[3] Conroy, M. *et al*, Sci. Reports **7** (2017), 13274.

[4] Pacific Northwest National Laboratory is a multi-program national laboratory operated for the U.S. Dept. of Energy by Battelle Memorial Inst. under Contract DE-AC06-76RLO 1830. Parts of this work were carried out in the University of Minnesota Characterization Facility, a member of the NSF-funded Materials Research Facilities Network via the MRSEC program.

High Energy EELS with Direct Detection and Electron Counting

Mitra L. Taheri[1], James L. Hart[1], Andrew C. Lang[1]
[1.] Department of Materials Science, Drexel University, Philadelphia, PA 19104, USA

Electron energy loss spectroscopy (EELS) in the scanning transmission electron microscope (STEM) is a characterization technique which provides nanoscale measurement of elemental composition, chemical bonding, dielectric properties, and molecular vibrations. Unfortunately, EELS measurements of core-loss edges above ~2 keV – which provide valuable information relating to local bonding and can be crucial for elemental identification – are generally impractical. For such high energy edges, synchrotron X-ray absorption spectroscopy (XAS) and energy dispersive spectroscopy (EDS) within the (S)TEM allow for more straight forward acquisition. However, the spatial resolution of synchrotron XAS is generally limited to several microns, and the energy resolution of STEM-EDS is limited to >10 eV, preventing fine structure analysis. The development of an EELS system capable of spectral acquisition from 2-10 keV would allow more quantitative elemental identification and nanoscale measurement of the radial distribution function (through extended edge fine structure analysis). These capabilities would greatly benefit the physical sciences.

The first step to achieving this goal is optimization of the optical coupling between the TEM and spectrometer to prevent fold-over of the diffraction pattern and to ensure an appropriate collection angle at high energy [1]. However, even if these conditions are met, the low signal for high energy scattering presents a significant challenge, particularly for high energy elemental mapping and fine structure analysis. Here, we apply direct detection (DD) and electron counting to this problem using the GIF Quantum K2 system. As we have previously shown, DD EELS significantly improves the spectrum signal-to-noise ratio (SNR) and offers a superior combination of energy resolution and energy field of view [2]. Below we show that with DD, elemental mapping at high energy is practical and in some cases superior to STEM-EDS. We also discuss ongoing efforts to perform extended fine structure analysis with EELS at >5 keV.

To demonstrate high energy mapping with DD EELS, we investigated an annealed high entropy alloy (HEA). In its as prepared state, the HEA is a single phase solid solution of Zr, Cr, Mn, Fe, Co, and Ni. After high temperature annealing, the transition metals segregate into distinct phases. With DD EELS, we performed elemental mapping using edges from 2.2 keV up to 8.3 keV. Despite the high energies of the mapped edges, the elemental signal maps show high SNR. We also mapped the Cr *K* edge at ~6 keV with traditional EELS (with a scintillator/fiber-optical/CCD camera) and with STEM-EDS (Oxford EDS silicon drift detector, 90 mm^2). Equivalent acquisition time and beam parameters were used for the DD EELS, CCD EELS, and EDS measurements, specifically, a 1.5 nm probe size, ~1 nA of current, and 20 min acquisition time.

To quantify the quality of the Cr *K* edge map, we selected an area with a nominally uniform Cr concentration shown by the square in the upper right hand corner of Figure 1h. The SNR of the Cr signal map was then determined by taking the average value within the area (the signal) and dividing by the standard deviation of the signal within the area (the noise). The calculated SNR values for DD EELS, CCD EELS, and EDS are shown in Figures 1f, 1g, and 1h, respectively.

The DD EELS signal map shows the highest SNR, followed by EDS, and then CCD EELS. This comparison demonstrates the usefulness of DD EELS for high energy elemental mapping. We note that the sample thickness within the selected area is ~0.7 inelastic mean free paths (MFP). At the bottom of the mapped area, the thickness is >1.0 MFP, and the EDS SNR is superior to that of DD EELS. This result is not surprising, as thicker samples tend to be problematic for EELS and advantageous for EDS. We anticipate that for samples thinner than 0.6 MFPs, the performance benefits of DD EELS relative to EDS will be further increased.

We are currently working to perform extended edge fine structure analysis using DD EELS. This technique could be used to locally measure the radial distribution function of a given element. This technique requires experimental data with exceptionally high SNR, because determination of the radial distribution function involves Fourier analysis. For this analysis, DD EELS is critical for maximizing SNR. Initial results will be presented here [3].

References:

[1] I MacLaren *et al*, Microscopy **67** (2017), p. i78-i85
[2] J Hart *et al*, Scientific Reports **7** (2017), p. 8243
[3] The authors acknowledge funding from the NSF MRI award #1429661. The authors acknowledge helpful discussions and advice from Prof. Ian MacLaren.

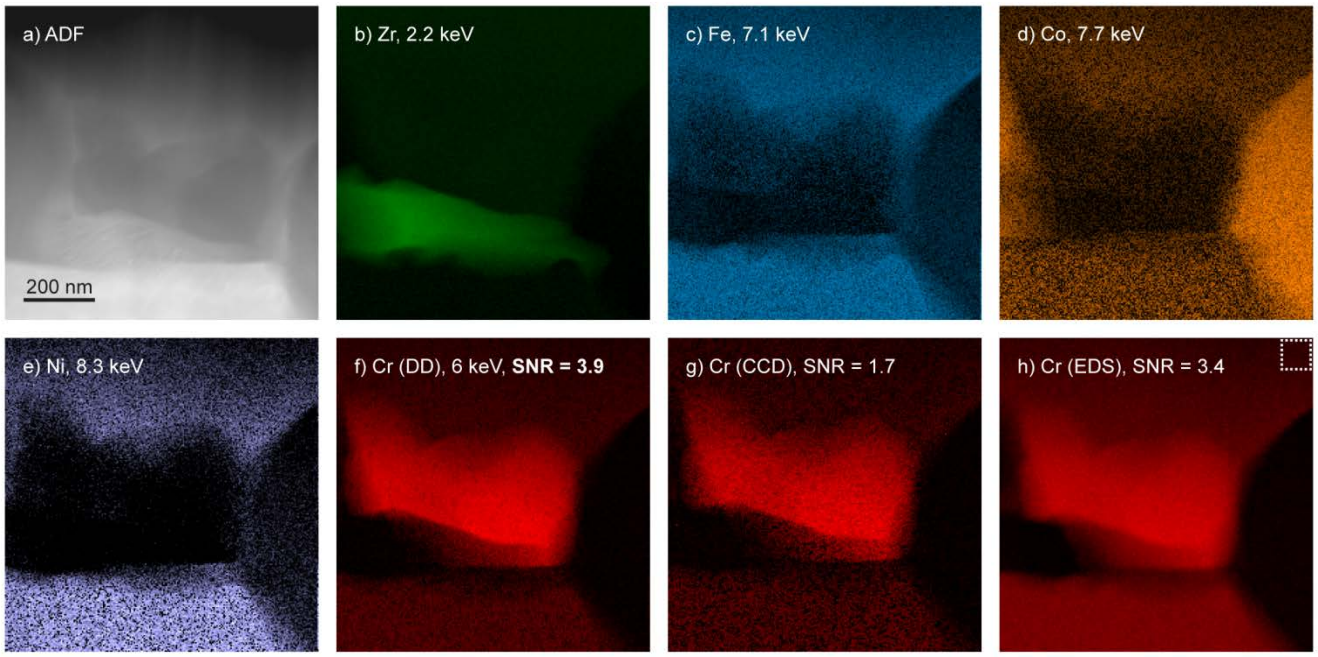

Figure 1. *Demonstration of elemental mapping with high energy edges using DD EELS. A high entropy alloy is investigated after annealing.* ***a)*** *ADF image.* ***b)-f)*** *DD EELS signal maps of different edges.* ***g)*** *A CCD (traditional) EELS map of the Cr K edge.* ***h)*** *EDS map of the Cr K edge.* ***g)*** *and* ***h)*** *should be compared with the Cr K edge mapped with DD EELS in* ***f)****. The SNR from each Cr K edge map was measured within the square region shown in* ***h)****.*

Knowledge from Atomically Resolved Images: Deep Learning Meets Statistical Physics

R. K. Vasudevan[1,2], L. Vlcek[2,3], M. Ziatdinov[2,3,4], S. Jesse[1,2], S. V. Kalinin[1,2]
[1]Center for Nanophase Materials Sciences, Oak Ridge National Laboratory, Oak Ridge TN
[2]Institute for Functional Imaging of Materials, Oak Ridge National Laboratory, Oak Ridge TN
[3]Chemical Sciences Division, Oak Ridge National Laboratory, Oak Ridge TN 37831
[4]Computer Science and Engineering Division, Oak Ridge National Laboratory, Oak Ridge TN

The capture of atomically resolved images or image sequences on a large variety of samples is now almost routine, but the wealth of information stored within these images is still not fully harnessed. This can often be broken into a two-part problem with the first being the isolation of the relevant parts of the images, including mapping all atomic coordinates, isolating the defects, classifying the symmetry, determining local strain fluctuations, and more mundane issues including background subtraction and image denoising. In many or all these areas, deep learning provides a robust tool that can be used in near real-time on atomically resolved images and can be trained on simulated images without need for expensive experiments to capture large training sets [1-3]. In this talk I will present our recent results in using deep learning for, atom and defect identification, symmetry classification, and mapping of dynamic defect trajectories. I will explain how these can fit into a larger experimental materials genomics library that can in future be mined for structure-property relationships at the atomic scale.

In parallel, once the local atomic configurations are identified, the question becomes how to use such information to understand the system and its interactions, and ultimately use them to build models with predictive capabilities. The key insight, from statistical physics, is that the fluctuations of the system (which are encoded within the statistics of the configurations) contain information that can be used to determine the system's response to thermodynamic variables [4,5]. I will explore our recent results at utilizing this statistical physics framework to turn atomically resolved images into generative models, developing effective Hamiltonians that can describe the effective interaction strengths between constituents, and the future avenues to combine such approaches with both dynamic data and adversarial deep learning methods.

References

[1] M Ziatdinov, O Dyck, A Maksov, X Li, X Sang, K Xiao, R. Unocic, R. Vasudevan, S. Jesse and SV Kalinin, ACS Nano 11 (2017), p. 12742 .
[2] R Vasudevan, N Laanait, EM Ferragut, K Wang, DB Geohegan, K Xiao, M Ziatdinov, S Jesse, O Dyck and SV Kalinin, npj Computational Materials 4 (2018), p. 30.
[3] M Ziatdinov, O Dyck, A Maksov, B Hudak, A Lupini, J Song, P Snijders, R Vasudevan, S Jesse and SV Kalinin, arXiV (2018), p. 1801.05133
[4] L Vlcek, RK Vasudevan, S Jesse and SV Kalinin, J. Chem. Theor. Comp. 13 (2017), p. 5179.
[5] L Vlcek, M Pan, RK Vasudevan and SV Kalinin, ACS Nano 11 (2017), p. 10313.
[6] The work was supported by the U.S. Department of Energy, Office of Science, Basic Energy Sciences and Materials Sciences and Engineering Division (R.K.V., S.V.K., L.V.). This research was conducted at the Center for Nanophase Materials Sciences, which also provided support (SJ) and is a US DOE Office of Science User Facility.

Effect of Non-Uniform Coverage of Dielectric Layer on the Localized Surface Plasmon Resonance

Canhui Wang[1,2], Wei-Chang D. Yang[1,2], Amit Agrawal[1,2], Alina Bruma[1,2], and Renu Sharma[1*].
[1.] Center for Nanoscale Science and Technology, National Institute of Standards and Technology, Gaithersburg, USA.
[2.] Maryland NanoCenter, University of Maryland, College Park, USA.

Excitation of localized surface plasmon resonance (LSPR) in metal nanoparticles has been shown to provide energy for photochemical reactions, allowing certain reactions to occur at room temperature. Recently, hybrid plasmonic-catalytic systems have been proposed as an efficient route towards channeling energy from a plasmonic nanoparticle to the adsorbed reactants on catalytic metal particles [1-2]. However, the stochastic nature of catalyst particle distribution on the nanoparticle surface may not allow efficient energy flow pathway from a localized plasmonic hotspot of reaction relevant energy to the adsorbed reactants. A mechanism to modify the location of the plasmonic hotspots will extend the control on engineering the plasmonic-catalytic systems. Here we propose a non-uniform thickness coating of dielectric layer as a new way to modulate the LSPR energy and intensity distribution on the plasmonic particles, in addition to the shape and size of the particles. This will provide additional control to modify the local plasmonic response at sub-particle scale, which in turn could be used in nanoparticle engineering to achieve an optimal catalytic efficiency.

We use Al/Al_2O_3 core-shell nanoparticle as a model system to investigate the effect of non-uniform coverage of dielectric material on modulating the LSPR at sub-nanoparticle scale. Electron energy-loss spectra (EELS) imaging, with different energy dispersions, is used to acquire both elemental and LSPR maps from the same particle. This allows us to identify the Al particles with a non-uniform coverage of Al_2O_3 layer and determine the relationship between the local Al_2O_3 layer thickness and the LSPR energy and intensity distribution (Fig. 1). The results show that at thicker local Al_2O_3 coverage the LSPR shifts to the lower energy, and vice versa. Non-negative matrix factorization (NMF) machine learning algorithm [3] is then used to decipher the principle components of the LSPR and map the intensity of each component (Fig. 2). This further allow us to identify the principle LSPR modes that are associated with Al_2O_3 layer thickness distribution. The result shows that, in the two modes that can be associated with the alumina layer thickness, the distribution of LSPR principle component with a lower energy overlaps with the location of higher Al_2O_3 layer thickness, and vice versa. Our result shows that a non-uniform dielectric layer can be utilized as an additional parameter to modulate the LSPR distribution on a sub-nanoparticle scale with high localization, adding to the flexibility of engineering the nanoparticles for plasmonic applications [4].

References:

[1] U. Aslam, S. Chavez, and S. Linic, Nature nanotechnology, **12(10)** (2017), p.1000.
[2] D. Swearer, et al. Proceedings of the National Academy of Sciences **113.32** (2016): 8916-8920.
[3] O. Nicoletti, et al. Nature **502.7469** (2013): 80.

[4] The authors acknowledge funding from the Cooperative Research agreement between the University of Maryland and the National Institute of Standards and Technology Center for Nanoscale Science and Technology, Award 70NANB14H209, through the University of Maryland.

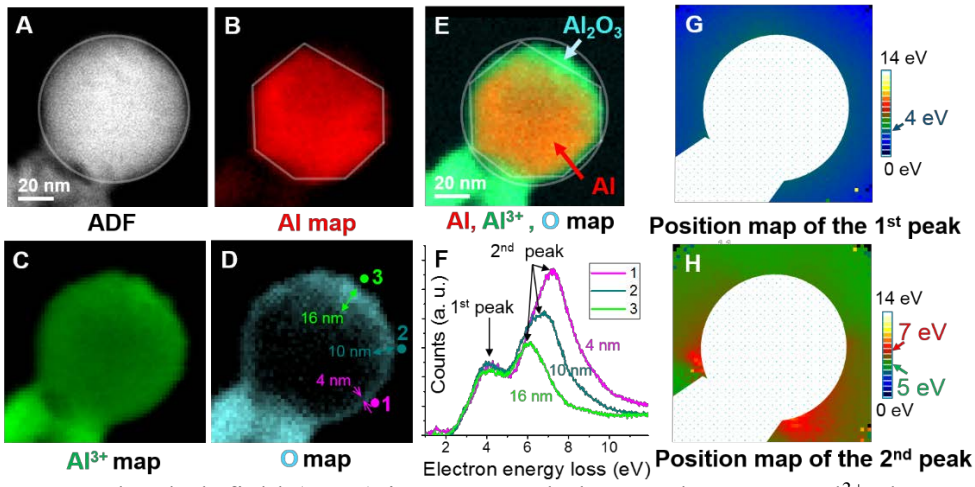

Figure 1. **A,** Annular dark field (ADF) image; **B**, Al elemental map; **C**, Al^{3+} elemental map; **D**, O elemental map showing a non-uniform Al_2O_3 shell coverage. The thickness of Al_2O_3 layer increases from 4 nm at position 1 to 16 nm at position 3; **E**, Combined Al, Al^{3+} and O elemental maps showing an Al/Al_2O_3 core-shell structure. ***F****, EEL spectra are extracted from position 1, 2 and 3 in D. It's clear that the 2nd LSPR peak shifts to lower energy as the thickness of the* Al_2O_3 layer increases. **G**, The position of the 1st LSPR peak is mapped across the area shown in A. **H**, The position of the 2nd LSPR peak is mapped across the area shown in A. The energy distribution of the first and second peaks shows dependence on the local thickness of Al_2O_3 shell (D) surrounding the Al core. The center position of the second peak (around 7eV) exhibits strong correlation with the Al_2O_3 layer thickness shown in D, while the center position of the first peak (around 4 eV) is not affected.

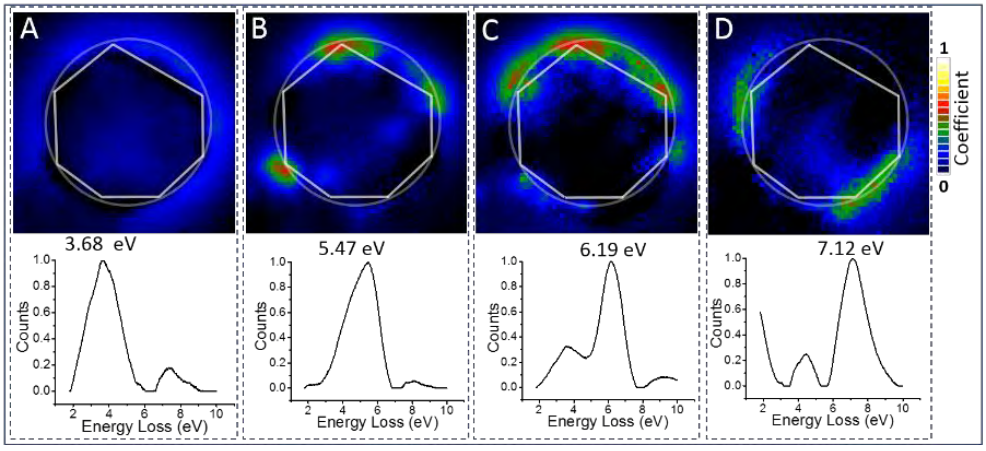

Figure 2. **A-D**, NMF algorism is used to decouple the principle components of the EELS as well as to generate the intensity distribution of each component, showing the probability distribution of different LSPR modes that are excited. Comparison of C, D and Fig. 1D shows the effect of the local Al_2O_3 thickness on the probability distribution of these two modes. The probability distribution of LSPR principle component with a lower energy (C) overlaps with the location where there is a Al_2O_3 layer with a higher thickness, and vice versa (D).

Atomic Structure, Defects, and Stacking of Clay Particles by Low-Dose, High Resolution (Cryo)-TEM

Michael L. Whittaker[1,2], Christian Kisielowski[3], Colin Ophus[3], Benjamin Gilbert[1], and Jillian F. Banfield[1,2]
[1.] Energy Geoscience Division, Lawrence Berkeley National Laboratory, Berkeley CA
[2.] Department of Earth and Planetary Science, University of California Berkeley, Berkeley CA
[3.] National Center for Electron Microscopy, Lawrence Berkeley National Laboratory, Berkeley CA

Clay minerals play important roles in myriad natural phenomena and engineered systems, from earthquakes and mudslides to barriers for nuclear waste storage and caprocks for anthropogenic carbon sequestration. Swelling clays are especially important, with chemical-mechanical behavior that arises from the competing forces between hydrated and charged layers 1 nm thick and up to a few microns wide. Establishing models for the effect of clay minerals on large-scale system function is a major cross-cutting goal in the Earth and Environmental Sciences, but this effort is limited by incomplete knowledge of the structures of clay layers, including isomorphic substitutions and the strain induced by them. Here, we present new low-dose high-resolution observations of strain within individual single-crystalline clay layers with 1-Angstrom resolution and demonstrate the coupling of this strain across multiple layers in a particle stack, a significant step towards a comprehensive model of intermolecular forces in swelling clays.

Unprecedentedly high resolution images of single layers of montmorillonite were obtained using a Nelsonian illumination scheme to minimize the total dose delivery in image-corrected low-dose high-resolution transmission electron microscopy (HRTEM). Electron-beam induced damage, the prevailing limitation to high-resolution imaging of clays, was found to initiate at the silicate layers and is hypothesized to be the result of water radiolysis.[1] Damage is minimized when particles are exfoliated to single layers, allowing water to be completely removed. At total electron doses less than ~500 e^-/Angstrom^2, a maximum resolution of 1 Angstrom along the [001] zone axis (face-on) was achieved (Figure 1). This increased dose-tolerance allows for focal-series image acquisition for exit-wave reconstruction. Single-layer images revealed the existence of strain variations on the few-nanometer length scale clearly associated with lattice defects. Edge structures were also resolved for the first time (Figure 2), showing far more disorder than expected from commonly used structural models based on micas.

Stacking of layers into particles was investigated by low-dose high-resolution cryo-TEM tomography. We directly measure the average interlayer separation while simultaneously tracking relative particle orientations with up to 2 Angstrom resolution. Loss of resolution is compensated for by increased beam-stability, which allowed for over 100x increased dose tolerance for the (020) and (110) lattice spacings. Evidence for a new, mid-range rotational ordering motif that is distinct from the textbook description of 'turbostratic' random orientation is identified. This ordering is dependent on the interlayer cation concentration and type, which suggests that it may play a significant role in controlling clay particle assembly in natural systems.

[1] M Whittaker *et al*, Microscopy and Microanalysis 24 (2018) p. 1958.

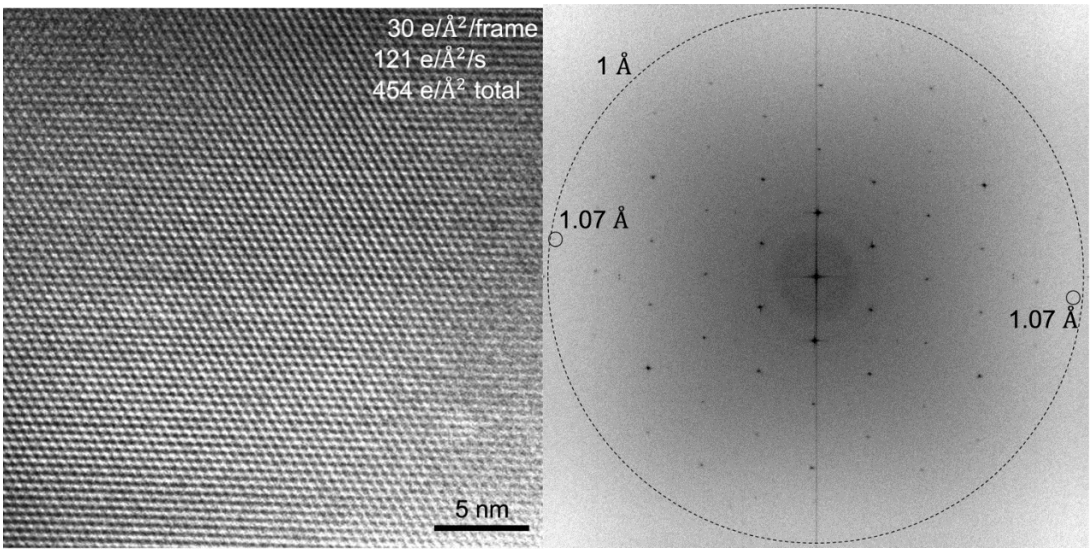

Figure 1. *Low-dose, HRTEM image of single-crystalline montmorillonite layer along the [001] zone axis (left) and associated FFT (right).*

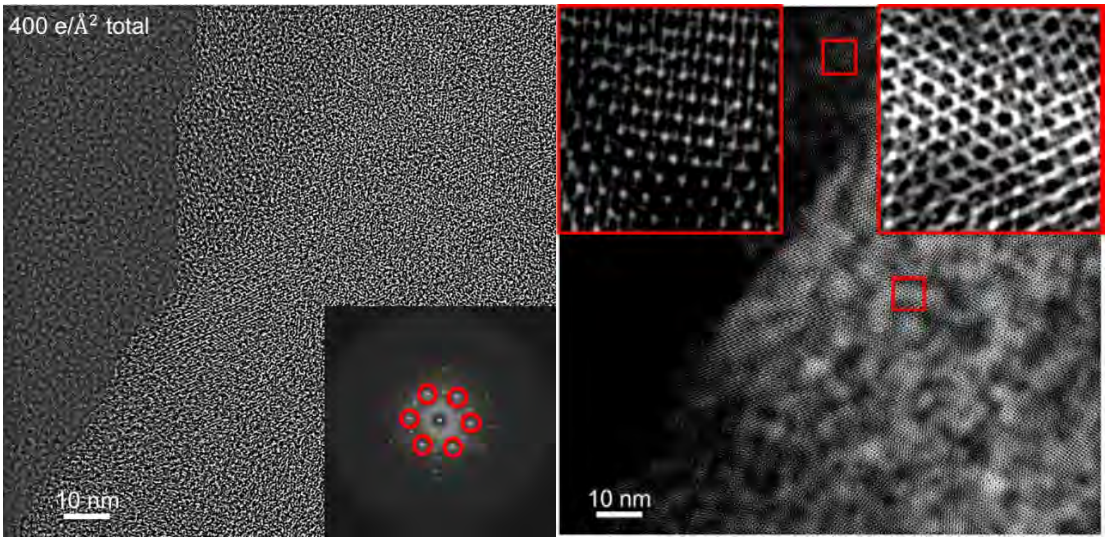

Figure 2. *Low-dose HRTEM exit-wave reconstructed image of montmorillonite particle stacks consisting of a total of three layers oriented along the [001] zone axis (left). Fourier-filtered associated FFT (right).*

Identification of Localized Surface Plasmon Mode-Selective Responses to Carbon Monoxide Adsorption on Gold Nanoparticles using Machine Learning Algorithm

Wei-Chang David Yang[1,2], Henri J. Lezec[1], and Renu Sharma[1]
[1.] Center for Nanoscale Science and Technology, National Institute of Standards and Technology, Gaithersburg, Maryland 20899, USA.
[2.] Maryland NanoCenter, University of Maryland, College Park, Maryland 20742, USA.

Optically-excited localized surface plasmon (LSP) resonances have been used to initiate a number of chemical reactions, such as hydrogen dissociation [1], water splitting [2], and ethylene epoxidation [3]. The use of plasmonic nanostructures is believed to harness light and to transfer energy from metal nanoparticles to reactants on their surface using the energized charge carriers that supply the chemical energy for LSP-induced reactions. However, sub-particle level information, regarding the LSP mode energy and intensity antinode along with their response to reactants that are adsorbed on plasmonic metal surface, has not been obtained by variants of optical spectroscopy.

Herein, we use a focused electron beam of an environmental scanning transmission electron microscope (ESTEM) to excite LSP resonances on plasmonic metal nanoparticles and to spatially resolve mode energy and intensity maximum at the sub-particle level, which correspond to the location of CO adsorption on the surface of a triangular Au nanoprism on TiO_2 support. ESTEM, operated at 80 kV and equipped with a monochromated electron source with energy resolution of 0.08 eV, enables *in situ* low- and core- loss electron energy loss spectroscopy (EELS) mapping to probe both LSP mode intensity distribution (low-loss EELS) and CO adsorption sites (core-loss EELS). The relevant LSP mode, which potentially mediates the energy transfer between the Au nanoprism and adsorbed CO molecules, is identified using machine learning algorithm that decomposes *in situ* hyperspectral imaging data. A core-loss scanning transmission electron microscopy (STEM) EELS map (Figure 1a) acquired in CO environment (P_{CO} = 110 Pa) shows the accumulated carbon K-edge signal (spectrum 1, Figure 1b) at the nanoprism edge. The excess signal can be derived by subtracting the C K-edge signal from the environment CO (spectrum 2, Figure 1b), as shown in spectrum 3. Raster-scan of electron beam in CO environment excites the LSP resonance on the Au nanoprism (ADF image of Figure 1c), which initiates room-temperature CO disproportionation that produces carbon deposits at the nanoprism edge near the cantilevered corner (Figure 1c). The carbon product, identified as amorphous carbon in Figure 1d, labels the actual reaction site on the Au nanoprim, where the maximum CO adsorption superimposes the strongest field enhancement indicated by LSP resonance intensity antinode, excited by electron beam. The LSP mode intensity distributions measured by low-loss STEM-EELS maps match closely to the electromagnetic boundary element method (BEM) calculations using the MNPBEM tool box [4]. The non-negative matrix factorization (NMF) algorithm learns LSP mode distributions based on the low-loss STEM-EELS maps (Figure 2). By comparing EELS maps of the same Au nanoprism in vacuum, CO environment, and after CO evacuation, we find certain mode shows changes in energy and intensity that can be linked to the occurrence of energy transfer from metal nanoparticle to adsorbed gas molecules. Our findings provide, for the first time, detail experimental information on sub-particle localization of plasmonic catalysis with nanometer

scale precision.

References:
[1] S Mukherjee *et al*, Nano Lett. **13** (2013), p. 240.
[2] Z Liu *et al*, Nano Lett. **11** (2011), p. 1111.
[3] P Christopher *et al*, Nat. Chem. **3** (2011), p. 467.
[4] U Hohenester, Comput. Phys. Commun. 185, 1177-1187 (2014).
[5] WDY acknowledge support under the Cooperative Research Agreement between the University of Maryland and the National Institute of Standards and Technology Center for Nanoscale Science and Technology, Award 70NANB14H209, through the University of Maryland.

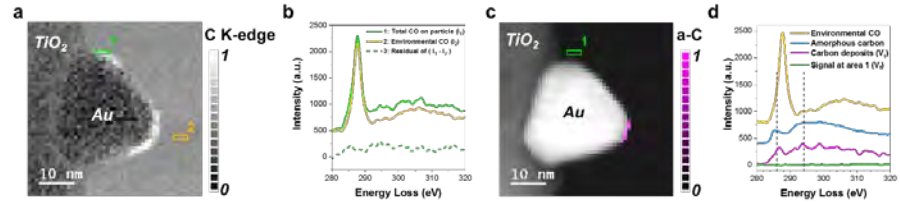

Figure 1. Room temperature CO disproportionation initiated by LSP resonance excited by electron beam. (a) STEM-EELS map of carbon K-edge in CO environment showing the accumulated CO signal at the nanoprism edge, indicating CO adsorption. (b) EEL spectra acquired from areas 1 and 2, marked in (a) showing the carbon K-edge of adsorbed CO (spectrum 1), environmental CO (spectrum 2), and their difference (spectrum 3). (c) STEM-EELS map of carbon K-edge (magenta) after CO evacuation, overlaid with an ADF image of the Au nanoprim on TiO_2 (gray scale), showing the location of carbon deposit from the LSP-induced reaction. (d) EEL spectra of environmental CO (yellow), amorphous carbon of lacey carbon grid (blue), carbon deposit (magenta), and the same area 1 (green) in both (a) and (c) after CO evacuation.

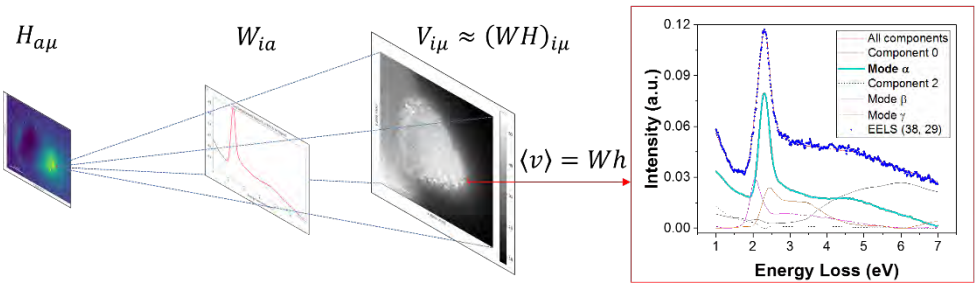

Figure 2. Non-negative matrix factorization decomposition of a low-loss STEM EELS spectrum image. Iterative algorithm finds an approximate factorization $V_{i\mu}$ by converging a local maximum for the objective function, $F = \sum_{i=1}^{n}\sum_{\mu=1}^{m}\left[V_{i\mu}\log(WH)_{i\mu} - (WH)_{i\mu}\right]$. LSP modes α, β, and γ, which are localized at the cantilevered nanoprism corner, two other nanoprism corners anchored to TiO2, and the rest of nanoprism, respectively, can be identified in the derived components at individual pixel of the original spectrum image.

Liquid Phase Electron Microscopy Study of Dynamic Phenomena at Solid-Liquid Interfaces

Haimei Zheng
[1]*Materials Sciences Division, Lawrence Berkeley National Laboratory, Berkeley, California 94720.*
[2]*Department of Material Science and Engineering, University of California, Berkeley, California 94720.*

An understanding of how materials grow and transform in their working environments is essential to the development of functional materials for various applications. My group studies a variety of physical and chemical processes of materials in liquids (including gases) by developing and applying *in situ* liquid phase transmission electron microscopy (TEM). In this talk, I will present our recent study of deposition-dissolution of alkali metal, such as Li and Na, at the electrode-electrolyte interfaces using our development of electrochemical liquid cells. I will also show our study of PbSe quantum dots superlattice transformations during ligand displacement. With the systematic study, we have been able to control the reactions and overcome the air sensitivity and other issues of PbSe nanoparticles during ligand exchange reactions. The *in situ* liquid phase TEM in combination with other advanced electron microscopy techniques on data collection and image processing allow us to achieve an unprecedented level of detail on PbSe quantum dots superlattice transformations.

Interfacially-driven Nanoparticle Nucleation Biases Hematite Crystallization towards Oriented Attachment

Guomin Zhu[1, 2], Maria Sushko[2], John Loring[2], Jinhui Tao[2], Ben Legg[2], Jennifer Solits[2], Chongmin Wang[2], James De Yoreo[1,2,*]

[1.] Department of Materials Science and Engineering, University of Washington, Seattle, Washington 98195, United States"

[2.] Physical Sciences Division, Pacific Northwest National Laboratory, Richland, WA, 99352, USA

A diverse class of materials exhibit characteristics of mesocrystals: single crystals composed of distinct nano-sized domains that are atomically aligned. The formation of such structures is often attributed to crystallization through oriented attachment (OA). However, many unanswered questions about the fundamental drivers and dynamic progression of this processes remain. Here we focus on the crystallization of hematite (hm, Fe_2O_3) from ferrihydrite (fh) as an example. In pure solution the resulting hm crystals are well faceted cuboctahedra, but in the presence of oxalate hm forms a nanoporous spindle-shaped single crystal elongated along [001]. The spindles are hierarchically organized at two length scales. At the shortest length scale, they consist of atomically aligned nanometer size domains. These then form a second order structure consisting of chains of the hm domains. We have applied in situ heating liquid phase TEM to investigate the process. We added hm seed into the solution of fh as a way to investigate the crystallization of hm. We directly observed the nucleation of new hm at the seeded hm/ solution interface, and followed by attachment to the hm seed at a solution temperature of 70 degree celsius. Post analyses after disassembling the liquid cell by using EDX mapping and electron diffraction confirmed the growth of spindle hematite in the liquid phase TEM. In addition, we developed a freeze-and-look approach using indexed TEM grids to cycle samples between the growth reactor and the TEM in order to track the pathway of crystallization over time, the results of which is in line with the in situ experiments. Based on ATR FTIR measurements of the relative binding strength of oxalate to the (001) and (012) faces, and calculations of chemical potential gradients near the interface, we propose that oxalate plays the role of inhibiting classical monomer-by-monomer growth of the hematite particles while promoting the nucleation of new hm particles at the hm/solution interface. Consequently, by inhibiting classical growth and driving all nucleation to occur near existing hm particles, the ligands bias the growth process towards oriented attachment.

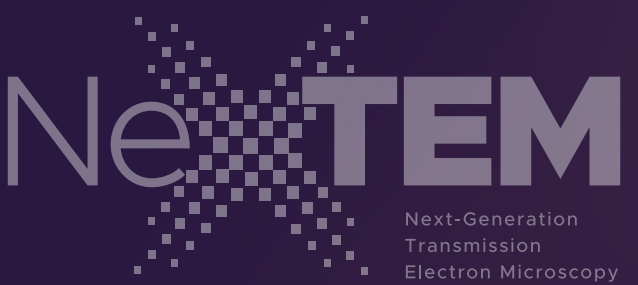
NeXTEM
Next-Generation
Transmission
Electron Microscopy


Pacific Northwest
NATIONAL LABORATORY